ANL-75-51

CHEMICAL ENGINEERING DIVISION
ENVIRONMENTAL CHEMISTRY
ANNUAL REPORT

July 1974—June 1975

by

P. T. Cunningham, B. D. Holt, B. R. Hubble,
S. A. Johnson, S. Siegel, W. I. Wilson,
F. A. Cafasso, and L. Burris

ARGONNE NATIONAL LABORATORY, ARGONNE, ILLINOIS

Prepared for the U. S. ENERGY RESEARCH
AND DEVELOPMENT ADMINISTRATION
under Contract W-31-109-Eng-38

Printed in the United States of America
Available from
National Technical Information Service
U. S. Department of Commerce
5285 Port Royal Road
Springfield, Virginia 22161
Price: Printed Copy $5.50; Microfiche $2.25

Distribution Category:
Environmental Control Technology
and Earth Sciences (UC-11)

ANL-75-51

ARGONNE NATIONAL LABORATORY
9700 South Cass Avenue
Argonne, Illinois 60439

CHEMICAL ENGINEERING DIVISION

ENVIRONMENTAL CHEMISTRY ANNUAL REPORT

July 1974—June 1975

by

P. T. Cunningham, B. D. Holt, B. R. Hubble,
S. A. Johnson, S. Siegel, W. I. Wilson,
F. A. Cafasso, and L. Burris

Earlier work on Environmental Chemistry was reported in the following Physical Inorganic Chemistry Reports:

ANL-8023 January—June 1973
ANL-8123 July 1973—June 1974

TABLE OF CONTENTS

TABLE OF CONTENTS (cont'd)

LIST OF FIGURES

LIST OF FIGURES (cont'd)

LIST OF FIGURES (cont'd)

LIST OF FIGURES (cont'd)

LIST OF TABLES

CHEMICAL ENGINEERING DIVISION
ENVIRONMENTAL CHEMISTRY ANNUAL REPORT
July 1974—June 1975

by

P. T. Cunningham, B. D. Holt, B. R. Hubble, S. A. Johnson,
S. Siegel, W. I. Wilson, F. A. Cafasso, and L. Burris

ABSTRACT

Analysis of ambient urban aerosols using infrared spectroscopic techniques has revealed the presence of acidic sulfate species. Field sampling has also revealed that the chemistry of submicrometer-sized particulates in different geographic regions is characterized more by similarity than differences. Established analytical techniques have been improved, and new approaches, including attenuated total reflectance spectroscopy, have been explored.

Study of the oxygen isotope ratios in sulfate, prepared by differing processes in the laboratory, has shown that the oxygen-18 enrichment of the product depends on the specific formation process used. This observation suggests that the oxygen isotope ratio measurements may provide a basis for determining the formation mechanism of sulfate in atmospheric particulates. Preliminary results, based on samples collected at Argonne during winter months, indicate that the sulfate was formed predominantly by a heterogeneous mechanism involving surface-adsorbed species. Details of the oxygen isotope measurement technique are described.

X-ray diffraction, optical microscopy, electron microprobe, and TGA studies have been directed toward an understanding of the molecular processes associated with the cyclic use of dolomite in sulfur emission control. Kinetic data are presented for the half-calcination, sulfation, reduction, and carbonation reactions. Other topics discussed include the development of a mathematical model to describe kinetic data, the elucidation of a structural and morphological model, the development and use of synthetic dolomites, the feasibility of a solid-solid regeneration reaction, the formation of the binary sulfate, $Mg_3Ca(SO_4)_4$, and the study of procedures to control the morphology of half-calcined dolomite.

SUMMARY

Chemistry of Airborne Particulates

The chemistry of airborne particulate materials is being studied in laboratory experiments and by field sampling and analytical activities. Attempts to observe the formation of aerosol material in a laboratory flow reactor have not been successful, but the reactor has been used with seed aerosols to obtain samples of acid sulfate that have infrared spectra very like those of

samples collected in urban areas. Suitable standards have been prepared for the quantitative determination of sulfate in particulate samples using infrared spectrophotometric techniques. Preliminary evaluation of attenuated total reflectance (ATR) spectroscopy as a technique for the determination of aerosol chemistry has been encouraging. A rudimentary sampling device for use with ATR analysis has been designed and tested. Techniques are being developed for recovering particulate samples from filter media for subsequent infrared analysis. The major problem relates to maintaining the integrity of the sample chemistry during the recovery process.

Field sampling has been conducted in the Chicago and St. Louis areas, as well as at Riverside, California. Acid sulfate has been identified in the submicrometer-sized particulate samples from Chicago and St. Louis; some degree of acidity is present in 21% of the Chicago samples. The samples collected at Riverside contain significantly greater amounts of nitrate than do the samples from the midwestern area but are remarkably similar to midwestern samples in other observed features.

Oxygen-18 Analysis in the Study of Atmospheric Sulfate Aerosols

Sulfate, prepared by two hydrolysis-oxidation methods in the laboratory from SO_2, excess water, and air oxygen, all of known ^{18}O content, was shown by oxygen isotope ratio analysis to have the form $SO_sO_sO_wO_w^{2-}$ (two oxygens originating from the SO_2, two from the water, and none detectable from air oxygen). Sulfate prepared by an oxidation-hydrolysis sequence, using the same reagents and exciting the SO_2 in dry air by a Tesla-coil spark, was shown to consist partially of air oxygen--the relative amount depending on the duration of exposure of the SO_2-air mixture to the spark.

In the application of the demonstrated distinguishableness of sulfates by oxygen isotopy according to their sequence of formation from SO_2 (i.e., hydrolysis-oxidation or oxidation-hydrolysis), field samples of concurrently collected ambient sulfate aerosols, SO_2, and water vapor were analyzed for ^{18}O. The initial results suggest that if the sulfate aerosols collected at the Argonne meteorological station during winter months (November-February) were produced in the atmosphere from coincident SO_2, water, and air, they were probably formed predominantly by a heterogeneous mechanism involving surface-adsorbed intermediate molecular ions of the forms $SO_sO_sO_wO_aO_a^{2-}$ and $SO_aO_aO_wO_aO_a^{2-}$.

Sulfur Emission Control Chemistry

Studies are being made to gain information on the fundamental aspects of the chemical reactions and structural properties related to the cyclic use of limestones and other reagents to control sulfur emissions. Exploratory experiments were conducted to determine those factors that influence reaction rates, the degree of reagent utilization, ease of sorbent regeneration, and the extent of decrepitation. Techniques used to obtain the experimental data included thermogravimetric analysis (TGA), differential thermal analysis (DTA), x-ray diffraction, optical microscopy, electron microscopy, electron microprobe, and infrared spectroscopy.

A rudimentary mathematical model was developed to assist in interpreting the experimental data. This model successfully fits much of the sulfation data presently available, but certain parameters still lack physical

significance. Nevertheless, this model has been useful for suggesting lines of investigation and will serve as a point of departure for a more satisfactory model.

The sulfation of half-calcined dolomite has been studied by several experimental approaches. Detailed analysis of the crystallographic structure and morphology of the stone before and after sulfation has provided considerable insight into the nature of the sulfation process on a microscale. Similar structural studies of the half-calcination reaction suggest that the crystallographic nature of the half-calcined stone is determined by the calcining conditions and that properties desirable in subsequent reactions may be selectively produced.

Synthetic dolomites were prepared with the expectation that such materials will permit study of the fundamental chemical and physical changes that take place during sulfation and regeneration without interference by impurities present in natural stones. Preliminary results are encouraging. A new phase, $Mg_3Cs(SO_4)_4$, has been identified in the sulfation product of synthetic dolomite and in the sulfated form of natural dolomite that was sulfated and half-calcined simultaneously.

The reactions used in the two-step regeneration process (reduction and carbonation) were investigated using TGA. In addition, an alternative one-step regeneration process based on the solid-solid reaction of CaS and $CaSO_4$ was explored. The structural and morphological character of the various sorbent reagents was examined on a microscale in an effort to determine those factors that contribute to stone hardness and thereby influence decrepitation rates.

I. CHEMISTRY OF AIRBORNE PARTICULATES
(P. T. Cunningham and S. A. Johnson)

The need to understand the chemistry of airborne particulate material is becoming increasingly important as the role played by particulates in the health and environmental effects of atmospheric pollutants becomes more apparent.[1] The importance of secondary particulates, those particles formed in the atmosphere from gaseous precursors, is especially great since they contribute a substantial fraction of the mass of material in the size range from about 0.1 to 2.0 micrometers--a size which interferes with visibility and is most easily respirable.[2] During the period covered by this report, exploratory laboratory experiments and field sampling activities were conducted to gain information necessary to improve present sampling and analytical procedures,[3,4] to develop new techniques, to deduce particulate formation mechanisms, and to determine how the chemistry of atmospheric particulates differs on a regional basis.

A. Laboratory Studies (S. A. Johnson and L. Holley*)

The laboratory studies conducted during this period included (1) use of the flow reactor apparatus, described in a previous report,[3] to provide insight into the chemical nature and mechanism of formation of some secondary particulates, (2) preliminary testing of infrared attenuated total reflectance spectroscopy as a technique for the determination of the chemistry of airborne particulate material, (3) development of additional calibration standards for the quantitative determination of substances present in particulate samples, using infrared spectrophotometric techniques, and (4) preliminary study of techniques appropriate to the extraction of particulate samples from filter media without alteration of sample chemistry and subsequent analysis using infrared spectrophotometry. Since much of the work is still incomplete, and since some ideas or concepts have been shown to be less fruitful than originally believed, what is presented here should not be considered to be final findings.

1. Flow Reactor Studies

The flow reactor, described in some detail in a previous report,[3] is utilized to simulate the formation of airborne particulate material and to test various proposed formation mechanisms. Briefly, it is a cylindrical Pyrex chamber 15 cm in diameter and 3.5 m long into which seed aerosol, reactive gases, and dilution air can be introduced at one end, while emerging aerosol is monitored and collected at the other end. The reactor has a volume of about 64 liters, and the residence time in the reactor can be controlled by adjusting the total flow rate.

In a number of experiments, reactive gases such as SO_2, NO, NO_2, and NH_3 have been introduced into the reactor with and without various seed aerosols and at a variety of total flow rates and relative humidities. To date, there has been no evidence of aerosol formation. When seed aerosol that was not expected to be highly reactive has been used (*e.g.*, sodium chloride), there has been no evidence of aerosol growth nor has any new substance (*e.g.*, sulfate)

---

*Undergraduate Research Participant.

been found in the aerosol collected from the reactor that could indicate that a reaction had taken place. When reactive seed aerosol, such as sulfuric acid, was introduced into the reactor, neutralization by ammonia has been observed resulting in modification of the aerosol chemistry.

One problem noted in early flow reactor experiments is the long memory effect (presumably due to adsorption and subsequent desorption of reactive gases on the reactor walls) exhibited by the reactive gases, especially ammonia. For example, after ammonia has been used in the reactor at a low ppm level, seed aerosol of sulfuric acid or ammonium bisulfate has emerged from the reactor as ammonium sulfate for periods of several hours after introduction of ammonia has terminated. This observation is general and extends to other seed aerosols of an acidic nature, such as iron sulfate and aluminum sulfate.

One positive result obtained from flow reactor studies relates to the identification of acid sulfate in ambient particulate samples by infrared spectroscopy. As previously reported[3] (and discussed in greater detail later in this report), the infrared spectra of some submicrometer-sized atmospheric particulate samples were quite similar to those of mixtures of ammonium sulfate and sulfuric acid, but the peak heights of the various bands were in poor agreement. It was observed that if aerosol produced by bubbling clean dry air through a solution containing sulfuric acid and ammonium sulfate in various proportions was allowed to age during transit through the flow reactor, the aged aerosols gave spectra that agreed very closely in all respects with those of various ambient particulate samples. An example is shown in Fig. I-1. This observation has considerably strengthened confidence in the capability of infrared spectroscopy as an analytical method in the study of particulate chemistry.

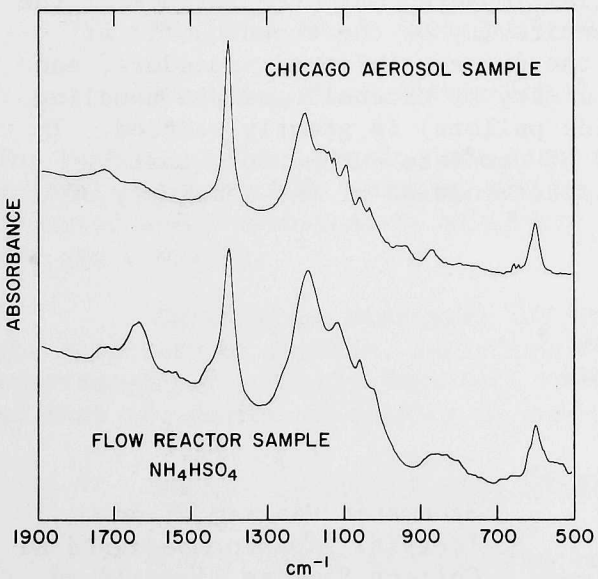

Fig. I-1.

Infrared Spectra: upper curve, acid sulfate-containing submicrometer-sized particulate material collected in Chicago, and lower curve, acid sulfate-containing aerosol obtained from a flow reactor.

2. Attenuated Total Reflectance Spectroscopy

The infrared spectroscopic methods presently used to analyze particulate samples[3,4] require that the sample first be recovered from the collection substrate (either an impactor collection film or some filter medium) and then incorporated into a potassium bromide pellet before an infrared spectrum is obtained (see the following section of standards for quantitative analysis). Attenuated total reflectance (ATR) spectroscopy appears to offer a means of avoiding this tedious procedure.

The ATR technique is based on the fact that light that is totally reflected at the interface between two media having different refractive indexes is, in fact, partially absorbed or attenuated by material that may be in contact with that interface. A detailed discussion of this phenomenon and some of its applications has been presented by Harrick.[5] The technique is most applicable to the infrared spectral region.

In practice, infrared light is focused on the bevelled end of a thin plate of material that is not infrared-absorbing in the spectral region of interest. The bevel angle is chosen so that the light is totally reflected within the plate a number of times (the exact number depends on the plate thickness, entrance angle, etc.)[5] before emerging from the plate through the bevelled surface at the other end. The spectrum of material in intimate contact with the plate's surfaces can thus be obtained.

The concept envisioned here is to use an ATR plate as the impaction surface in an inertial impactor and to obtain the infrared spectrum of the material collected. A rudimentary device was fabricated along these lines from available impactor parts and is shown schematically in Fig. I-2. Preliminary evaluation of this concept has been encouraging. Samples collected from the flow reactor, as well as ambient air samples collected in Chicago, have indicated that the spectrum of material impacted onto the surface of the ATR plate can be easily obtained. The sensitivity of the technique is at least comparable with the sensitivity of the present infrared procedure, and the likelihood of altering the sample chemistry by extensive sample handling (as in the procedure with potassium bromide pellets) is greatly reduced. In addition, the technique has the potential of complete automation, thereby providing a technique for near real-time determination of the chemistry of airborne particulates.

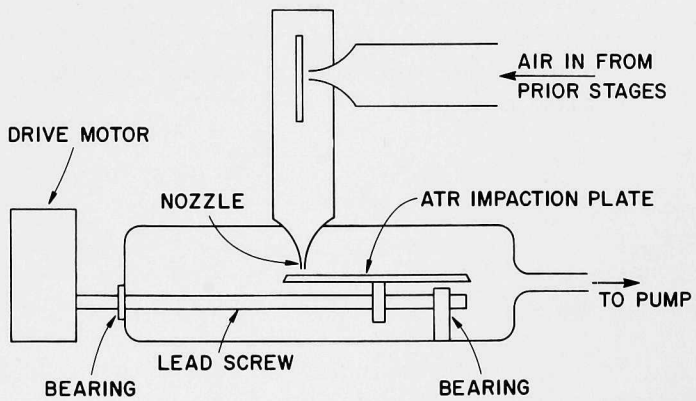

Fig. I-2.

Schematic Diagram of an Inertial Impactor Designed to Collect Samples Directly on ATR Plates to Simplify Subsequent Analysis.

3. Standards for Quantitative Analysis

The desirability of quantitative, as well as qualitative, information on the chemistry of particulate material is clear. An earlier report[3] described difficulties and initial favorable results in establishing quantitative standards appropriate for the infrared spectrophotometric methods presently being used. More recent results are reported here.

Potassium bromide pellets containing known amounts of reagent grade ammonium sulfate were prepared by first thoroughly mixing easily weighed amounts of these materials and then mixing various proportions of that mixture with additional potassium bromide to obtain pellets containing 5 to 250 μg of ammonium sulfate. Both mixing steps were carried out in an agate ball mill to achieve complete and uniform mixing. The infrared spectra of these samples were obtained, and peak heights of the sulfate bands at 620 and 1110 cm^{-1} and of the ammonium band at 1400 cm^{-1} were measured in absorbance units. Plots of peak absorbance versus weight of ammonium sulfate are shown in Figs. I-3 through I-5. It is evident that Beer's law is followed for all three bands over the concentration range studied here. It is noted that infrared absorption has been previously proposed as a means of quantitative sulfate determination and that the calibration curve reported for the 1110 cm^{-1} sulfate band agrees with the curve reported here within the experimental uncertainty. By assuming a spectrum with a reasonable base line and freedom from other interfering species in the sample (which is usually the case for the 620 cm^{-1} sulfate band), the following equations were obtained by a linear regression analysis of the data presented in Figs. I-3 through I-5; these equations can be used to determine the weight, in micrograms, of ammonium and sulfate (as ammonium sulfate) in particulate samples.

$$\text{Wt } (NH_4)_2SO_4 = \text{Absorption } (1400\ cm^{-1}) \times 3.24 \times 10^2$$

$$\text{Wt } (NH_4)_2SO_4 = \text{Absorption } (1110\ cm^{-1}) \times 2.91 \times 10^2$$

$$\text{Wt } (NH_4)_2SO_4 = \text{Absorption } (620\ cm^{-1}) \times 6.54 \times 10^2$$

For typical ambient particulate samples, these equations are estimated to be accurate within ±10%; however, the necessary comparative studies between this infrared spectrophotometric procedure and standard analytical procedures are not yet complete.

Calibration standards for other substances have been prepared, but, for a variety of reasons, satisfactory results have not been obtained. It is considered particularly important to develop standards for ammonium bisulfate so that the degree of acidity of ambient particulate samples can be determined.

4. Sample Extraction From Filter Media

A difficulty in comparing results obtained using the airborne particulate sampling and analysis procedures developed in this program,[3,4] which is, in fact, a difficulty common to much of the atmospheric pollution monitoring work, is that the variety of sampling techniques in use makes comparison of results difficult. Sampling devices vary from the traditional Hi-Vol filter

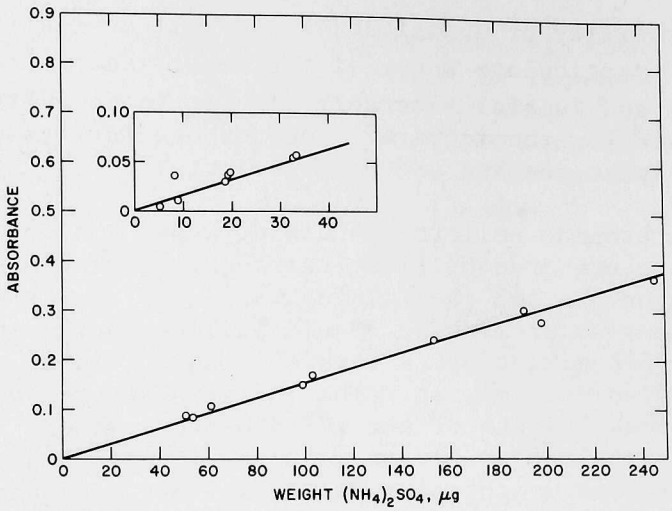

Fig. I-3. $(NH_4)_2SO_4$ Weight in a Standard Pellet Versus Absorbance of the 620 cm^{-1} Sulfate Band.

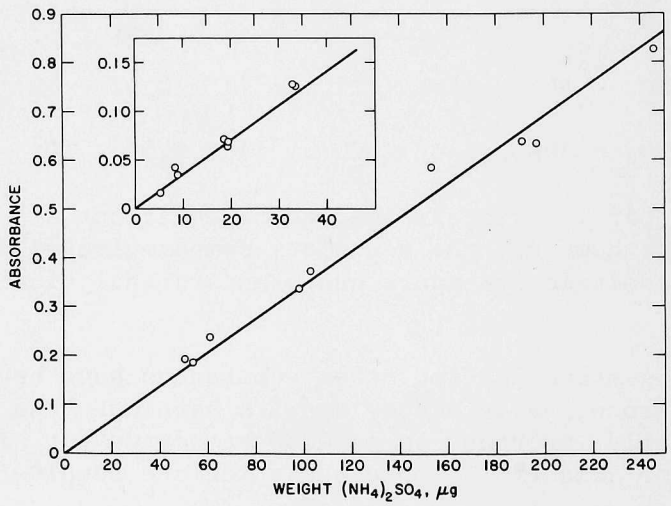

Fig. I-4. $(NH_4)_2SO_4$ Weight in a Standard Pellet Versus Absorbance of the 1110 cm^{-1} Sulfate Band.

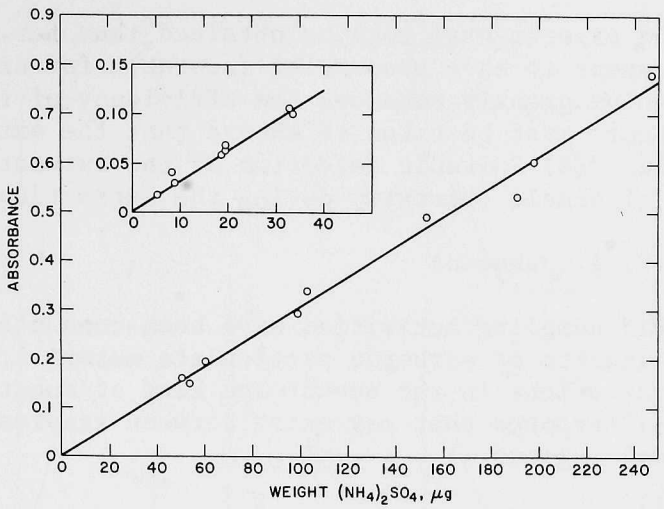

Fig. I-5. $(NH_4)_2SO_4$ Weight in a Standard Pellet Versus Absorbance of the 1400 cm^{-1} Sulfate Band.

sampler, which provides no size classification of the sample and only limited time classification (24-hour samples are common), to a variety of filter samplers with and without time classification. For these samplers, a variety of filter media and impaction substrates is used. To bridge the gap among the various sampling techniques, attempts are being made to develop techniques whereby samples could be recovered from a variety of substrates and made available for subsequent analysis by a common technique.

In particular, efforts have been directed toward developing a procedure for recovering material from the backup filter (used with the Lundgren cascade impactor employed in this program) in a way that permits subsequent analysis by the infrared spectrophotometric methods already developed. To date, fluid extraction methods have received the most attention, and three problems can be identified: (1) The extraction medium (water, benzene, cyclohexane, methanol) interacts with many substrate materials, resulting in interferences and/or incomplete extraction. (2) Any single extraction fluid tends to be selective in the materials extracted, necessitating multiple extraction if several different substances must be analyzed. (3) The extraction process tends to alter the chemistry of the sample and thereby introduces considerable uncertainty in interpreting the analytical results in terms of ambient particulate composition. This third difficulty is especially bothersome when the degree of acidity associated with particulate samples is to be determined since neutralization appears to occur, at least in part, during the extraction process. Recent work at Brookhaven National Laboratory[6] indicates that by proper selection of the extracting fluid, the acidity of the sample can be determined; this concept deserves further investigation.

No satisfactory extraction process has yet been developed. Although it is unlikely that an extraction process will prove to be as satisfactory as direct analysis of the as-collected sample, the development of an extraction process is necessary if the comparability of various atmospheric particulate sampling procedures is to be established. The following generalizations can

be made, based on the experimental results obtained thus far. (1) Teflon fiber filter media appear to have properties favorable for extraction processes. (2) Ultrasonic agitation greatly enhances the efficiency of the extraction process. (3) Great care must be taken to ensure that the extraction fluid is free of contamination. (4) Suitable selection of the extraction fluid may minimize alteration of sample chemistry during the extraction process.

B. Field Studies (S. A. Johnson)

A number of field sampling activities have been conducted to determine the major chemical constituents of airborne particulate material, to determine the nature of temporal variations in the amount and kind of substances present, and to examine the differences that may exist between samples collected in different geographical regions.

1. Field Sampling in Chicago

During the past several years, a large number of samples has been collected in the metropolitan Chicago area and have been subsequently analyzed by infrared spectrophotometry. Many of the results have already been reported. The earlier work showed that the chemistry of airborne particulate material is dependent on the particle size, with large particles comprising primarily silicates and carbonates, whereas particles smaller than about one micrometer in aerodynamic diameter are principally ammonium sulfate. The variations in chemistry with particle size are consistent with the theory that the large-particle-size range is dominated by mechanically injected primary particulates, whereas the smaller-particle-size range comprises, for the most part, secondary particulates formed in the atmosphere from gaseous precursors. Thus, the spectra of submicrometer-sized particles are dominated by the infrared active vibrational modes, $\nu_3(F_2)$ and $\nu_4(F_2)$, for the ammonium and sulfate tetrahedral ions, which are observed at 3140 and 1400 cm^{-1} for ammonium and at 1110 and 620 cm^{-1} for sulfate.[7] It was previously reported[3] that variations in the spectra of the submicrometer-sized particles were observed, and it was suggested that these variations were due to the presence of acid sulfate. That this is indeed the case seems now to be well established, based on the flow reactor studies described above and on more complete analyses of the observed spectral variations.

The nature of the spectral variations caused by the presence of acid sulfate can be seen in Fig. I-6, which shows the spectra of a sequence of samples collected with three-hour time resolution in Chicago during the fall of 1973. The two bands associated with sulfate (620 and 1110 cm^{-1}, curves *a* and *q* in Fig. I-6) diminish in intensity and are replaced by four prominent bands at 1205, 1063, 869, and 600 cm^{-1} (see curves *e* and *i*) and two weaker bands at 1118 and 675 cm^{-1} (see curves *f* through *h*). The four prominent bands correspond reasonably well with those reported for bisulfate ion;[8] the following assignments have been made: 1205 cm^{-1}, $\nu_4(E)$; 1063 cm^{-1}, $\nu_1(A_1)$; 869 cm^{-1}, $\nu_2(A_1)$; 600 cm^{-1}, $\nu_3(A_1)$ and/or $\nu_6(E)$. The samples with weaker bands at 1118 and 675 cm^{-1} are believed to be more acidic than bisulfate on the basis of comparison with samples prepared in the flow reactor.

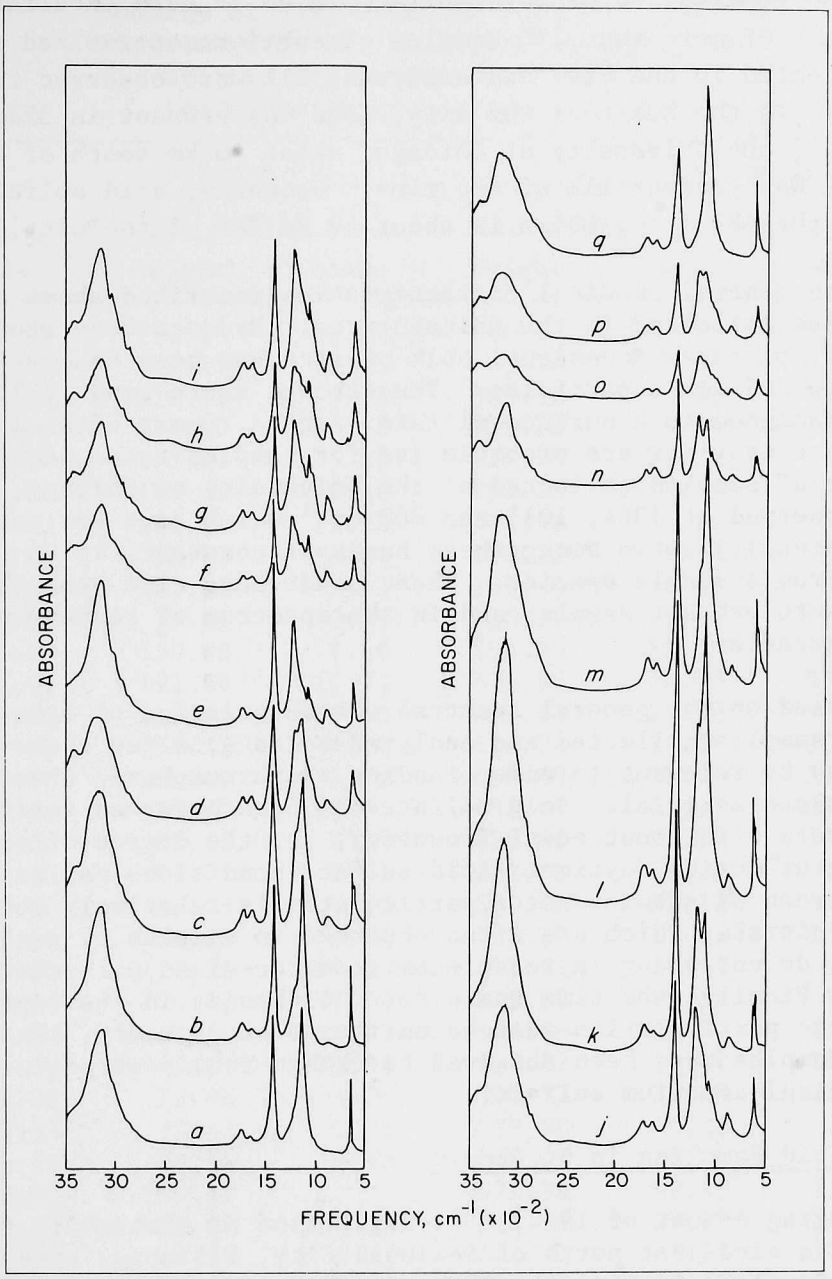

Fig. I-6.

Infrared Spectra For a Series of Samples Collected in the City of Chicago. Each sample was collected during a three-hour interval, starting at 20:00 for curve *a*, and including a total period of 51 hours. Variations in the spectra reflect the changing degree of acidity of the sample: neutral--curves *a* and *q*; weakly acidic--curves *b*, *c*, *l* and *m*; moderately acidic--curves *d*, *k*, *n* and *p*; strongly acidic--curves *e*, *i*, *j* and *o*; very strongly acidic--curves *f*, *g* and *h*. All spectra were obtained with 8 cm^{-1} resolution and are plotted in the same scale of absorbance.

The observation of acid sulfate is not a rare occurrence in the Chicago area. Of more than 250 samples of submicrometer-sized particulate samples collected in the city and analyzed, 21% were observed to be acidic to some degree. In the heart of the city, acid was present in 33% of the samples; at the site of the University of Chicago, about 10 km south of the city's center, acid was present 11% of the time. Recently, acid sulfate has been observed at the ANL site, which is about 40 km WSW of the city's center.

The general chemical characteristics described above apply to most of the samples collected in the Chicago area. Hydrocarbons are usually present, and, on a few occasions, bulk nitrate has been observed in samples of both large and small particles. The strong, sharp band at 1385 cm^{-1}, previously assigned to a surface nitrate species,[4] most often is observed when high NO_x concentrations are probable (as for samples taken near an expressway). For a number of samples collected at the University of Chicago, however, three bands are observed at 1364, 1035 and 808 cm^{-1} which have not yet been assigned. Since the intensity ratio among these bands is constant, it is assumed that they arise from a single species. These bands have also been observed in the spectra of auto exhaust samples and in the spectrum of benzene used to clean a Soxhlet extractor.

Based on the general spectral characteristics of a large number of particulate samples collected and analyzed to date, a few observations can be made that may be relevant to understanding the atmospheric chemistry associated with particulate material. Acid sulfate has been observed during daytime and nighttime hours with about equal frequency, but the degree of acidity is usually greater during daytime. Acid sulfate conditions can exist even when the total burden of submicrometer particulates is relatively low. Hydrocarbon and surface nitrate, which are often observed in samples of particles of all size ranges, do not occur in those submicrometer-sized particle samples that are acidic. Finally, the time scale for the changes in the degree of acidity of atmospheric particulation must be on the order of hours, since sequential three-hour samples have been observed to change from a strongly acidic character to neutral ammonium sulfate.

2. Field Sampling in St. Louis

During August of 1974, a 24-day period of continuous sampling was conducted at a site just north of National City, Illinois, at a point about 12 km NW of downtown St. Louis. This site was also occupied by a Regional Air Monitoring System (RAMS) station being operated by the U.S. EPA as a part of the Regional Air Pollution Study (RAPS). It was anticipated that considerable data on meteorology and gaseous pollutant concentration would be available to assist in interpreting the particle chemistry data, but operating difficulties greatly reduced the amount of supplemental information available. Nevertheless, the experience gained in continuously operating a sampler at a site remote from ANL and in analyzing the samples collected has proved valuable. The data collected during this sampling period are presented in Table I-1. Each sample weight represents the weight of sample recovered from the Mylar substrate of the stage III and stage IV impactor stages and as such represent a minimum for the weight actually collected. Similarly, since the atmospheric loading is based on the recovered weight and is not corrected for impactor losses, it represents the minimum loading for particulate material

Table I-1. Summary of Data Obtained During a Field Sampling Experiment at St. Louis During Late Summer, 1974.
1. Weights are in micrograms.
2. Loads are in micrograms per cubic meter.

Date	Start Time	Stage III Sample Weight	Stage III Sample Load	Stage IV Sample Weight	Stage IV Sample Load	Stage IV Sulfate Weight	Stage IV Sulfate Load
8/ 5/74	12:00	21.26	1.19	26.67	1.50	0.51	0.03
8/ 5/74	15:00	17.01	0.95	91.76	5.14	32.46	1.82
8/ 5/74	18:00	116.93	6.55	380.92	21.35	123.25	6.91
8/ 5/74	21:00	457.09	25.62	559.11	31.34	129.84	7.28
8/ 6/74	0:00	172.21	9.65	417.20	28.39	137.96	7.73
8/ 6/74	3:00	110.55	6.20	292.36	16.39	74.56	4.18
8/ 6/74	6:00	199.84	11.20	371.32	20.81	55.28	3.10
8/ 6/74	9:00	51.02	2.86	170.72	9.57	33.47	1.88
8/ 6/74	12:00	23.39	1.31	100.30	5.62	50.21	2.81
8/ 6/74	15:00	17.01	0.95	100.30	5.62	37.02	2.08
8/ 6/74	18:00	150.95	8.46	394.79	22.13	170.92	9.58
8/ 6/74	21:00	191.34	10.73	476.95	26.73	139.98	7.85
8/ 7/74	0:00	167.95	9.41	454.54	25.48	83.69	4.69
8/ 7/74	3:00	255.12	14.30	428.93	24.04	108.03	6.06
8/ 7/74	6:00	280.63	15.73	488.69	27.39	106.00	5.94
8/ 7/74	9:00	125.43	7.03	488.69	27.39	149.11	8.36
8/ 7/74	12:00	87.17	4.89	420.40	23.56	108.54	6.08
8/ 7/74	15:00	46.77	2.62	362.78	20.34	66.44	3.72
8/ 7/74	18:00	125.43	7.03	501.49	28.11	130.35	7.31
8/ 7/74	21:00	150.95	8.46	514.29	28.83	155.71	8.73
8/ 8/74	0:00	116.93	6.55	471.61	26.44	97.89	5.49
8/ 8/74	3:00	196.65	11.02	475.88	26.68	97.89	5.49
8/ 8/74	6:00	191.34	10.73	347.84	19.50	114.12	6.40
8/ 8/74	9:00	248.74	13.94	697.82	39.12	154.19	8.64
8/ 8/74	12:00	72.28	4.05	390.52	21.89	127.30	7.14
8/ 8/74	15:00	30.83	1.73	539.90	30.26	76.59	4.29
8/ 8/74	18:00	53.15	2.98	446.01	25.00	78.11	4.38
8/ 8/74	21:00	129.69	7.27	524.96	29.43	110.57	6.20
8/ 9/74	0:00	65.91	3.69	614.59	34.45	109.05	6.11
8/ 9/74	3:00	89.29	5.01	422.53	23.68	187.66	10.52
8/ 9/74	6:00	80.79	4.53	234.74	13.16	69.99	3.92
8/ 9/74	9:00	34.02	1.91	106.70	5.98	57.31	3.21
8/ 9/74	12:00	91.42	5.12	181.83	10.19	58.12	3.26
8/ 9/74	15:00	46.77	2.62	117.04	6.56	26.82	1.50
8/ 9/74	18:00	61.65	3.46	127.49	7.15	30.80	1.73
8/ 9/74	21:00	89.29	5.01	169.29	9.49	40.24	2.26
8/10/74	0:00	1.06	0.06	85.69	4.80	16.39	0.92
8/10/74	3:00	38.27	2.15	41.80	2.34	15.90	0.89
8/10/74	6:00	85.04	4.77	50.16	2.81	6.46	0.36
8/10/74	9:00	35.08	1.97	39.71	2.23	22.85	1.28
8/10/74	12:00	72.28	4.05	60.61	3.40	19.87	1.11
8/10/74	15:00	38.27	2.15	35.53	1.99	14.41	0.81
8/10/74	18:00	31.89	1.79	81.51	4.57	22.35	1.25
8/10/74	21:00	44.65	2.50	77.33	4.33	40.73	2.28

Table I-1. (Cont'd.)

Date	Start Time	Stage III Sample Weight	Stage III Sample Load	Stage IV Sample Weight	Stage IV Sample Load	Stage IV Sulfate Weight	Stage IV Sulfate Load
8/11/74	0:00	97.80	5.48	96.14	5.39	19.87	1.11
8/11/74	3:00	12.76	0.72	68.97	3.87	17.39	0.97
8/11/74	6:00	1.06	0.06	91.96	5.15	20.86	1.17
8/11/74	9:00	12.76	0.72	43.89	2.46	9.93	0.56
8/11/74	12:00	17.01	0.95	52.25	2.98	14.41	0.81
8/11/74	15:00	4.25	0.24	22.99	1.29	15.40	0.86
8/11/74	18:00	4.25	0.24	10.45	0.59	2.98	0.17
8/11/74	21:00	76.54	4.29	100.32	5.62	15.40	0.86
8/12/74	0:00	65.91	3.69	171.38	9.61	21.36	1.20
8/12/74	3:00	89.29	5.01	196.46	11.01	29.80	1.67
8/12/74	6:00	138.19	7.75	181.83	10.19	47.69	2.67
8/12/74	9:00	138.19	7.75	346.94	19.45	121.20	6.79
8/12/74	12:00	44.65	2.50	75.24	4.22	54.14	3.03
8/12/74	15:00	70.16	3.93	56.43	3.16	20.86	1.17
8/12/74	18:00	102.05	5.72	119.13	6.68	34.27	1.92
8/12/74	21:00	114.80	6.44	117.04	6.56	22.35	1.25
8/13/74	0:00	87.17	4.89	154.66	8.67	35.76	2.00
8/13/74	3:00	104.17	5.84	74.19	4.16	18.38	1.03
8/13/74	6:00	77.60	4.35	88.82	4.98	21.36	1.20
8/13/74	9:00	77.60	4.35	88.82	4.98	20.86	1.17
8/13/74	12:00	46.77	2.59	98.23	5.43	38.75	2.14
8/13/74	15:00	85.04	4.70	60.61	3.35	6.95	0.38
8/13/74	18:00	104.17	5.76	79.42	4.39	10.93	0.60
8/13/74	21:00	380.55	21.04	158.84	8.78	25.83	1.43
8/14/74	0:00	159.45	8.82	123.31	6.82	18.88	1.04
8/14/74	3:00	82.91	4.58	91.96	5.08	13.91	0.77
8/14/74	6:00	97.80	5.41	173.47	9.59	37.75	2.09
8/14/74	9:00	38.27	2.12	163.02	9.01	60.10	3.32
8/14/74	12:00	34.02	1.88	261.25	14.44	123.69	6.84
8/14/74	15:00	10.63	0.59	374.11	20.68	252.84	13.98
8/14/74	18:00	23.39	1.29	309.32	17.10	174.35	9.64
8/14/84	21:00	70.16	3.88	227.81	12.59	103.82	5.74
8/15/74	0:00	110.55	6.11	252.89	13.98	60.10	3.32
8/15/74	3:00	85.04	4.70	280.06	15.48	72.03	3.98
8/15/74	6:00	53.15	2.94	275.88	15.25	85.44	4.72
8/15/74	9:00	29.76	1.65	432.63	23.92	115.74	6.40
8/15/74	12:00	31.89	1.76	240.35	13.29	90.90	5.03
8/15/74	15:00	25.51	1.41	321.86	17.79	127.16	7.03
8/15/74	18:00	48.90	2.70	296.78	16.41	162.93	9.01
8/15/74	21:00	57.40	3.17	108.68	6.01	77.49	4.28
8/16/74	0:00	10.63	0.59	211.09	11.67	58.12	3.21
8/16/74	3:00	114.80	6.35	177.65	9.82	44.21	2.44
8/16/74	6:00	193.47	10.70	209.00	11.55	55.63	3.08
8/16/74	9:00	127.56	7.05	434.72	24.03	131.63	7.28
8/16/74	12:00	38.27	2.12	79.42	4.39	24.84	1.37
8/16/74	15:00	31.89	1.76	48.07	2.66	20.86	1.15
8/16/74	18:00	31.89	1.76	45.98	2.54	24.34	1.35
8/16/74	21:00	61.65	3.41	83.60	4.62	13.91	0.77

Table I-1. (Cont'd.)

Date	Start Time	Stage III Sample Weight	Stage III Sample Load	Stage IV Sample Weight	Stage IV Sample Load	Stage IV Sulfate Weight	Stage IV Sulfate Load
8/17/74	0:00	17.01	0.94	83.60	4.62	4.97	0.27
8/17/74	3:00	121.18	6.70	231.99	12.83	23.84	1.32
8/17/74	6:00	161.58	8.93	248.71	13.75	38.75	2.14
8/17/74	9:00	46.77	2.59	244.53	13.52	117.23	6.48
8/17/74	12:00	31.89	1.84	38.84	2.24	11.17	0.64
8/17/74	15:00	36.14	2.08	124.68	7.19	48.58	2.80
8/17/74	18:00	31.89	1.84	151.26	8.72	97.65	5.63
8/17/74	21:00	104.17	6.01	143.08	8.25	63.15	3.64
8/18/74	0:00	31.89	1.84	98.11	5.66	40.32	2.32
8/18/74	3:00	59.53	3.43	114.46	6.60	56.35	3.25
8/18/74	6:00	29.76	1.72	81.76	4.71	37.41	2.16
8/18/74	9:00	10.63	0.61	28.62	1.65	10.69	0.62
8/18/74	12:00	11.69	0.67	10.22	0.59	4.86	0.28
8/18/74	15:00	10.63	0.61	14.31	0.82	6.80	0.39
8/18/74	18:00	25.51	1.47	212.58	12.26	125.34	7.23
8/18/74	21:00	167.95	9.68	402.67	23.22	166.14	9.58
8/19/74	0:00	163.70	9.44	459.90	26.52	111.73	6.44
8/19/74	3:00	110.55	6.37	531.44	30.64	101.05	5.83
8/19/74	6:00	267.88	15.44	527.35	30.40	142.34	8.21
8/19/74	9:00	125.43	7.23	351.57	20.27	177.32	10.22
8/19/74	12:00	27.64	1.59	249.37	14.38	52.95	3.05
8/19/74	15:00	17.01	0.98	241.19	13.91	50.52	2.91
8/19/74	18:00	112.68	6.50	435.37	25.10	124.85	7.20
8/19/74	21:00	55.28	3.19	290.25	16.73	129.71	7.48
8/20/74	0:00	63.78	3.68	343.39	19.80	133.59	7.70
8/20/74	3:00	104.17	6.01	386.32	22.27	133.11	7.67
8/20/74	6:00	229.61	13.24	972.94	56.10	228.81	13.19
8/20/74	9:00	93.54	5.39	447.64	25.81	57.81	3.33
8/20/74	12:00	34.02	1.96	134.90	7.78	5.34	0.31
8/20/74	15:00	38.27	2.21	114.46	6.60	7.29	0.42
8/20/74	18:00	106.30	6.13	412.89	23.81	81.13	4.68
8/20/74	21:00	68.03	3.92	476.25	27.46	92.30	5.32
8/21/74	0:00	82.91	4.78	402.67	23.22	141.85	8.18
8/21/74	3:00	74.41	4.29	398.58	22.98	158.37	9.13
8/21/74	6:00	128.62	7.42	364.85	21.04	139.91	8.07
8/21/74	9:00	128.62	7.42	364.85	21.04	140.40	8.09
8/21/74	12:00	36.14	1.97	71.06	3.88	45.20	2.47
8/21/74	15:00	8.50	0.46	166.15	9.06	82.95	4.52
8/21/74	18:00	17.01	0.93	447.26	24.39	158.46	8.64
8/21/74	21:00	53.15	2.90	405.46	22.11	182.30	9.94
8/22/74	0:00	125.43	6.84	470.25	25.65	227.50	12.41
8/22/74	3:00	223.23	12.17	461.89	25.19	192.73	10.51
8/22/74	6:00	323.15	17.62	532.95	29.07	141.07	7.69
8/22/74	9:00	87.17	4.75	175.56	9.57	87.92	4.80
8/22/74	12:00	46.77	2.55	217.36	11.85	124.18	6.77
8/22/74	15:00	31.89	1.74	273.79	14.93	123.69	6.75
8/22/74	18:00	61.65	3.36	321.86	17.55	162.43	8.86
8/22/74	21:00	140.32	7.65	372.02	20.29	130.14	7.10

Table I-1. (Cont'd.)

Date	Start Time	Stage III Sample Weight	Stage III Sample Load	Stage IV Sample Weight	Stage IV Sample Load	Stage IV Sulfate Weight	Stage IV Sulfate Load
8/23/74	0:00	240.24	13.10	359.48	19.61	80.47	4.39
8/23/74	3:00	182.84	9.97	357.39	19.49	106.30	5.80
8/23/74	6:00	331.66	18.09	361.57	19.72	91.90	5.01
8/23/74	9:00	136.06	7.42	257.07	14.02	123.69	6.75
8/23/74	12:00	87.17	4.75	171.38	9.35	95.87	5.23
8/23/74	15:00	91.42	4.99	114.95	6.27	50.67	2.76
8/23/74	18:00	85.04	4.64	173.47	9.46	80.97	4.42
8/23/74	21:00	82.91	4.52	177.65	9.69	51.16	2.79
8/24/74	0:00	48.90	2.67	102.41	5.59	34.77	1.90
8/24/74	3:00	108.43	5.91	181.83	9.92	36.76	2.00
8/24/74	6:00	112.68	6.15	156.75	8.55	78.48	4.28
8/24/74	9:00	223.23	12.17	384.56	20.97	180.31	9.83
8/24/74	12:00	133.94	7.30	537.13	29.29	313.44	17.09
8/24/74	15:00	59.53	3.25	240.35	13.11	158.95	8.67
8/24/74	18:00	10.63	0.58	146.30	7.98	63.58	3.47
8/24/74	21:00	199.84	10.90	315.59	17.21	96.86	5.28
8/25/74	0:00	99.92	5.45	248.71	13.56	51.16	2.79
8/25/74	3:00	51.02	2.78	154.66	8.44	66.07	3.60
8/25/74	6:00	21.26	1.16	167.20	9.12	45.70	2.49
8/25/74	9:00	10.63	0.58	186.01	10.14	36.26	1.98
8/25/74	12:00	68.03	3.71	275.88	15.05	57.12	3.12
8/25/74	15:00	40.39	2.20	267.52	14.59	74.01	4.04
8/25/74	18:00	91.42	4.99	407.55	22.23	152.50	8.32
8/25/74	21:00	221.10	12.06	472.34	25.76	108.29	5.91
8/26/74	0:00	206.22	11.25	558.03	30.43	145.05	7.91
8/26/74	3:00	261.50	14.26	355.30	19.38	91.40	4.98
8/26/74	6:00	369.92	20.18	514.14	28.04	185.78	10.13
8/26/74	9:00	170.08	9.28	539.22	29.41	103.82	5.66
8/26/74	12:00	51.02	2.78	493.24	26.90	70.04	3.82
8/26/74	15:00	85.04	4.64	777.48	42.40	89.91	4.90
8/26/74	18:00	99.92	5.45	591.47	32.26	189.25	10.32
8/26/74	21:00	233.86	12.75	589.38	32.14	123.19	6.72
8/27/74	0:00	250.68	13.68	463.98	25.31	146.54	7.99
8/27/74	3:00	76.54	4.17	277.97	15.16	114.75	6.26
8/27/74	6:00	210.47	11.48	227.81	12.42	41.23	2.25
8/27/74	9:00	27.64	1.51	48.07	2.62	19.87	1.08
8/27/74	12:00	51.02	2.78	50.16	2.74	13.91	0.76
8/27/74	15:00	46.77	2.55	85.69	4.67	14.41	0.79
8/27/74	18:00	48.90	2.67	79.42	4.33	13.41	0.73
8/27/74	21:00	57.40	3.13	66.88	3.65	7.45	0.41

Table I-1. (Cont'd.)

Date	Start Time	Stage III Sample Weight	Stage III Sample Load	Stage IV Sample Weight	Stage IV Sample Load	Stage IV Sample Weight	Stage IV Sample Load
8/28/74	0:00	61.65	3.36	43.89	2.39	12.42	0.68
8/28/74	3:00	65.91	3.59	45.98	2.51	10.93	0.60
8/28/74	6:00	55.28	3.01	83.60	4.56	21.86	1.19
8/28/74	9:00	63.78	3.48	156.75	8.55	38.25	2.09
8/28/74	12:00	142.44	7.77	179.74	9.80	37.75	2.06
8/28/74	15:00	42.52	2.32	108.68	5.93	22.85	1.25
8/28/74	18:00	102.05	5.57	33.44	1.82	5.96	0.33
8/28/74	21:00	91.42	4.99	85.69	4.67	13.91	0.76
8/29/74	0:00	121.18	6.61	106.59	5.81	16.89	0.92
8/29/74	3:00	78.66	4.29	73.15	3.99	9.44	0.51
8/29/74	6:00	137.13	7.48	100.32	5.47	18.88	1.03
8/29/74	9:00	137.13	7.48	107.63	5.87	13.91	0.76

in the size range collected by the respective impactor stages. The weight of sulfate found in the stage IV samples is based on the absorbance of the 620 cm^{-1} band and was calculated from the relation between absorbance and sulfate weight as determined with the calibration standards described earlier in this report.

The variations in total sample weight and sulfate weight were typical of what was also observed in the Chicago samples. In general, the spectra of the St. Louis samples were, in most respects, very like those of samples collected in Chicago. There were a few exceptions. Early in the sampling period, but not after the third day of sampling, the St. Louis stage IV (submicrometer) samples contained more nitrate than is typical of Chicago samples. Acid sulfate was observed in only 8% of the samples collected in St. Louis, nearly all of the observations occurring during the last third of the sampling period. This rate of occurrence is lower than expected on the basis of the Chicago samples and other observations of acid sulfate in the St. Louis area but could easily be a result of statistical variation. Sulfate was observed in stage II and stage III samples on a few occasions. Since most atmospheric sulfate is present in secondary particulates, it should not be associated with the supermicrometer particles collected on stages II and III. In this instance, the probable source of the sulfate, presumed to be calcium sulfate from the details of its spectral character, was a fertilizer plant located near the sampling point. Wind data necessary to confirm this conclusion are not available.

3. Field Sampling in Riverside, California

With the cooperation of the California Statewide Air Pollution Laboratory at the University of California, Riverside, particulate samples were collected near Riverside, California, on several occasions during the fall of 1974. This site provided an opportunity to compare the chemical characteristics of aged particulate material that originated in the Los Angeles

basin and is associated with photochemical smog with those of the midwestern urban particulate collected in Chicago and St. Louis. The comparison is more striking for the similarities than for the differences.

Figure I-7 shows a spectrum typical of a heavy Riverside sample of submicrometer-sized particles. The only outstanding difference between this spectrum and similar spectra of Chicago area samples is the presence in the Riverside sample of a considerable amount of bulk nitrate and a very strong surface nitrate band. Analysis of the Riverside samples is still not complete and will eventually include quantitative analysis for both sulfate and nitrate, as well as qualitative interpretation of other spectral features.

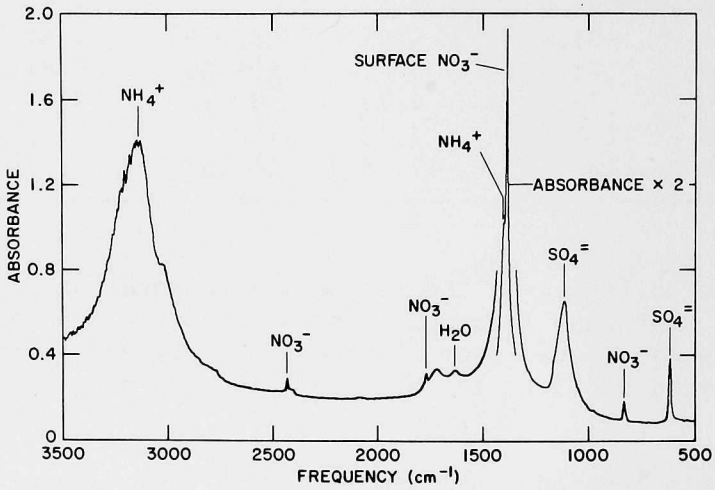

Fig. I-7.

Typical Spectrum Obtained From a Heavy Three-Hour Sample of Submicrometer-Sized Particulate Material Collected in Riverside, California.

II. OXYGEN-18 ANALYSIS IN THE STUDY OF ATMOSPHERIC SULFATE AEROSOLS

(P. T. Cunningham and B. D. Holt)

Atmospheric sulfate aerosols, particularly in acid forms, are becoming generally recognized as potentially hazardous to man, animals, plants, and inanimate objects (buildings, bridges, sculpture, paintings, etc.). A major fraction of sulfate aerosols found in the atmosphere orginates as oxides of sulfur injected into the atmosphere as a by-product of man's production of energy by combustion of fossil fuels. The increasing demand for energy from sulfur-containing fossil fuels and the potential hazards of sulfate aerosols in the atmosphere are, therefore, serious yet inseparable problems. The problem of energy demand is here to stay; hence, elimination or reasonable control of the pollution problem deserves consideration. Impressive advances in the reduction of sulfur oxides emissions may continue for a while as the limits for legal compliance are tightened, but each gain becomes more and more costly. In the long run, tolerable pollution levels must be maintained at sustainable cost.

Pertinent to this dilemma are the following questions. Assuming that emission controls are not perfect, what forms of oxidized sulfur are the most offensive to the environment? Can the conditions that are conducive to the formation of the offensive forms of oxidized sulfur be avoided or minimized? To deal with these questions, it is important to learn as much as possible about the origin and mechanism of formation of sulfate from SO_2 in the atmosphere.

This section describes the application of oxygen isotopy to a study of atmospheric sulfate formation by isotopically comparing sulfates produced in the laboratory under controlled, varied conditions with ambient sulfate aerosols collected at or near the site of Argonne National Laboratory. The project was started in the current fiscal year and therefore is described for the first time in this annual report.

Mizutani and Rafter[9] outlined two possible mechanisms of formation of sulfate aerosols from atmospheric SO_2 as follows:

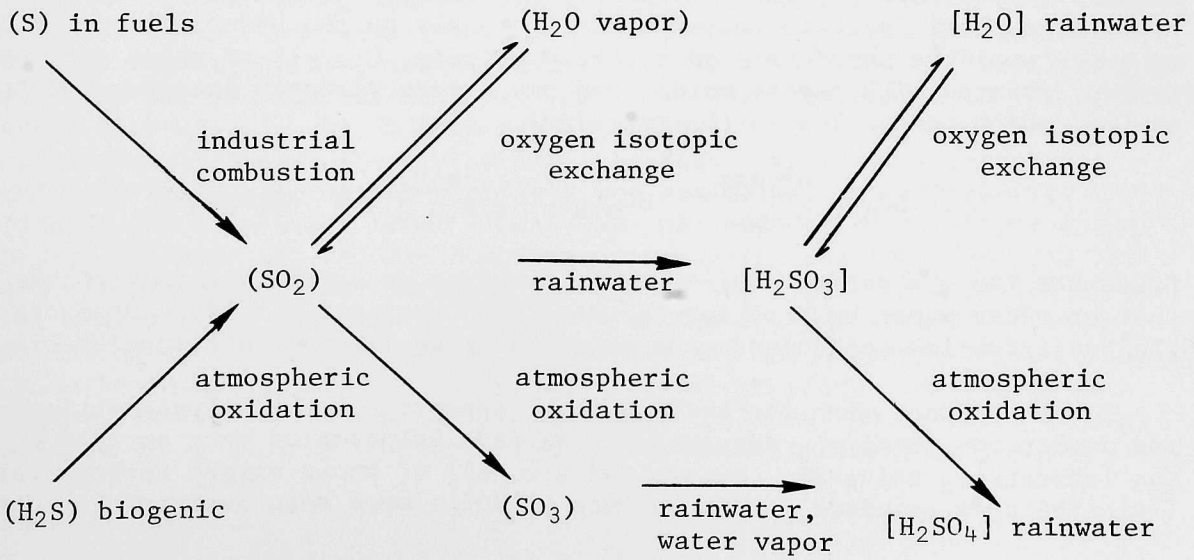

The hydrolysis of SO_2 to sulfurous acid with subsequent oxidation to sulfate is usually referred to as a heterogeneous mechanism, whereas the photo-oxidation to SO_3, with subsequent hydrolysis to sulfate, is a homogeneous mechanism. There is still some disagreement as to which of the two routes of formation of sulfate predominates.

The photo-oxidation-hydrolysis process depends upon the intensity of solar radiation (wavelength range of 0.29 to 0.50 μm), SO_2 concentration, concentrations of other air pollutants (NO_2, O_3, hydrocarbons, etc.), temperature, and relative humidity.[10,11] Hydrolysis-oxidation reactions are thought to occur in water droplets of fog or rain or on solid aerosol particles coated with a film of moisture. The hydrolysis-oxidation process is catalytically enhanced by trace amounts of metal ions, particularly manganese, iron, nickel, and copper. Hydrolysis-oxidation reaction rates also depend upon the pH of the aqueous aerosols, tending to be suppressed by the low pH of the acid product but enhanced by the pH-elevating effect of atmospheric ammonia.[12]

The specific objective at the outset of this work was to determine the applicability of oxygen isotopy to the assessment of the relative roles of the two classes of sulfate-formation processes, oxidation-hydrolysis and hydrolysis-oxidation. It was expected that the ^{18}O content of the sulfate product would be reproducibly relatable to the sequence of its formation reactions, because of the remarkably low rate of exchange of oxygen isotopes between water and sulfate ions (halftime about 2000 years at pH 7 and 25°C),[13] in contrast to the assumed relatively rapid rate of exchange between water and sulfite ions.[14]

Disregarding fractionation effects, which were to be assessed and accounted for later, it was expected that each sulfate ion formed homogeneously in the atmosphere by a photo-oxidation-hydrolysis sequence would contain two oxygen atoms originating from the SO_2 molecule, one from the air oxidant, and one from atmospheric water. The sequence of reactions may be represented as follows:

$$SO_sO_s \xrightarrow[1/2(O_aO_a)]{\text{air}} SO_sO_sO_a \xrightarrow[H_2O_w]{} SO_sO_sO_aO_w^{2-} \qquad (1)$$

where s, a, and w subscripts on the oxygen atoms indicate their initial association with SO_2, air O_2, and atmospheric H_2O vapor, respectively. On the other hand, atmospheric sulfate formed heterogeneously by the hydrolysis-oxidation sequence would be characterized by three oxygens, O_e, all of which had been preequilibrated with excess water, and one oxygen directly incorporated from air oxidation, according to the reactions,

$$SO_sO_s \xrightarrow[H_2O_w]{\text{excess}} SO_eO_eO_e^{2-} \xrightarrow[1/2(O_aO_a)]{\text{air}} SO_eO_eO_eO_a^{2-} \qquad (2)$$

Since the isotope ratio, $^{18}O/^{16}O$, of air oxygen is easily distinguishable from that of water vapor by mass spectrometry, the respective sulfate products of the two formation mechanisms were expected to be likewise distinguishable.

In accordance with the basic plan of the project, hydrolysis-oxidation and oxidation-hydrolysis sequences of sulfate preparation were carried out in the laboratory, using SO_2, water, and air, all of known oxygen isotope ratios (relative to a standard). The sulfate products were then analyzed to confirm

the expected isotope chemistry. Collection of samples of atmospheric sulfates, atmospheric sulfur dioxide, rain (or snow), and sedimentary dust was started for isotopic analysis. Since the isotope ratio of air oxygen is known to be fairly invariant, measurements of the ratios in concurrently sampled atmospheric SO_2, water vapor, and sulfate aerosol were expected to provide sufficient information to indicate the predominant mechanism of formation of the sulfate from the SO_2.

The experimental information obtained thus far has not substantiated all of the expected results outlined above. However, equally valuable alternative interpretations of observed oxygen isotope chemistry have emerged and are discussed below.

A. Experimental (B. D. Holt, A. Engelkemeir* and S. A. Johnson)

Experimental procedures are described or referred to in this subsection for the following operations: hydrolysis-oxidation formation of sulfate, oxidation-hydrolysis formation of sulfate, preparation of $BaSO_4$ and subsequent conversion of the oxygen in SO_4^{2-} to CO_2, conversion of air oxygen to CO_2, conversion of the oxygen in water to CO_2, and field sampling of sulfate aerosol, atmospheric SO_2, water vapor, precipitation, and sedimentary dust. The CO_2 was prepared for subsequent mass spectrometric analysis.

1. Hydrolysis-Oxidation Formation of Sulfate

Two methods were used to prepare sulfate by a hydration-oxidation process. In the first method, SO_2 and oxygen-free water were equilibrated in a sealed container before air was admitted; in the second, SO_2 was injected into an aqueous alkaline solution.

a. First Method. Figure II-1 shows the apparatus used for carrying out the hydrolysis-oxidation reactions in a sealed container. The 250-ml flask, connected as shown in Fig. II-1a, was evacuated and then charged with 50 ml of water. The water was degassed by freezing, pumping off the released gases, thawing, refreezing, and repumping. With the water frozen at liquid nitrogen temperature, a measured quantity ($\sim$85 μmoles) of SO_2 was cryogenically transferred to the flask, and the flask was separated from the vacuum line by sealing off at the side arm. The sealed glass container was placed in a mechanical shaker and agitated several hours for oxygen isotope equilibration between the SO_2 and the excess H_2O. The flask was then sealed to the stopcock assembly shown in Fig. II-1b with a seal breaker, and a seal-off constriction was provided as shown. The system was evacuated, the lower stopcock was closed, and the break-seal to the flask was fractured. By appropriate manipulation of the stopcocks, about 2 ml of NH_3 was added, the flask was filled with dry, CO_2-free air to near atmospheric pressure, and the flask was again sealed off at the constriction. It was shaken for eight hours on the mechanical shaker and then allowed to stand unopened for one week to allow air oxidation of the sulfite solution. The flask was then opened and the solution was made to volume in a 100-ml volumetric flask and stored for subsequent analysis. Variations of this basic procedure included the addition of small quantities (1 μg to 1 mg) of $FeCl_3 \cdot H_2O$ to the water to increase reaction rates.

---

*Analytical Chemistry Laboratory, ANL.

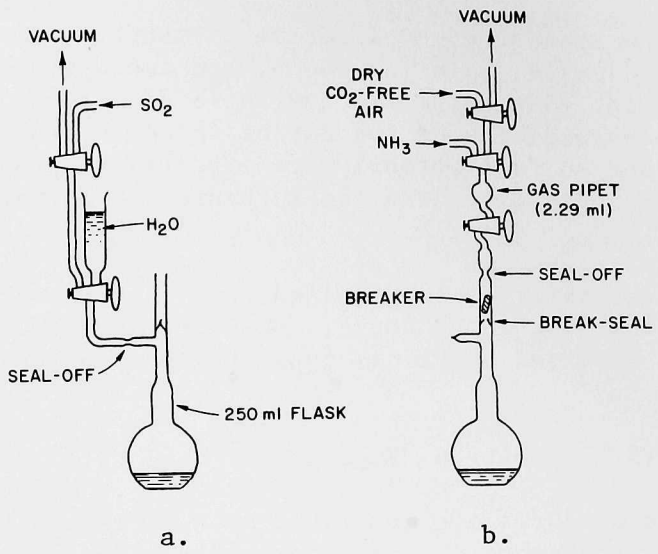

Fig. II-1. Apparatus for Hydrolysis-Oxidation Formation of Sulfate in a Sealed Container.

b. Second Method. The hydrolysis-oxidation procedure was later carried out by using equipment diagramed in Fig. II-2. Fifty milliliters of SO_2 was injected from a syringe through rubber tubing into about 450 ml of aqueous solution contianing 2 g KOH and 1 ml glycerol. The solution had been pulled up into the inverted separatory funnel by the rubber-bulb pump. Tiny bubbles of insoluble gas impurities from the 50 ml of SO_2, which were collected at the top of the container as the SO_2 was discharged into the alkaline solution, had a volume of about 1 ml. The sulfite solution was oxidized to sulfate by adding three drops of liquid bromine and heating for several minutes on a steambath.

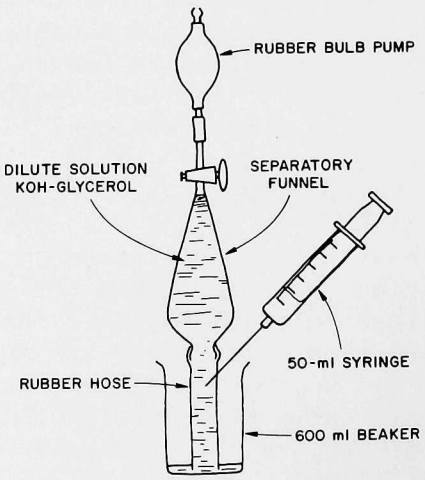

Fig. II-2. Apparatus for Adding SO_2 to Alkaline Solution.

2. Oxidation-Hydrolysis Formation of Sulfate

Oxidation of SO_2 to SO_3, prior to hydrolysis to sulfuric acid, was carried out in the apparatus shown in Fig. II-3. A measured quantity of SO_2 ($\sim$85 μmoles) was cryogenically transferred to the side arm of the evacuated reaction chamber (Fig. II-3a). The reaction chamber was then filled with dry air to a pressure of about 600 torr and was sealed off at the constriction. A high-voltage spark (Fig. II-3b) was passed across a 1-cm gap between platinum electrodes embedded in the end wall of the glass chamber. The other end of the reaction chamber was cooled with ice water to ensure condensation of the SO_3 as it was formed. During the first half hour of each exposure to the spark coil, the gas mixture turned brown, indicating the presence of NO_2. A white condensate also appeared on the inner walls of the reaction chamber. In addition to SO_3, some S_2O_5 and some polysulfur peroxides were probably present in the condensate.[15]

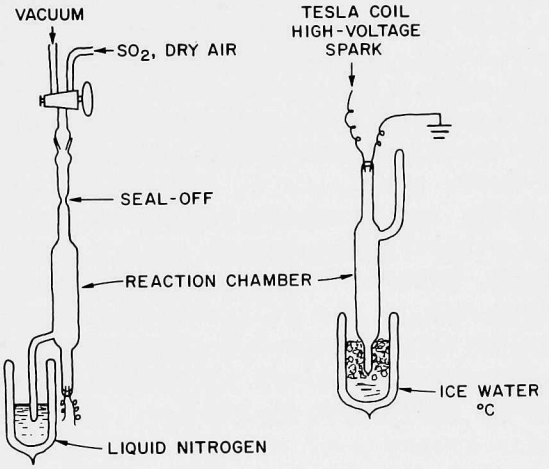

Fig. II-3. Apparatus for Oxidation-Hydrolysis Formation of Sulfate. a. Confinement of SO_2 and dry air. b. Activation of oxidation by high voltage discharge.

3. Preparation of $BaSO_4$ for Reduction by Graphite

The sulfate of each sample was converted to $BaSO_4$ by a conventional precipitation procedure used in gravimetric analysis.[16] The $BaSO_4$ precipitate was not filtered on fine, low-ash filter paper for subsequent ashing at 800°C as in the conventional procedure, however, because the oxygen isotope composition of the $BaSO_4$ would be subject to change as a result of charring of the paper during combustion--i.e., the $BaSO_4$ could be partially reduced under these conditions and then be reoxidized by air oxygen.

Two other procedures considered for the preparation of $BaSO_4$ (for subsequent conversion of its contained oxygen to CO_2 by graphite reduction) were filtration on fritted glass media and centrifugation. Both of these techniques required tedious, preferably quantitative transfer of washed and dried $BaSO_4$ from either glass frit or a centrifuge tube to a container suitable for the intimate mixing of $BaSO_4$ with graphite powder for enclosure in a graphite crucible.

A filtration procedure was worked out that avoided the problems of paper charring, incomplete transfer, and hand mixing with graphite powder. The precipitated $BaSO_4$ was cofiltered with graphite powder (added to the supernatant solution) through a porous graphite capsule. Figure II-4 shows the capsule (made from a spectrographic cup) mounted in a glass holder that extends into a 250-ml suction flask. A short segment of rubber hose sealed the capsule to the holder and supported a glass funnel, into which the suspension of $BaSO_4$ and graphite powder was poured. The steps of the procedure were as follows:

Take a sample aliquot containing about 9 mg SO_4^{2-}, dilute to 50 ml, make slightly acid, and add 1 ml excess HCl. Heat the solution to boiling to destroy carbonates, and slowly add 3 ml of 10% $BaCl_2$ solution with vigorous stirring. Digest the solution on a steambath for one hour, and let stand at room temperature for at least two hours. Install the graphite capsule as shown in Fig. II-4, and wash a few times with reagent-grade acetone. Decant the supernatant liquid from the $BaSO_4$ precipitate into the funnel for filtration. Add about 50 mg spectroscopic-grade graphite powder to the beaker that contains the residual $BaSO_4$ precipitate, and (using hot water from a wash bottle) transfer the $BaSO_4$ and graphite powder to the funnel for collection in the capsule. Use a rubber policeman to effect complete transfer of the $BaSO_4$, and wash the $BaSO_4$-graphite powder mixture with hot water until negligible chloride is detected in the filtrate by silver nitrate test. Wash the funnel and upper edges of the capsule 5-6 times with acetone from a plastic wash bottle. Remove the capsule, close it with a threaded graphite plug, and leave it in a drying oven overnight at 110°C.

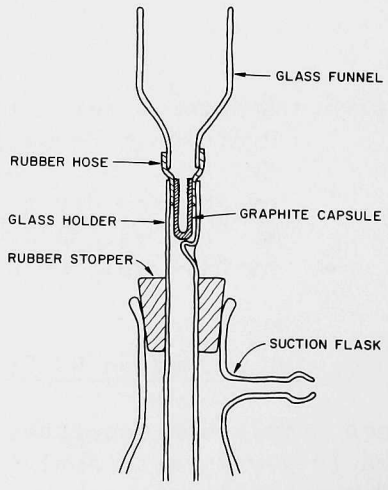

Fig. II-4. Filtration of $BaSO_4$ in Graphite Capsule.

This filtration procedure permits only a small amount of $BaSO_4$ to be lost by passage into the filtrate. The filtration losses were measured on four samples, the average being 0.4 mg SO_4^{2-}.

Although the rate of oxygen isotope exchange between the sulfate ion and water is known to be extremely low at pH 7 and room temperature,[13] the effects of the higher acidity and higher temperatures during the precipitation and digestion procedure were suspected sources of error and therefore were checked on four aliquots of a sulfate solution. The acidity was varied from slightly acid to strongly acid (1.5 ml concd. HCl excess); the temperature treatment was varied from heating to near boiling, with a one-hour digestion on the steambath, to a five-minute boiling period, followed by overnight digestion on the steambath. The isotopic results for the four samples were in excellent agreement (within the error of the mass spectrometric measurements), indicating that high acidity and elevated temperature during the relatively brief precipitation procedure had negligible effects.

4. Conversion of Oxygen in $BaSO_4$ to CO_2

The sulfate sample, in the form of $BaSO_4$ mixed with finely divided graphite in a graphite capsule as described above, was reduced to CO_2 and CO by heating the capsule at ∿1150°C in an inductively heated graphite furnace. The CO was disproportionated to CO_2 and carbon in a high-voltage discharge; then all of the CO_2 was combined, measured, and stored for subsequent mass spectrometric analysis.

A procedure for the conversion of oxygen in $BaSO_4$ to CO_2 by graphite reduction was described by Clayton and Epstein[17] in 1958, and variations of the method have since been used by others.[13, 18-20] Clayton and Epstein,[17] Lloyd,[13] and Longinelli and Craig[18] mixed the $BaSO_4$ with graphite powder by mortar-and-pestle grinding, compressed the mixture into a pellet, and placed the pellet in a graphite crucible for the high-temperature reaction by induction heating. Rafter[19] placed the powdered mixture of $BaSO_4$ and graphite in a platinum boat, and the boat was heated in a quartz tube enclosed in a resistance-wire furnace. Mizutani[20] used a small folded sheet of platinum to function both as the boat for containing the powdered $BaSO_4$-graphite mixture and as the heater, by passing sufficient electrical current through it to raise its temperature to 1000°C.

These methods all entailed the multiple operations of filtering the $BaSO_4$, drying, batchwise mixing with graphite powder, and charging into a suitable container for the thermal conversion to CO_2. The technique described here of cofiltering the graphite powder with the $BaSO_4$ in a graphite capsule combines all of these operations into one.

a. Apparatus. The apparatus used for converting the oxygen in the $BaSO_4$ to CO_2 is shown in Fig. II-5. The main components, connected in a loop arrangement, are the graphite furnace, a high-voltage discharge tube, a cold trap, a Toepler pump, a capillary manometer, gas sample bulbs, and a thermocouple gauge. The Toepler pump was used to circulate gases through the loop. Vacuum (∿5 x 10^{-4} torr) was provided (through a liquid nitrogen cold trap) by a mechanical rotary pump, and purified tank helium was provided for flushing the loop when a sample was being introduced. Four-way stopcocks (labeled 4, 6, 8, and 14 in Fig. II-5) were used to connect or disconnect components or groups of components from the main loop as needed.

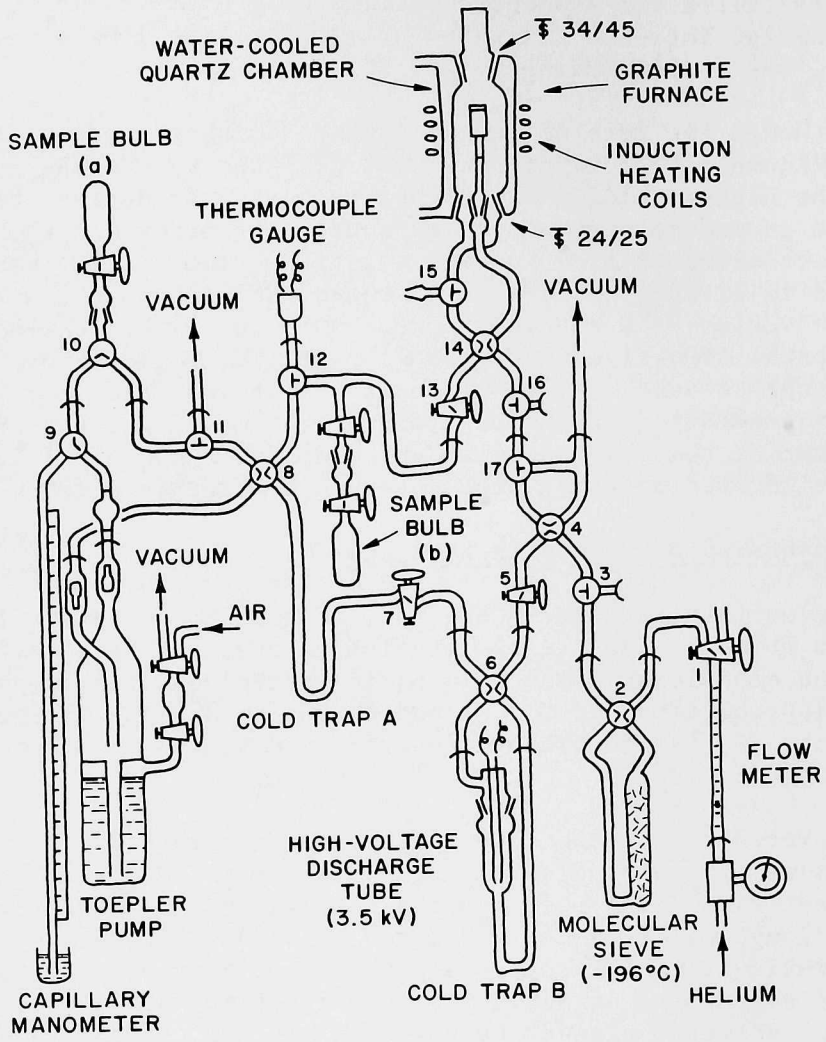

Fig. II-5. Apparatus for Converting Samples to CO_2.

A detail of the crucible assembly in the water-cooled "graphite furnace" is shown in Fig. II-6. The inductively heated graphite crucible was isolated from the silica standard-taper joint holder by a short segment of platinum tubing. The CO and CO_2 produced by the carbon reduction of the $BaSO_4$ diffused through the porous walls of the enclosed graphite capsule into the analytical loop.

The high-voltage discharge tube is shown in Fig. II-7. The platinum plates, 32 mm x 6 mm x 0.25 mm, were spaced about 3 mm apart. The U-tube portion of the chamber served as a cold trap for CO_2.

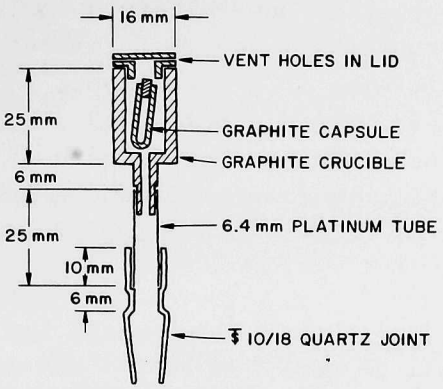

Fig. II-6. Graphite Crucible Assembly.

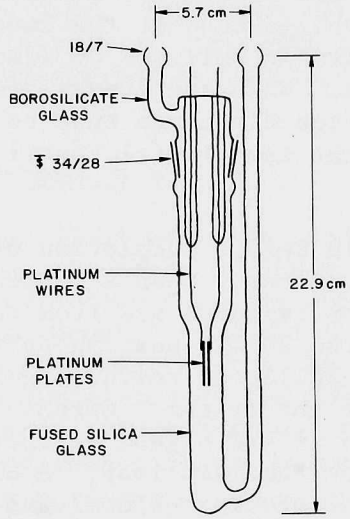

Fig. II-7. High-Voltage Discharge Tube.

b. Procedure. The basic steps of the procedure follow. Arrange the stopcocks and thoroughly outgas all loop components. Close stopcock 17, and allow helium to pressurize the loop (∿50 torr above atmospheric pressure) through stopcocks 4,8, and 14 so that it flows out of the graphite furnace when the 34/45 joint is opened. Open the joint and, with 10-inch tweezers, remove the graphite lid from the crucible, insert a sample capsule, replace the lid, and replace the glass joint. Close stopcock 3 and rotate stopcock 4 one-quarter turn to isolate the loop. Evacuate the loop through stopcock 17, and energize the induction heating coil to heat the crucible to very dull redness (575-600°C). The thermocouple gauge will register a temporary increase in pressure as the sample capsule is outgassed. Maintain this temperature for 5 minutes.

Rotate stopcock 17 one-half turn to isolate the loop from the vacuum manifold. Close stopcocks 7 and 13. Immerse the high-voltage discharge tube (trap B) in liquid nitrogen to a level about 3 cm below the platinum plates. Turn on the high-voltage discharge (∿3.5 kV), and increase the power on the induction heater such that the temperature of the crucible increases to ∿1150°C. As the $BaSO_4$ begins to react with the graphite, CO_2 will begin to condense in the inlet leg of cold trap B and a blue corona discharge of CO will appear at the electrodes.

After heating at this temperature has continued for 10 min, reduction of the $BaSO_4$ will be near completion and most of the CO will be disproportionated in the high-voltage discharge to CO_2 and carbon. Rotate stopcock 6 one-quarter turn and shut off the high voltage. Lower the liquid nitrogen container and increase the trap B temperature to room temperature. (This allows release of appreciable amounts of CO that are cocondensed with the CO_2 in the form of C_2O_3.) Recondense the CO_2 at the bottom of the discharge tube. Raise the level of the liquid nitrogen 3-4 cm, and turn on the high voltage again. A fairly strong blue corona will briefly persist, caused by the released CO. After the corona has subsided, use a gas torch to heat the glass walls of the discharge tube at the level of carbon deposits near the platinum plates. This treatment releases CO adsorbed by the activated carbon deposits on the inner walls. When the corona discharge resulting from this operation subsides, reopen the discharge tube to the main loop by rotating stopcock 6. Continue to heat the crucible until a total heating period of 20 min has elapsed.

About 3-5 min before completion of the 20-min heating period, rotate stopcock 8 one-quarter turn, open stopcock 7, and start the Toepler pump in order to collect the residual gas from the loop in the capillary manometer. At the end of the 20-min heating period, rotate stopcock 14 one-quarter turn. Measure the collected residual gas (usually ∿3-4 μmoles) as a check on the performance of the system. Circulate the residual gas through the high-voltage tube again at the higher pressure that is allowed by exclusion of the graphite furnace from the main loop. A blue corona may briefly appear again, and, on re-collection of the residual gas in the capillary manometer, the amount may be typically reduced to about 1 μmole. Close stopcock 13, and discard the residual gas to the vacuum manifold through stopcock 11. Turn off the high voltage.

Place dry ice-acetone coolant on cold trap A, remove the liquid nitrogen from trap B, and turn on the Toepler pump to transfer the CO_2 through the dry-ice cold trap to the capillary manometer for measurement. Using liquid nitrogen, cryogenically transfer the measured CO_2 to sample bulb (b) for storage for subsequent mass spectrometric analysis. (Sample bulb (a) is provided for occasional sampling of noncondensible gases in other analyses.)

In preparation for the next sample, another sample bulb is attached for outgassing, and the high-voltage discharge unit is removed for minimal cleaning and is then replaced for degassing. The discharge unit is removed by rotating stopcock 6 one-quarter turn and detaching at the 18/7 ball joints beneath the stopcock. Remove the electrode assembly from the unit at the 34/38 joint. With a hand torch, flame the platinum electrodes to redness to burn off the carbon deposit. Reassemble the unit, reattach at the ball

joints, and reevacuate through stopcock 6. Flame the quartz chamber with the hand torch to thoroughly outgas the carbon deposits on the inner walls. (When the carbon deposit accumulates to a heavy film, the quartz chamber should be cleaned with a 10% solution of nitric acid containing a few drops of hydrofluoric acid.)

c. Blanks. For three graphite capsules that were carried through the filtration procedure (with the addition of 50 mg of graphite powder) and the carbon-reduction procedure, the average CO_2 blank was 0.8 ± 0.4 μmoles CO_2, equivalent to about 0.04 mg SO_4^{2-}.

d. Recoveries. It was important that the procedure should allow quantitative conversion of oxygen in $BaSO_4$ to CO_2 in order to avoid isotope fractionation. Recoveries for the combined precipitation, filtration, and carbon-reduction procedures were determined by analyzing four aliquots of a solution of known sulfate concentration. (The solution was assayed for sulfate by a conventional gravimetric procedure.) After filtration-loss corrections of 0.9 mg $BaSO_4$ were made for each sample, the four aliquots, each containing 4.46 mg SO_4, averaged 99 ± 2% recovery.

e. Interference by SiO_2. SiO_2 does not interfere. A test was made by pulverizing a few milligrams of SiO_2 with graphite powder and heating in a graphite capsule by the prescribed procedure. The CO_2 yield did not exceed the blank.

5. Conversion of the Oxygen in SO_2 to CO_2

The vacuum loop (Fig. II-5) was also used for converting the oxygen in SO_2 to CO_2 for ^{18}O analysis. A sample of about 2 ml (STP) of SO_2 was transferred cryogenically to cold trap A of the evacuated loop through stopcock 3. The loop was isolated at stopcock 4, and the SO_2 was Toepler-pumped into the capillary manometer for measurement. With the empty graphite crucible heated to 1300°C, the gas was circulated by the Toepler pump through the entire loop for 20 min to quantitatively reduce the SO_2 to CO. A remeasurement in the manometer at this time confirmed that the quantity of gas had doubled. The high-voltage conversion of CO to CO_2 was made by the procedure used in the $BaSO_4$ analysis. The average recovery of CO_2 from seven measured SO_2 samples was 99 ± 1%.

The elemental sulfur produced by the carbon reduction of SO_2 was deposited as a film on the water-cooled walls of the graphite furnace. Although the accumulation of the sulfur film appeared to have no deleterious effect on subsequent use of the equipment, the quartz chamber was cleaned and the graphite crucible was replaced before the furnace was used for other types of samples (i.e., O_2, H_2O, and $BaSO_4$).

6. Conversion of O_2 in Air to CO_2

Tank oxygen was quantitatively converted to CO_2 by the same procedure as was used for SO_2. This procedure was not applicable to oxygen in air, however, because of interference by nitrogen in the formation of nitrogen oxides by the high voltage discharge. For determining oxygen in air, it was necessary to operate at a lower graphite temperature in the presence of platinum catalyst to quantitatively convert the air oxygen directly to CO_2

without the formation of CO. A technique used by Horibe *et al.*[21] was adapted to our equipment. The graphite crucible was covered with platinum gauze and operated at ∿800°C. As the sample was circulated through the loop for 20 min, the CO_2 was collected in cold trap B at -196°C with no high voltage on the electrodes. Mass spectrometric analysis of the residual gas from each of three such conversions showed the composition to be 96.8% N_2, 1.2% Ar, ≤2.0% CO (difficult to determine in excess N_2 by mass spectrometry), <0.01% O_2 and <0.005% CO_2. The necessity of covering the graphite crucible with platinum gauze was demonstrated by operating at 800°C without the platinum; the residual gas then contained about 20% CO.

7. Conversion of Oxygen in H_2O to CO_2

The most commonly used method of preparing a CO_2 sample for determining the oxygen isotope composition of water by mass spectrometric analysis is to equilibrate a measured quantity of degassed water with a measured quantity of CO_2 of known isotopic composition. The equilibration is carried out by frequently shaking the water in contact with the CO_2 for about three days at a constant temperature. An isotope separation factor for that temperature is then applied, and a mass spectrometric comparison of the $^{18}O/^{16}O$ ratios in the CO_2 before and after equilibration allows the isotopic composition of the water oxygen to be calculated.[22]

Majzoub[23] developed a method for converting all of the oxygen in microquantities of water to CO_2 for mass spectrometric analysis. The method consists of hot graphite reduction of the water to CO and H_2, separation of the H_2 from the CO through a palladium membrane, and conversion of the CO to CO_2 and carbon on a nickel catalyst. This carbon-reduction method of preparing water samples for mass spectrometric analysis appeared to be more attractive than the CO_2-H_2O equilibration method for the following reasons: (1) The technique is very similar to that already in use for the analysis of $BaSO_4$, SO_2, and O_2 and therefore could be done on the same apparatus with some modifications. (2) Only microquantities of water samples are required; this could be advantageous when dealing with atmospheric water-vapor water. (3) The long (three-day) equilibration requirement would be avoided. After modification to accommodate the method, our apparatus differed from Majzoub's apparatus in design and operation, but not in the principle of operation.

a. Apparatus. The graphite furnace unit of our basic apparatus (Fig. II-5) was modified for water analysis, as shown in Fig. II-8. A palladium-tube assembly was added at the 34/45 joint and connected to the main loop through stopcock 16. The cooling water for the quartz chamber of the graphite furnace was confined to a closed system so that it was maintained at boiling-water temperature during furnace operation. (Apiezon H stopcock grease was used in the heated standard-taper joints.) The palladium tube was maintained at 400°C by a heater tape covering the exterior walls of the palladium-valve unit. The stopcock assembly (stopcocks 13-16) was also maintained at ∿100°C by a heater tape. A water sampler unit was attached, the use of which is described below.

The only change necessary to reconvert the apparatus to use for a $BaSO_4$ analysis after a water analysis is to substitute the closed-end 34/45 joint (Fig. II-5) for the palladium tube unit at the top of the furnace.

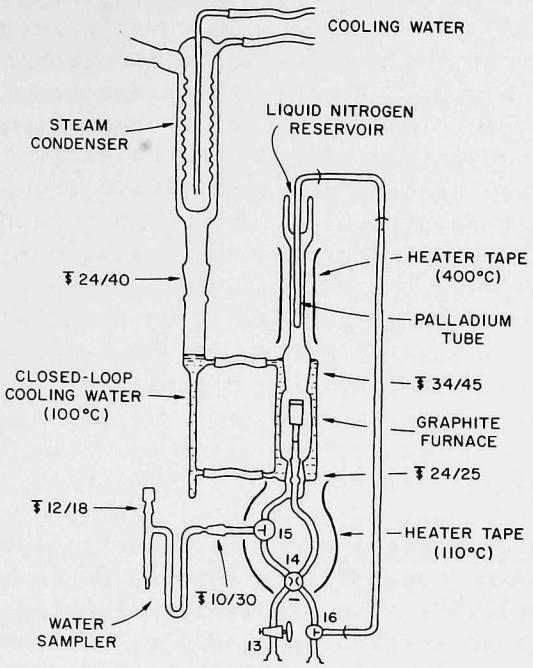

Fig. II-8. Apparatus for Graphite Reduction of H_2O.

b. Procedure. After thorough outgassing of the system, manipulate the stopcocks to allow dried helium to flow out of the water sampler when the 12/18 joint on the sampler is opened. With helium flowing out, deposit a 2-μℓ sample of water from a micropipet into the lower end of the sampler tube. Emplace the 12/18 cap, close stopcock 3, and rotate stopcock 4 one-quarter turn. Immerse both the sampling tube and the adjacent U-tube in liquid nitrogen. Evacuate the entire system through stopcock 17 to $\sim 5 \times 10^{-4}$ torr. Rotate stopcock 14 one-quarter turn to isolate the graphite-furnace loop from the main loop.

To transfer the water sample from the sampler to the furnace loop, fill the reservoir on the palladium tube unit with liquid nitrogen, and remove the liquid nitrogen from the water sampler. Allow for complete cryogenic transfer of the water sample, and rotate stopcock 15 one-half turn. With the palladium tube connected to the vacuum system through stopcock 16, energize the induction heating coil to heat the graphite crucible to ∿1150°C for 20 min. The water vapor, confined to the heated furnace loop, ≥100°C, is converted to H_2 (which diffuses through the palladium wall at 400°C) and CO (which is retained).

Rotate stopcock 17 one-half turn to isolate the evacuated main loop. Rotate stopcock 16 one-half turn, and close stopcocks 5, 7, and 13. Immerse cold trap B in liquid nitrogen, as in the procedure for $BaSO_4$ analysis, and turn on the high voltage. Rotate stopcock 14 one-quarter turn, and slowly open grooved stopcock 5 to throttle the flow of CO into the discharge unit. Carry out the conversion of CO to CO_2 and subsequent operations as in the $BaSO_4$ procedure.

c. Fractionation and Memory Effects. Two potential sources of error in the isotopic analysis of oxygen in water are (1) fractionation of the isotopes by loss of part of the samples through evaporation and (2) interference by residual microscopic amounts of water that remain on inner surfaces of the system from previous samples (memory effect). Provisions to avoid fractionation by evaporation during sample introduction to the apparatus were (1) deposition of the sample on a surface that is not directly in the purge stream of helium (used to avoid contamination by ambient water vapor in the room atmosphere), and (2) evacuation of the sample through the U-tube cold trap. Memory effects were minimized by maintaining the entire furnace loop at or above 100°C during the conversion of H_2O to CO and H_2. Also, when a run was preceded by a run with a sample differing by several parts per thousand in isotope ratio, the apparatus was conditioned by interposing a preliminary run and discarding the CO produced in that run.

8. Field Sampling

a. Atmospheric Sulfate Aerosols. Particulate matter from the atmosphere was collected on paper filter sheets, 20 cm x 25 cm, in a Misco Hi-Vol air sampler, Model 260. The sampler was located about six meters above ground level at the Argonne meteorology station, well away from any point sources of sulfate or SO_2. Sampling periods varied from one-day to three-day duration, and flow rates were 40-80 m^3/hr.

After collection of the sample, the sheet of filter paper was divided into quarters, one or two quarters being taken for analysis and the others reserved for rechecks or future reference. A 1/4-sheet aliquot was leached in 50 ml water, acidified with 1 ml concd. HCl, heated to boiling, and filtered through Whatman No. 42 filter paper. The filtrate was reserved for $BaSO_4$ precipitation and analysis, as described above.

Sulfate blanks were determined for three grades of filter paper. The amount of sulfate per sheet was 2.2 mg for Schleider & Schnell Grade 25, 0.7 mg for Whatman No. 1, and 0.3 mg for Gleman Spectro Grade, Type A.

b. Atmospheric SO_2. There appears to be no feasible way of collecting from the atmosphere a sample of SO_2 that is suitable for oxygen isotope analysis, without converting the SO_2 to some other chemical form in the process. For example, if SO_2 is collected cryogenically, it is obtained as sulfurous acid, sulfites, or sulfates, depending on the other condensible atmospheric gases and vapors cocondensed with the SO_2. Likewise, if the SO_2 is adsorbed on an active surface or if it is absorbed in an alkaline solution or on a moist filter impregnated with an alkaline reagent, it is not retrievable as SO_2; rather, it is combined and influenced isotopically by its collection environment.

To determine the isotopic composition of atmospheric SO_2, it is therefore necessary to collect it in some well-defined chemical form and to know precisely what chemical and isotopic changes occur during collection and during subsequent conversion to sulfate before analysis by the methods described above. A method of collection should provide a product that can be reproducibly characterized and should be capable of quantitatively collecting milligram quantities of SO_2 at ppb concentrations from the atmosphere. Incomplete collection would tend to result in fractionation errors in the isotopic data.

The method that we adopted was to collect the SO_2 on filter paper impregnated with KOH and glycerol according to the recommendations of Huygen.[24] The filter holder of the Misco Hi-Vol air sampler was modified to accommodate two 20 cm x 25 cm filter sheets, mounted in series and separated by appropriate stainless steel screens. An inert, glass-fiber paper filter (Gelman Spectro Grade, Type A) was placed in the upper position and an alkaline-treated, cellulose paper filter (Whatman No. 1) in the bottom position. Thus, the upper filter collected SO_2-free sulfate aerosols; concurrently, the lower filter collected sulfate-free SO_2. The SO_2 collection filter was prepared by soaking the paper in a 20% KOH-10% glycerol-water solution, squeezing out the excess liquid with a rubber roller on a flat surface, and drying for about 20 min in an oven at 110°C.

It became evident during the early part of the investigation that under the conditions of sampling SO_2 by this procedure and of subsequent storage for analysis, the oxidation state of the sulfur on the SO_2-collection filter paper changed progressively from sulfite to sulfate. Huygen[24] had determined that absorbed sulfite on the paper was stable with respect to oxidation for many days if kept dry. Our sampling conditions, however, frequently involved high humidities. The method used to check the oxidation state of the sulfur on the alkaline filter paper was the ASTM Method C for testing sulfite ion concentration in water.[25]

In preparation for the ^{18}O analysis, a measured fraction of the exposed alkaline filter paper was leached with water, to which 2-3 drops of liquid bromine were added to ensure complete oxidation. The pH of the solution was adjusted with HCl (diluted with an equal volume of water) to near neutral but slightly basic, and the solution was heated to boiling and filtered into a 100-ml volumetric flask. Heating the solution while it was strongly basic was avoided because oxygen isotope exchange between sulfate and water is enhanced under such conditions.

c. Water Vapor. The isotopic composition of oxygen in atmospheric water vapor varies seasonally and with prevailing weather conditions. Such variations were indicated in the data of Cortecci and Longinelli[26] who compared oxygen isotope ratios between H_2O and SO_4^{2-} in rainwater collected in Pisa, Italy. Generally, atmospheric water is enriched in the lighter oxygen isotope as it moves from the tropic regions toward the poles. Since the isotopic composition of water vapor in the atmosphere varies, a study of sulfate formation in the atmosphere from SO_2, water vapor, and oxygen necessarily requires concurrent sampling of water vapor, SO_2, and sulfate aerosols.

The apparatus used for sampling atmospheric water vapor consisted of a glass cold trap (cooled with dry ice) and a small diaphragm pump to draw the air through the trap at about 8 ℓ/min. Essentially all of the water vapor in the air sample was collected in the first few centimeters of a cold path of 40-50 cm in the trap. This provided quantitative removal and avoided isotope fractionation.

The amount of water collected varied (5-70 ml/day), depending on temperature, relative humidity, and flow rate. Very little water-vapor water was needed for the isotope analysis (2 μℓ per sample), but the larger quantities were collected for some experiments (to be described later) in which the SO_2 filter papers were leached with ambient water-vapor water.

d. Rain and Snow. Snow samples were gathered from "clean" ground areas, away from buildings and roadways, on the Argonne site during the winter months of 1974-75. Rain was collected through a shallow funnel (1 m x 1.5 m) fabricated from plastic sheeting and attached to a metal frame atop an automobile. The automobile was parked in open areas, away from buildings and trees. Some of the rain samples were collected at Argonne and some at Hinsdale, Illinois, 16 km northeast of Argonne.

For the isotopic analysis of dissolved sulfate, two liters of each sample of precipitation were evaporated to ∿75 ml, filtered through Whatman No. 42 paper, and diluted to 100 ml in a volumetric flask. A few milliliters of each original water sample was also reserved for isotopic analysis of the H_2O oxygen.

e. Dust. To ascertain the oxygen isotope variations in the sulfates of dust that settles out on the ground, a monthly sample of dust was collected according to a standard ASTM method.[27] An open-topped cylinder (15 cm diam by 30 cm high), half filled with antifreeze solution (40% isopropyl alcohol in water) in winter months and distilled water containing ∿60 mg $CuCl_2 \cdot 2H_2O$ (bactericide) in summer months, was mounted ∿2.5 m above ground level in an open field away from buildings and roadways. Each sample was collected over a period of one month. The sample solution was then filtered through Whatman No. 42, and made to volume in a 100-ml volumetric flask.

9. Mass Spectrometric Analysis

Oxygen isotope data are expressed in del units (‰) which are parts per thousand deviation of the $^{18}O/^{16}O$ ratio from that of a standard. The commonly accepted standard is SMOW (Standard Mean Ocean Water) obtainable from the International Atomic Energy Agency, Vienna, Austria. We obtained some of the SMOW reference water, converted it to CO_2 by the procedure described above, and compared it mass spectrometrically with a supply of tank CO_2. The tank CO_2 was then used as a secondary standard for the analysis of samples. Its del value with respect to SMOW was $\delta^{18}O_{SMOW} = 20.2 \pm 0.3‰$ for five analyses.

The mass spectrometer was a Nier-type, double-beam, isotope-ratio instrument designed for gas analysis. In the analysis, the standard CO_2 and sample CO_2 flow continuously, each through a capillary leak into the instrument. They are alternately sampled several times by an automatic switching arrangement. The electronic components have been modernized,[28] and the precision for ^{18}O analysis is $\pm 0.2‰$.

B. Results and Discussion (B. D. Holt)

1. Laboratory Preparations of Sulfates

Figure II-9 shows the results obtained on sulfates prepared in the laboratory by both the hydrolysis-oxidation and the oxidation-hydrolysis

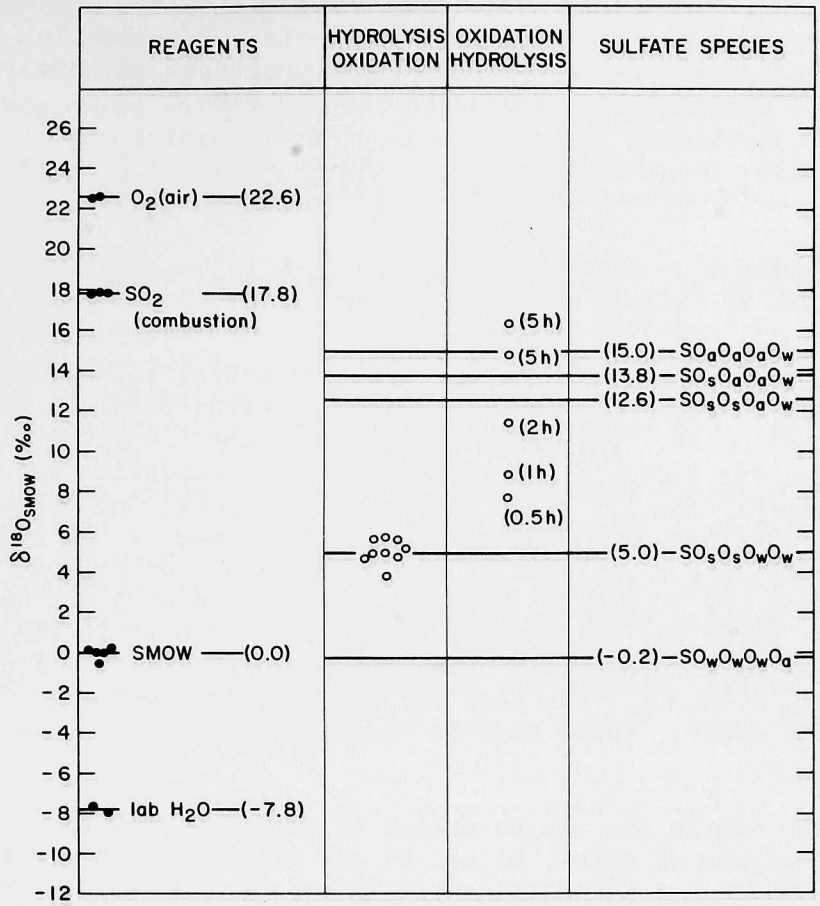

Fig. II-9. Isotopic Composition of Oxygen in Sulfate from Hydrolysis-Oxidation and Oxidation-Hydrolysis Preparations.

procedures. The left-hand column shows the del values,* with respect to SMOW, of the reagents used to prepare the sulfates. The reagents were air, at 22.6‰; SO_2 (prepared in the laboratory by combusting sulfur in air) at 17.8‰; and laboratory distilled water at -7.8‰. Experimental values are plotted as points and the mean values as horizontal lines. The value for air is lower than the generally accepted value of about 23.5‰; although it is expected that this discrepancy will soon be resolved by special attention to its cause, the precise value for air is not essential to the comparative analyses that follow.

---

*A del value is the deviation of the $^{18}O/^{16}O$ ratio of a sample from that of a standard in units of parts per thousand (‰).

$$\delta^{18}O_{std} = \frac{\left(^{18}O/^{16}O\right)_{sample} - \left(^{18}O/^{16}O\right)_{std}}{\left(^{18}O/^{16}O\right)_{std}} \cdot 1000$$

The right-hand column shows the sulfate species that can conceivably be produced by the reagents of known ^{18}O contents. For example, if $SO_sO_sO_aO_w^{2-}$ is produced as described in the introductory paragraphs of this section, the del value should be 12.6‰ according to the equation,

$$\delta^{18}O_{SMOW}(‰) = \frac{2O_s + O_a + O_w}{4} = \frac{2(17.8) + 22.6 - 7.8}{4} = 12.6 \qquad (3)$$

where O_s, O_a, and O_w are the respective del values of the reagent SO_2, air, and water.

The two middle columns show the experimental values obtained for the products. The del values of the hydrolysis-oxidation products matched that of the $SO_sO_sO_wO_w^{2-}$ molecule. They were all close to the 5.0‰ level, although the time allowed for isotopic equilibration before oxidation was varied for some of the samples from 1.5 hr to 4 days. Also, small amounts of catalyst (1 μg to 1 mg $FeCl_3 \cdot 6H_2O$ per sample) were used in some of the hydrolysis-oxidation preparations of sulfate to speed up the air oxidation. The same product (matching the $SO_sO_sO_wO_w^{2-}$ molecule) was formed when SO_2 absorbed in alkaline excess water was oxidized by bromine. Not shown in Fig. II-9 are two other sets of data for hydrolysis-oxidation preparations; a different SO_2 supply ($\delta^{18}O_{SMOW}$ = 10.3‰) was used for one, and snow water ($\delta^{18}O_{SMOW}$ = -15.6‰) was used for the other. These results also correspond well with the $SO_sO_sO_wO_w^{2-}$ ion.

The mechanism for the formation of $SO_sO_sO_wO_w^{2-}$ by the oxidation of SO_2 in a large excess of water, either by air oxidation (in the presence of a catalyst) or by bromine, was not identified by our limited observations. Its formation would require that the two original oxygen atoms of the SO_2 were retained by the sulfur, without appreciable exchange with water, and that the two oxygen atoms incorporated by hydrolysis and oxidation were both supplied by the water medium. A test was made for hydrogen that might be produced during the equilibration of SO_2 and water in a sealed air-free container. After equilibration, the container was opened and degassed in a vacuum system, but no hydrogen was detected.

The sulfate formed by the oxidation-hydrolysis procedure, described in the Experimental section above, varied in ^{18}O enrichment, mainly with time of exposure to the Tesla discharge. The exposure times are noted in parentheses with each del value in Fig. II-9. The higher 5-hr value was for a sample that was flamed occasionally to decompose (or distill) the white condensate that formed on the walls of the vessel near the platinum electrodes. Presumably, for those samples with del values above the expected product of $SO_sO_sO_wO_w^{2-}$, the condensates may have contained extra air oxygen (22.6‰) by polysulfur peroxide formation.[15] Oxides of nitrogen (from the air) may also have been involved in the oxidation process.

Not shown in Fig. II-9 are the results of an experiment performed to try to enrich ^{18}O in the sulfate by carrying out the Tesla-discharge reaction between SO_2 and pure O_2 in a sealed, isothermally heated chamber at 120°C (well above the decomposition temperature of the condensates). The ^{18}O enrichment was surprisingly small, indicating the enrichment may occur more by incorporation of air oxygen into condensed phases or by interaction with oxides of nitrogen than by isotopic exchange between SO_2 and O_2.

2. Analysis of Field Samples

Sulfate aerosol samples and water vapor samples were collected during each month, beginning in July 1974, by the methods described above. Collections of SO_2 samples, precipitation (snow and rain), and sedimentary dust were also started in 1974. Analytical results for many of these samples, collected up to about February 1975, are shown in Fig. II-10.

The del values for sulfate aerosol samples collected on the inert filter paper of the Misco Hi-Vol air sampler are plotted in Fig. II-10 and joined by a line labeled "SO_4." Several samples collected in August, September, and October have not yet been analyzed. The ^{18}O data obtained from the sulfate samples formed by collection of SO_2 on filter papers treated with KOH (or K_2CO_3) and glycerol are also plotted as connected points and are labeled "K."

It may be noted that the ^{18}O del values of sulfates in dust and atmospheric precipitation are generally within the range of $11 \pm 4‰$, which coincides with the average Hi-Vol sulfate values. The ^{18}O in the water of atmospheric precipitation is also within the general range of the water vapor samples, although the limited amount of data at hand indicate that the precipitation water may be somewhat richer in ^{18}O than is the water vapor. This may be because of the higher vapor pressure of the lighter isotope.

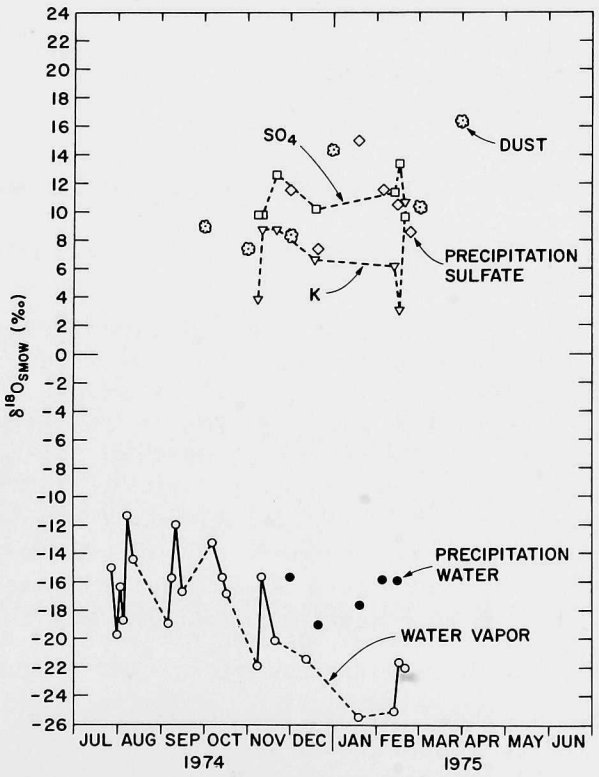

Fig. II-10. Analytical Results for Field Samples.

Hi-Vol air samples and simultaneous water vapor samples were usually collected in sets of three consecutive 3-day runs. These sets are connected with solid lines. The water-vapor data varied considerably from sample to sample, with an apparent summer-to-winter seasonal trend toward depletion of the heavier isotope. A corresponding trend is not clearly indicated by the limited amount of Hi-Vol data.

The del values for atmospheric SO_2 are not shown as measured data on Fig. II-10. They are calculated from the "K" data and therefore depend upon the isotopic composition assumed for the sulfate formed from the SO_2 collected on the treated paper. In the following discussion, three different assumed isotopic compositions are considered for the calculation.

It was observed from the laboratory preparations of sulfate by hydrolysis-oxidation procedures that a product having a del value approximating that of $SO_sO_sO_wO_w^{2-}$ was consistently formed when SO_2 was dissolved in an alkaline solution containing a large excess of water, and then oxidized (1) by bromine or (2) by air in the presence of a catalyst. It could be assumed that equivalent conditions prevailed on the procedure used for the collection of SO_2 on alkaline filter papers. That is, according to the procedure, the potassium sulfite formed on the dry filter paper was leached in several milliliters of water-vapor water which was collected concurrently with the sulfite. The hydrolyzed sample was then oxidized with bromine in the excess water-vapor water. The sulfate product, K, could be assumed to consist of two oxygens from the SO_2 and two oxygens from the ambient water-vapor water in which it was dissolved.

$$K = SO_sO_sO_wO_w^{2-} = \frac{2\,O_s + 2\,O_w}{4} \qquad (4)$$

The del value for atmospheric SO_2, $O_s = \delta^{18}O_{SMOW}(SO_2)$ could then be calculated:

$$O_s = 2K - O_w \qquad (5)$$

A problem with assuming that the K values correspond to the $SO_sO_sO_wO_w^{2-}$ molecule is that the calculated del values for SO_2 were extremely high, varying from 28 to 43‰, as compared with 23‰ for air oxygen. A plausible mechanism for the production of such highly enriched SO_2 in the atmosphere is not readily apparent. As mentioned in the Experimental section, attempts were made to produce highly enriched SO_2 by heating normal SO_2 at 120°C with pure oxygen in sealed glass tube, through which a Tesla-coil spark discharge was passed for 5 hr. The ^{18}O del values for the products of two runs were only 1‰ and 4‰ above the level obtained for untreated SO_2. Any processes of exchange or fractionation reactions that may have occurred between the SO_2 and O_2 produced very little enrichment.

Based on the high del values calculated for SO_2, the corresponding levels for various sulfate compositions are plotted in Fig. II-11 for comparison with the measured sulfate aerosol values. The SO_4 aerosol data appear between the levels of $SO_sO_sO_wO_w^{2-}$ and $SO_sO_sO_wO_a^{2-}$, and approximately coincide with $SO_aO_aO_wO_a^{2-}$.

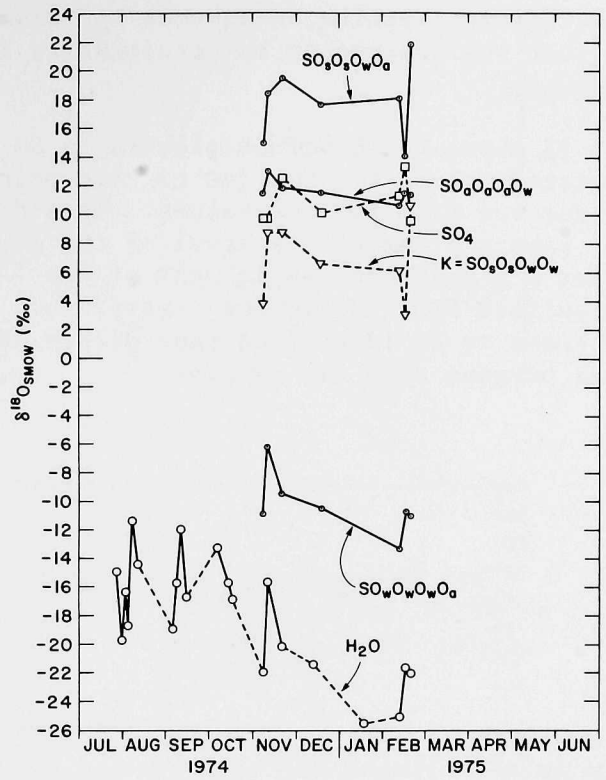

Fig. II-11. Relative ^{18}O Enrichment of Various Sulfur Compounds Assuming Molecule K to be $SO_sO_sO_wO_w^{2-}$.

Another objection to the assumption that the K values correspond to the $SO_sO_sO_wO_w^{2-}$ form became evident when sulfite analyses were performed on the exposed KOH-glycerol filter papers. The analyses revealed that the absorbed SO_2 did not quantitatively remain as sulfite on the filter paper prior to dissolution in ambient water-vapor water and to oxidation to sulfate by bromine in the excess water. Instead, in the presence of only molecular-film amounts of ambient water, large fractions (>50%) of the sulfite were oxidized to sulfate while still in the Hi-Vol sampler. Under these conditions, the sulfate molecule that might be reasonably expected is $SO_sO_sO_wO_a^{2-}$, where the oxidizing oxygen comes directly from the air rather than from the water solvent.

It was further observed from the measurements of sulfite on the treated filter papers that oxidation continued to proceed toward completion during storage in plastic bags prior to analysis and that the rate of oxidation varied from one sample to another. Some samples were found to be completely oxidized to sulfate after one day of storage, whereas others had appreciable sulfite remaining after 2 or 3 weeks.

When it was recognized that the sulfite on the SO_2-collection filter papers was being extensively oxidized, even while still in the Hi-Vol sampler, the procedure was revised to allow for complete oxidaiton of the sulfite to

sulfate on the paper before leaching in aqueous solution for $BaSO_4$ precipitation. The product that was assumed to be consistently formed under these conditions was $SO_sO_sO_wO_a^{2-}$.

Figure II-12 shows the K values plotted as $SO_sO_sO_wO_a^{2-}$, with the corresponding calculated values for SO_2 (as circled points) and for other sulfate molecules, derived from the SO_2 values. This display uniquely places the sulfate aerosol sample at about the level of the $SO_aO_aO_wO_a^{2-}$ molecule. This might imply that a significant enrichment of the ^{18}O occurs during the process of forming sulfate from SO_2 in the atmosphere. If such a process does occur, a mechanism needs to be identified that allows the sulfur to replace both of its original oxygens with air oxygens.

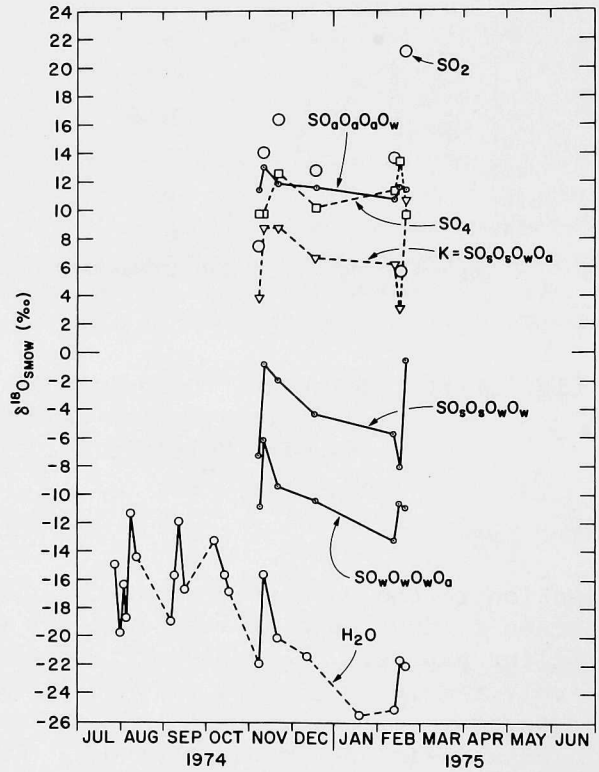

Fig. II-12. Plot of Calculated Data, Assuming K Values are for the Molecule $SO_sO_sO_wO_a^{2-}$.

A spike run was made in the field for experimental identification of the sulfate molecule formed on the unleached alkaline-treated filter paper. As illustrated in Fig. II-13, the intake of the Hi-Vol air sampler was connected to a 4-m length of plasticized fabric hose (75-mm dia), and SO_2 of known ^{18}O composition was slowly ($\sim$1 ml/min) injected from a syringe into the air stream, flowing at $\sim$1/3 m^3/min. After the SO_2 was collected on the KOH-glycerol-treated filter (in the lower position of the filter holder), the sampler was left to operate normally for 24 hours with an alkaline-treated filter in the

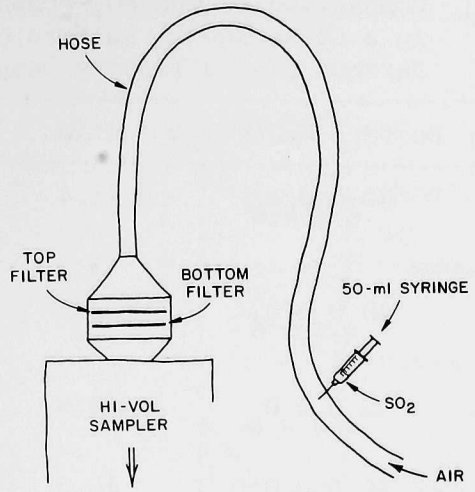

Fig. II-13. Arrangement for Adding SO_2 Spike to Hi-Vol Air Sampler.

top position of the holder to protect the spike sample from ambient SO_2 and sulfate aerosols. Ambient water vapor was sampled during the 24-hr exposure of the spike sample in the Hi-Vol sampler.

Although about two-thirds of the sulfite on the alkaline-treated filter of the spike was oxidized at the end of 24 hr in the Hi-Vol sampler, the completion of oxidation during storage was very slow. Even after 7 days in a covered dish maintained at 75% relative humidity with the sampled water-vapor water, oxidation was only about 80% complete. Since the oxidation of field samples was normally complete after 2-3 days, it was concluded that oxidation of the field samples was catalyzed by some atmospheric pollutants (O_3, NO_2, etc.) that passed through the inert filter, whereas the spike sample was protected from such pollutants by the alkaline-treated top filter that stripped out the ambient SO_2. To speed completion of oxidation of the sulfite in the spike sample, the alkaline-treated paper was finally exposed to some ozone generated in the storage container with a Tesla spark coil.

In Table II-1, the isotope results of the sulfate produced from the SO_2 spike are compared with sulfate molecules of various isotopic compositions that conceivably might be formed from the reagents, SO_2, water, and air. Included in the list is the $SO_sO_sO_wO_aO_a^{2-}$ molecule, which might be considered an unstable intermediate that could exist on a surface sufficiently long for isotopic equilibration to occur. By a mechanism of the type described by Novakov *et al.*,[29,30] the SO_2 and H_2O might be considered to coadsorb on an active surface and to form a surface sulfite (stabilized by the alkaline substrate). Air oxygen might be considered to combine with the adsorbed sulfite to form the intermediate molecule before decomposing to the stable sulfate. If fractionation effects are ignored, the sulfate product, SO_4^{2-}, would have the same isotopic composition as the SO_5^{2-} intermediate.

Table II-1. Comparison of the SO_2-Produced Sulfate in a Spike Run to Sulfate Molecules of Various Oxygen Isotope Compositions.

Reagents	$\delta^{18}O$	Sulfate Molecules	$\delta^{18}O$	SO_2 Spike	$\delta^{18}O$
SO_2	10.3	$SO_s O_s O_w O_w$	-1.4	Sulfate Product	10.7 10.8
H_2O (ambient)	-13.1 -13.0	$SO_s O_s O_w O_a$	7.5		
Air	22.6	$SO_a O_a O_w O_a$	13.6		
		$SO_s O_s O_w O_a O_a$	10.5		
		$SO_a O_a O_w O_a O_a$	15.5		

The results of the spiking experiment (Table II-1), which it is planned to repeat for substantiation, indicate that the SO_2-produced sulfate on the Hi-Vol alkaline-treated filter matches the $SO_s O_s O_w O_a O_a^{2-}$ form. The alkaline-filter sulfates (designated as K) for the field samples are assigned this composition in Fig. II-14; the calculated SO_2 values are again plotted as circled points. Also, the calculated levels for the various sulfate compositions are again shown to allow comparison with the ambient sulfate aerosol samples.

The ambient sulfate aerosols appear to be bracketed by the levels of the assigned $SO_s O_s O_w O_a O_a^{2-}$ and the calculated $SO_a O_a O_w O_a O_a^{2-}$ forms, the latter being a possible intermediate for atmospheric-oxidized H_2S. The concept that these two SO_5^{2-} molecules may generally constitute the upper and lower limits of the ambient sulfate aerosol (also having been formed as SO_5^{2-} on active sites of a surface) may be more defensible than the previous idea that the ambient aerosols are generally of the composition $SO_a O_a O_w O_a$.

A practical use of this concept may be in estimating the relative amounts of sulfate aerosols that come from H_2S and SO_2 emissions in a given area, providing that it can be shown that simultaneous homogeneous oxidation-hydrolysis formations of sulfate are relatively unimportant.

Another interesting aspect of the calculated data shown in Fig. II-14 is the apparently drastic variation in the ^{18}O content of ambient SO_2. If this is real, rather than caused by some artifact of the technique, the ^{18}O analysis may be useful in identifying SO_2 that originates from point sources. For example, in the data presented in Fig. II-14, the two very low del values for SO_2 were obtained when the wind was, at least part of the time, from the southwest (the direction of a major fossil fuel power plant and some oil refineries). None of the other samples was collected with a southwest component in the wind direction. If it should be confirmed by more direct measurements that the SO_2 emitted from the power plant is very low in ^{18}O in comparison with

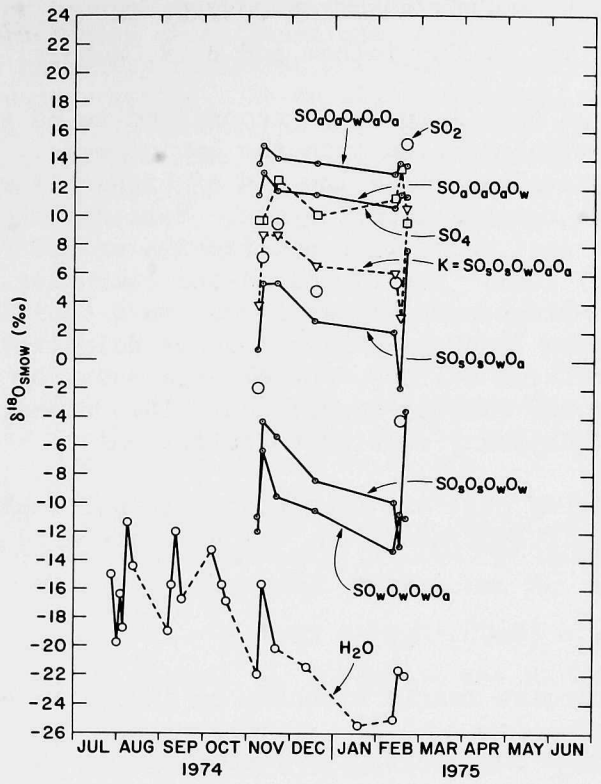

Fig. II-14. Plot of Calculated Data, Assuming K Values are for the Molecule $SO_sO_sO_wO_aO_a^{2-}$.

air oxygen, the reason for the low ^{18}O may be that appreciable amounts of oxygen originally associated with water (as well as from air) are combined with sulfur in the power plant furnaces.

III. SULFUR EMISSION CONTROL CHEMISTRY*

(P. T. Cunningham and B. R. Hubble)

The combustion of fossil fuels is recognized to be a major source of sulfur dioxide pollution emission into the environment. Many processes currently are being developed to allow use of high-sulfur-containing fossil fuels in an environmentally acceptable way. Most approaches involve the use of reagent materials that react with and fix SO_2 or H_2S formed from the combustion of the fossil fuel. The fluidized-bed combustor, one such process under development, employs combustion of coal in a fluidized bed containing a sulfur-fixing reagent (such as a limestone or dolomite) that reacts with the SO_2 to produce calcium sulfate. Other processes for SO_2 control such as panel bed filters employ similar approaches. This report presents results on the study of the chemistry related to sulfur emission control.

The sorbent reagent that has received principal emphasis in this program is dolomite in the half-calcined form, which is prepared as indicated by Eq. (6):

$$CaMg(CO_3)_2 \rightarrow [CaCO_3 \cdot MgO] + CO_2 \qquad (6)$$

The half-calcined dolomite reacts with SO_2 as indicated by Eq. (7):

$$[CaCO_3 \cdot MgO] + SO_2 + 0.5\ O_2 \rightarrow [CaSO_4 \cdot MgO] + CO_2 \qquad (7)$$

For obvious economic and environmental reasons, it is desirable to regenerate the reactive sorbent material from the product. Two such regeneration schemes that have received considerable attention are represented by Eqs. (8), (9), and (10).

$$[CaSO_4 \cdot MgO] + 4H_2 \rightarrow [CaS \cdot MgO] + 4H_2O \qquad (8a)$$

$$[CaSO_4 \cdot MgO] + 4CO \rightarrow [CaS \cdot MgO] + 4CO_2 \qquad (8b)$$

$$[CaS \cdot MgO] + H_2O + CO_2 \rightarrow [CaCO_3 \cdot MgO] + H_2S \qquad (9)$$

$$[CaSO_4 \cdot MgO] + H_2 \rightarrow [CaO \cdot MgO] + SO_2 \qquad (10)$$

Eqs. (8) and (9) represent a two-step regeneration scheme that can be performed at lower temperatures than the one-step process represented by Eq. (10). An important goal in the regeneration schemes is to obtain an off-gas that contains H_2S or SO_2 at a concentration sufficiently high for sulfur recovery in a Claus plant. Other regeneration schemes may be feasible. For example, preliminary results are presented below on another scheme represented by Eq. (11):

$$3[CaSO_4 \cdot MgO] + [CaS \cdot MgO] \rightarrow 4[CaO \cdot MgO] + 4SO_2 \qquad (11)$$

The reactions described by Eqs. (6) through (11) suggest the scope of the sulfur emission control chemistry program. The goal of the program is to develop an in-depth understanding of this chemistry. Specifically, chemical

---

*The work reported in this section is supported in part by the Division of Coal Conversion and Utilization of the ERDA-Fossil Energy Office.

reaction rates, extents of reactions, structural changes that take place in the solid reagents during these reactions, and the effect that these factors have on relevant chemistry represent information currently deemed necessary to develop this understanding. It is also considered desirable to develop a mechanistic model that is consistent with experimental results and that can be used to predict the behavior of dolomite and other reagents under various reaction conditions. Finally, it is believed that synthetic reagents will provide a valuable means for testing reaction theories and that they may also serve as alternative sorbent materials.

Emphasis has been placed on the examination of those factors that will ultimately have a bearing on the rates of reaction and on limitations of yield. A review of the extensive literature on the effects of stone type, particle and pore sizes, reacting gas pressures and temperatures, and chemical reaction rates indicates that detailed knowledge of the structural and morphological characteristics of the sorbent is not available. To that end, a basic study has been initiated that, it is hoped, will lead to a clearer picture of the various structural and morphological changes associated with sulfation and regeneration. Such an approach should improve the understanding of reaction mechanisms and should supply detailed information for refined mathematical modeling.

A. Experimental (L. H. Fuchs,* B. R. Hubble and S. Siegel)

The primary experimental tool for this work has been the thermogravimetric apparatus (TGA) used for chemical kinetic studies. This equipment allows measurement of changes in the weight of samples exposed to various reactive gases at elevated temperatures. It is recognized, however, that multiple chemical processes and complex morphological changes take place within the sorbent; accordingly, optical microscopy, electron microprobe analysis, and x-ray diffraction methods are used in conjunction with the TGA experiments.

1. TGA Experimental Techniques

The thermogravimetric unit used for most of the experiments reported herein has been described previously.[31] In that apparatus, the reactant gas mixture was prepared by controlling the flow of each constituent by means of a diaphragm-type regulator and a calibrated rotameter. Total flow was controlled in the range 200 to 400 cm^3/min. The water content of the reactant gas mixture was controlled by a thermostated humidifier, and sulfur dioxide was added to the gas stream after humidification. The sample, contained in a platinum basket, was suspended from one arm of an Ainsworth Model RVA balance, which provided continuous weight data over the range 0.2 to 1.0 g with an accuracy of ±0.1 mg, and was protected from corrosive gases by a purge flow of nitrogen or helium. Temperature in the reaction zone was maintained by a Marshall furnace with an accuracy of ±10°C up to about 950°C and was recorded along with sample weight on a strip chart recorder. The apparatus was fabricated of quartz and Type 304 stainless steel.

---

*Chemistry Division, ANL.

2. Improvements in TGA Apparatus

Considerable emphasis has been placed on improving the accuracy and reproducibility of TGA experiments. Figure III-1 is a schematic diagram of the apparatus that includes the modifications introduced to accomplish this goal. Prepared mixtures containing low concentrations of reactant gases have replaced the approach of blending the reactant gas mixture (by the use of rotameters) from the pure components. In addition, an improved procedure for the introduction of water vapor into the reactive gas stream has been adopted. In place of the thermostated humidifier technique, liquid water is pumped into the system at a constant rate, then evaporated, and finally mixed with the remaining constituents of the reactive gas mixture before being carried to the reaction tube. These changes in the apparatus should lead to the desired improvement in the accuracy and reproducibility of the TGA data.

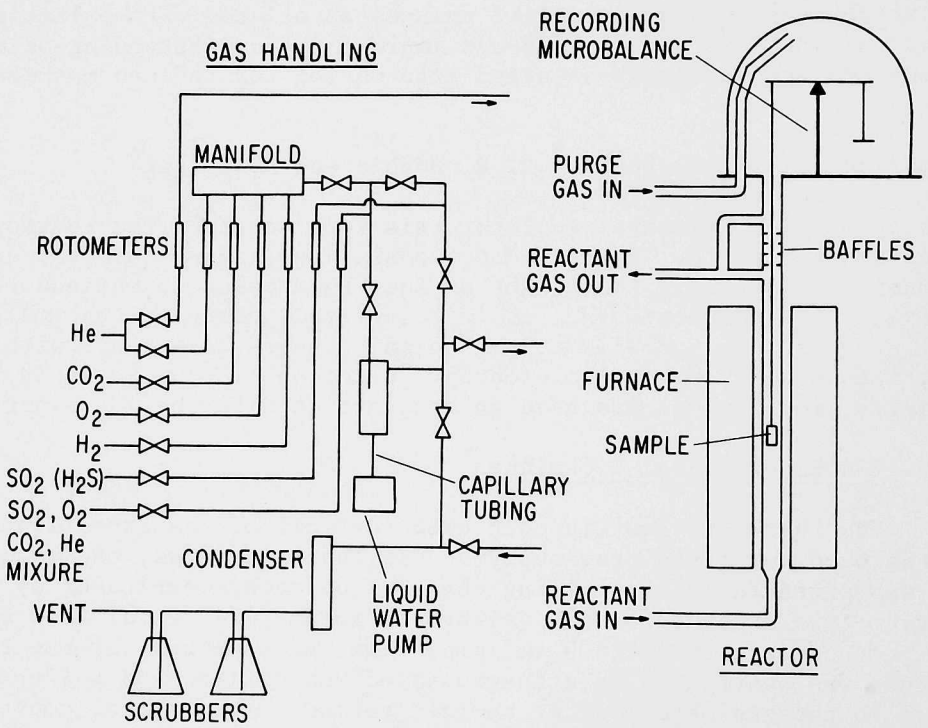

Fig. III-1. Schematic Diagram of the Improved Apparatus for Kinetic Studies.

3. Methods for Structural and Morphological Analysis

Techniques employed in these investigations to obtain structural information center on the use of aliquots of reagent stones removed at various stages during the reactions of interest. Room-temperature x-ray powder diffraction patterns of a random selection of stones from such an aliquot provide information on chemical phases present at that stage of reaction, as

well as details of crystallite size, preferred orientation, disordering, etc. Optical microscopic investigation of random stones from an aliquot provides information on chemical phases present and crystal sizes and, in addition, identifies the distribution of phases within a stone and the general morphological features. Electron microprobe studies are made on random stones from aliquots to determine the presence of Ca, Mg, and S as a function of position within a cross section of the stone. These techniques serve to complement each other, providing an excellent overall picture of the morphological changes that take place during the course of reactions under study.

B. Mathematical Modeling of Kinetic Data (C. A. Petty* and B. R. Hubble)

This section presents the results of efforts to develop a mathematical model that will describe the available kinetic data. Since the sulfation reaction, Eq. (7), has been studied the most extensively[31], these modeling efforts have been directed toward this reaction. A description of assumptions, development of the model, and testing of the model follows. The results presented suggest that limited success has been achieved in these initial efforts on the modeling aspect of the overall program.

A particle of half-calcined dolomite is known to be quite porous and to comprise a mixture of small crystallites of $CaCO_3$ and MgO. It is assumed in developing this model that rate limitations due to macropore diffusion in the particle can be neglected, *i.e.*, the concentration of gaseous reactants at the surface of the $CaCO_3$ crystallites is assumed to be the same as that in the reactant-gas stream. Further, it is assumed that the $CaCO_3$ crystallites are platelets (see Fig. III-2) and the reacting gases diffuse through a product layer of $CaSO_4$ to a moving reaction interface. The diffusion rate is

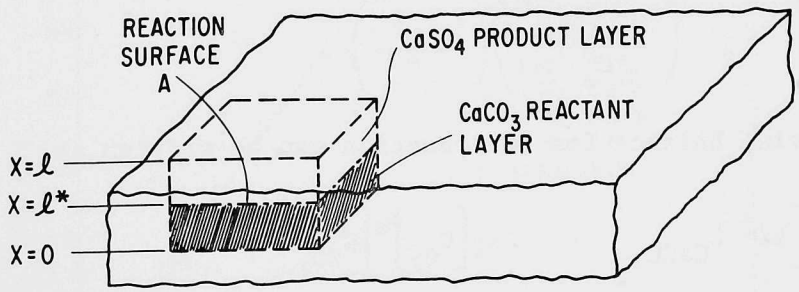

Fig. III-2. Schematic of a $CaCO_3$ Crystallite, Which is Assumed to be of a Rectangular Platelet Geometry, Found in Half-Calcined Dolomite Stone.

*Faculty Research Participant, Chemical Engineering Department, University of Delaware, Newark, Delaware.

assumed to be high compared with the movement of the reacting interface so that steady-state diffusion conditions exist within the product layer, with SO_2 diffusion being the rate-limiting process. The intrinsic reaction rate, r_1, for sulfation [Eq. (7)] is given by

$$r_1 = k_1\left(C_{O_2}\right)^m\left(C^*_{SO_2}\right) \tag{12}$$

where it is assumed that the reaction is first order with respect to the sulfur dioxide concentration.[31]

Using Eq. (12), the steady-state assumption mentioned above, and imposing suitable boundary conditions, the concentration of sulfur dioxide at the reaction interface, $C^*_{SO_2}$, can be represented as follows:

$$C^*_{SO_2} = \frac{C^\circ_{SO_2}}{1 + \dfrac{k_1\left(C_{O_2}\right)^m(\ell - \ell^*)}{D_e}} \tag{13}$$

where D_e is the effective diffusion coefficient, $C^\circ_{SO_2}$ is the sulfur dioxide concentration in the reactant-gas stream, and ℓ and ℓ^* are characteristic dimensions in the platelet (see Fig. III-2). If it is now assumed that the effective diffusion coefficient for SO_2 diffusing through the product layer of calcium sulfate is linearly dependent on the extent of the reaction, *i.e.*, $D_e = \xi^* D^\circ_e$ with $\xi^* \equiv \ell^*/\ell$, Eq. (13) can be rewritten as

$$C^*_{SO_2} = \frac{C^\circ_{SO_2}}{1 + \left(\dfrac{\ell k_1 \left(C_{O_2}\right)^m}{D^\circ_e}\right)\left(\dfrac{1 - \xi^*}{\xi^*}\right)} \tag{14}$$

The material balance for the reaction can be written as

$$\frac{d}{dt}\left[A\ell^* C_{CaCO_3}\right] = -AK_1\left[C_{O_2}\right]^m\left[C^*_{SO_2}\right] \tag{15}$$

where C_{CaCO_3} is the calcium carbonate concentration in the crystallite. Substituting Eq. (14) into (15) and rearranging terms gives

$$\frac{d\,\xi^*}{dt} = -\left\{\frac{k_1\left[C_{O_2}\right]^m\left[C^\circ_{SO_2}\right]}{\ell C_{CaCO_3}}\right\}\left\{\frac{1}{1 + \left[\dfrac{\ell k_1\left[C_{O_2}\right]^m}{D^\circ_e}\right]\left[\dfrac{1 - \xi^*}{\xi^*}\right]}\right\} \tag{16}$$

which can now be integrated to give

$$\frac{-\ln\,(1-\Psi)}{\Psi} = \frac{1}{\tau_D}\,\frac{t}{\Psi} - \left(\frac{\tau_R}{\tau_D} - 1\right) \tag{17}$$

where $\Psi \equiv 1 - \xi^*$, and physical constants associated with characteristic times for the reaction and diffusion have been collected so that

$$\frac{1}{\tau_R} = \frac{k_1\left[C_{O_2}\right]^m\left[C^\circ_{SO_2}\right]}{\ell\, C_{CaCO_3}} \tag{18}$$

$$\frac{1}{\tau_D} = \frac{D^\circ_e\left(C^\circ_{SO_2}\right)}{\ell^2\, C_{CaCO_3}} \tag{19}$$

The success of the model can be tested by ascertaining whether linear plots of $-\ln(1-\Psi)/\Psi$ versus t/Ψ are obtained for the experimental data. This has been done for the sulfation-reaction data previously reported,[31] and Figs. III-3 and III-4 show that the model does indeed fit the data. In addition, Fig. III-5 shows that the model also provides a reasonable fit for preliminary data obtained for the carbonation reaction (Eq. 9), which is discussed more fully below.

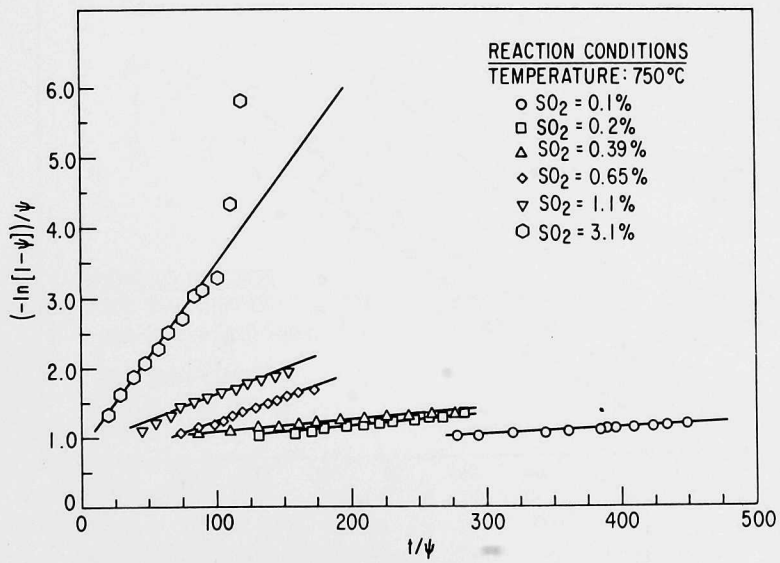

Fig. III-3. Plots of $(-\ln[1 - \Psi])/\Psi$ vs t/Ψ Employing Kinetic Data for Sulfation Reaction with H_2O Vapor Present in Reaction Gas Stream.

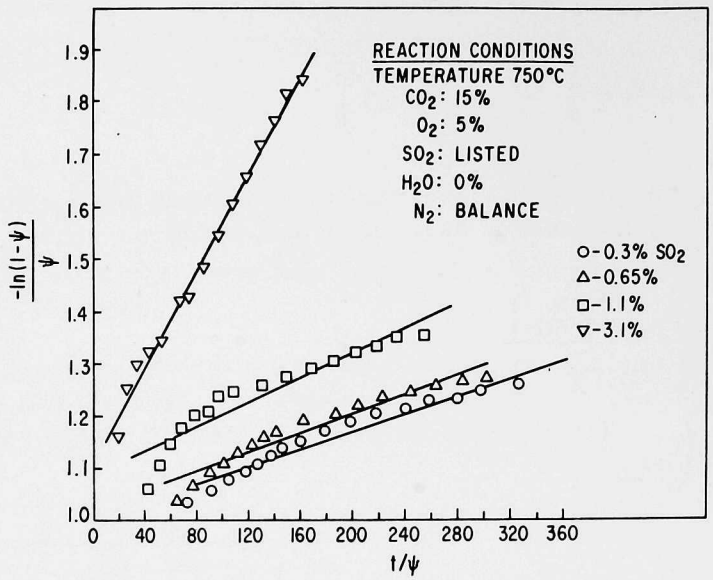

Fig. III-4. $-\ln(1 - \Psi)/\Psi$ vs t/Ψ Plots, Employing Kinetic Data for Sulfation Reaction without H_2O Vapor Present in Reactive Gas Stream.

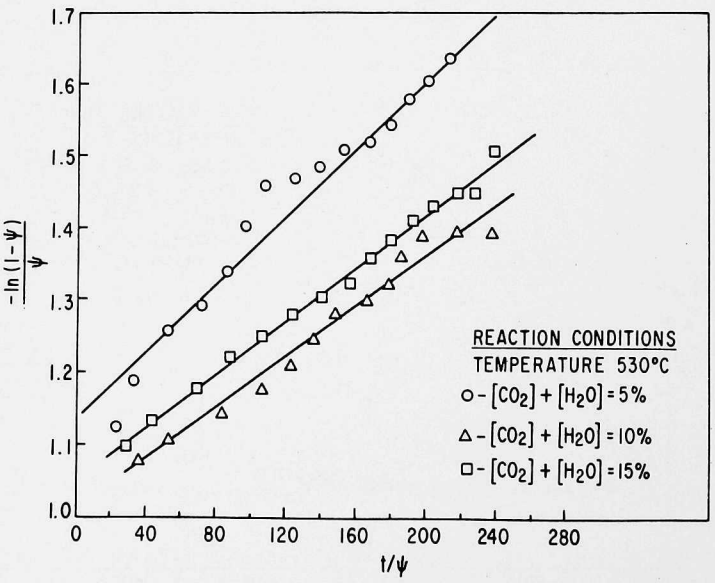

Fig. III-5. Plots of $-\ln(1 - \Psi)/\Psi$ vs t/Ψ, Employing Kinetic Data for Carbonation Reaction.

Equation 19 suggests a method whereby the order of reaction with respect to SO_2 concentration may be calculated via the model; that is, the slope of a plot of ln $(1/\tau_D)$ versus ln $C^\circ_{SO_2}$ is equal to the order of reaction with respect to SO_2 concentration:

$$\ln(1/\tau_D) = \ln C^\circ_{SO_2} + \ln D^\circ_e/\ell^2 C_{CaCO_3} \qquad (20)$$

Figure III-6 shows the results of such a calculation. For the sulfation reaction data with H_2O vapor present in the simulated flue gas, the slope is 0.99; for the sulfation reaction data without H_2O vapor, the slope is 0.85. The previously reported values[31] for this parameter, which were obtained from an analysis based on the initial reaction rates, are 1.08 for sulfation with H_2O vapor present and 0.77 for sulfation without H_2O vapor present in the reactive gas stream. The agreement of the results obtained with the two models is surprisingly good, especially since the mathematical model calculation of this parameter is based on kinetic data over the entire reaction time period.

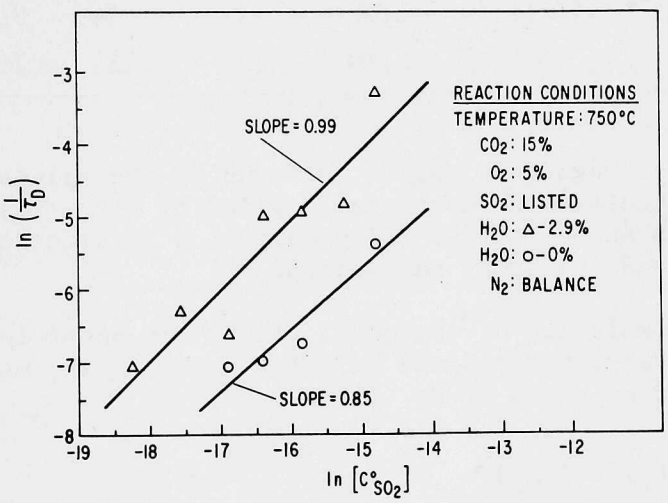

Fig. III-6. $\ln(1/\tau_D)$ vs $\ln\left[C^\circ_{SO_2}\right]$ Plots, Employing Kinetic Data for Sulfation Reaction.

Values of the model parameters of interest, τ_D and τ_R, can be obtained from the slopes and intercepts of plots of Eq. (17). Table III-1 summarizes the results of such calculation, obtained by analyzing the kinetic data for the sulfation reaction. From the data in this table, it is obvious that neither τ_D nor τ_R is a constant from experiment to experiment, but each varies with the SO_2 and H_2O concentrations. Equations (18) and (19) suggest that these model parameters should only be a function of SO_2 concentration since C_{O_2} is the same for each experiment reported in Table III-1. The last two columns in Table III-1 contain the values obtained when the values for τ_D and τ_R are multiplied by the $C^\circ_{SO_2}$ values; according to Eqs. (18) and (19), the values of these last two columns should be constant from experiment to experiment.

Table III-1. Summary of the Values Obtained for the Model Parameters τ_D and τ_R. Note: The oxygen concentration, C_{O_2}, was 5.95×10^{-7} mol/cc for each experiment.

SO_2, %	$C^\circ_{SO_2}$, mol/cc	C_{H_2O}, mol/cc	τ_R/τ_D	τ_D	τ_R	$\tau_D[C^\circ_{SO_2}]$	$\tau_R[C^\circ_{SO_2}]$
0.1	1.19×10^{-8}	3.47×10^{-7}	1.77	1170	2070	1.39×10^{-5}	2.46×10^{-5}
0.2	2.38×10^{-8}	3.47×10^{-7}	1.80	562	1010	1.34×10^{-5}	2.40×10^{-5}
0.39	4.64×10^{-8}	3.47×10^{-7}	1.95	746	1460	3.46×10^{-5}	6.77×10^{-5}
0.39	4.64×10^{-8}	0	2.00	1190	2380	5.52×10^{-5}	1.10×10^{-4}
0.65	7.74×10^{-8}	3.47×10^{-7}	1.55	148	229	1.14×10^{-5}	1.77×10^{-5}
0.65	7.74×10^{-8}	0	2.02	1080	2180	8.36×10^{-5}	1.69×10^{-4}
1.1	1.31×10^{-7}	3.47×10^{-7}	1.86	136	253	1.78×10^{-5}	3.31×10^{-5}
1.1	1.31×10^{-7}	0	2.08	842	1750	1.10×10^{-4}	2.29×10^{-4}
3.1	3.69×10^{-7}	3.47×10^{-7}	1.26	27	34	9.96×10^{-6}	1.26×10^{-5}
3.1	3.69×10^{-7}	0	2.10	215	452	7.93×10^{-5}	1.79×10^{-4}

However, an order of magnitude spread is found in the values, suggesting that the simple SO_2 concentration dependence implied by Eqs. (18) and (19) does not exist. The results shown in Fig. III-6 suggest a log-log relationship between SO_2 concentration and the model parameters.

Due to the formulation of the model, it is not possible to compute values of k_1 or D°_e separately, but instead only the ratio $D^\circ_e/\ell k_1$ may be obtained from values of intercept of plots of Eq. (17), *i.e.*,

$$\tau_R/\tau_D = D^\circ_e/\ell k_1 (C_{O_2})^m \tag{21}$$

where the quantity $(C_{O_2})^m$ is the same for each experiment. The value for C_{O_2} is given in Table III-1. Computed τ_R/τ_D ratios are also given in this table, where it is seen that if more than one significant figure is considered, the τ_R/τ_D values are not constant from experiment to experiment.

In the development of the model, the effect of H_2O concentration on the reaction rate observed experimentally[31] was ignored by explicitly assuming

$$r_1 = k_1\left(C_{O_2}\right)^m\left(C^*_{SO_2}\right) \tag{12}$$

where $C^*_{SO_2}$ is the SO_2 concentration at the reaction interface. However, it should be possible to separate the effect of H_2O concentration on the reaction rate by the following analysis. In Eq. (12) it is implied that the C_{H_2O} effect is included in the rate constant, k_1, *i.e.*,

$$k_1 = k_s(C_{H_2O})^n \tag{22}$$

where k_s is a more general intrinsic rate constant, C_{H_2O} is the gas-phase concentration of H_2O, and n is the order of the reaction with respect to water concentration. Equation (22) suggests that, for reactions with H_2O vapor present in the reactive gas mixture, Eq. (18) should be modified as follows:

$$(1/\tau_R)_{C_{H_2O}\neq 0} = k_s(C_{H_2O})^n(C_{O_2})^m(C^\circ_{SO_2})/\ell(C_{CaCO_3}) \qquad (23)$$

which suggests

$$(\tau_R)_{C_{H_2O}=0}/(\tau_R)_{C_{H_2O}\neq 0} = (C_{H_2O})^n \qquad (24)$$

Table III-2 summarizes the results of the calculations of such an analysis for the kinetic data in Table III-1. The results show that the $(C_{H_2O})^n$ values are not constant from experiment to experiment. However, the values of n, found in the last column, are in fairly good agreement with the value of n equal to zero[31] determined using initial reaction rates.

Table III-2. Effect of Water Concentration on Reaction Rate.

C_{SO_2}, %	C_{H_2O}, mol/cc	τ_R	$\frac{(\tau_R)_{C_{H_2O}=0}}{(\tau_R)_{C_{H_2O}\neq 0}} = (C_{H_2O})^n$	n
0.39	3.47×10^{-7}	1460		
0.39	0	2370	1.623	-0.03
0.65	3.47×10^{-7}	229		
0.65	0	2180	8.65	-0.14
1.1	3.47×10^{-7}	252		
1.1	0	1754	6.96	-0.13
3.1	3.47×10^{-7}	250		
3.1	0	453	1.81	-0.04

The parameters included in a model should possess certain qualities. Because the parameters are ratios involving physical constants and controlled experimental variables of the system under investigation, the values of these parameters should be constant and should not vary from experiment to experiment in an unexplainable fashion. Moreover, such parameters should provide information that can be interpreted physically. From the above analysis of the model parameters, it is difficult to draw conclusions that support the merit of the model. The results do not completely discredit the model, but strongly suggest that it is not complete as presently formulated. This situation may change when further, more accurate kinetic data become available for analysis and when further structural data are obtained.

It must be emphasized that the limited success of this model does not necessarily mean that it is an accurate description of the physical processes actually taking place in these reactions. It is, in fact, very difficult to rationalize, on the basis of some physical phenomena, the dependence of the effective diffusion coefficient on the degree of reaction. Nevertheless, the model does provide a mathematical description for the reaction under a variety of conditions and can serve as a point of departure for the development of a more satisfactory model by suggesting further experiments. The extent to which this process has already begun is pointed out below where kinetic results not explained by this early model are described. In addition, structural characteristics are presented indicating that the assumptions of the model are not correct. These structural characteristics suggest a more realistic model.

C. Sulfation Reaction of Half-Calcined Dolomite (L. H. Fuchs,* B. R. Hubble, S. Siegel and W. I. Wilson)

1. Initial TGA Experiments

The initial results obtained for the sulfation reaction, Eq. (7), presented in an earlier report,[31] are summarized again here for completeness. They indicate that the reaction is first order with respect to SO_2 concentration when H_2O vapor is present in the reactive-gas stream, and that the rate varies with the three-fourths power of SO_2 concentration when H_2O vapor is not present. Thus, it appears that the rate-determining step differs depending on whether or not water is present in the reactive gas. With water present, the reaction is 0.22 order with respect to oxygen concentration in the reactive-gas stream. An apparent activation energy of 7.3 kcal/mol was found; such a value does not point conclusively to a mechanism in which a chemical reaction is rate-controlling, but is somewhat greater than one might expect if the reaction is diffusion-controlled.

A number of other studies have now been performed on the sulfation reaction, Eq. (7), employing 1337 dolomite. These experiments are described below and have been performed (1) to test the simple mathematical model described above and (2) to initiate a study of the structural changes in the solid reagent that are associated with this reaction.

2. TGA Kinetic Experiments to Test Mathematical Model

The experimental procedure employed is the same as that used in the earlier study,[31] that is, with the TGA apparatus before it was modified to the form shown in Fig. III-1. The studies completed include the following: (a) experiments at low SO_2 concentrations in the reactant-gas mixture (0.39% and 0.65% SO_2) to determine whether the $CaCO_3$ available in half-calcined dolomite stones can be completely converted to $CaSO_4$ at low SO_2 concentrations, (b) experiments in which the SO_2 concentration in the reactant-gas mixture was increased from an initially low value (0.39% or 0.65%) to a high value (3.1%) at a later stage of the sulfation reaction, and (c) an experiment to test the effect on the reaction rate that might be caused by crushing the stone after

---

*Chemistry Division, ANL.

it had been partially sulfated. The results of these investigations are shown in Fig. III-7. For comparison, results obtained earlier[31] for 3.1% SO_2 are also included.

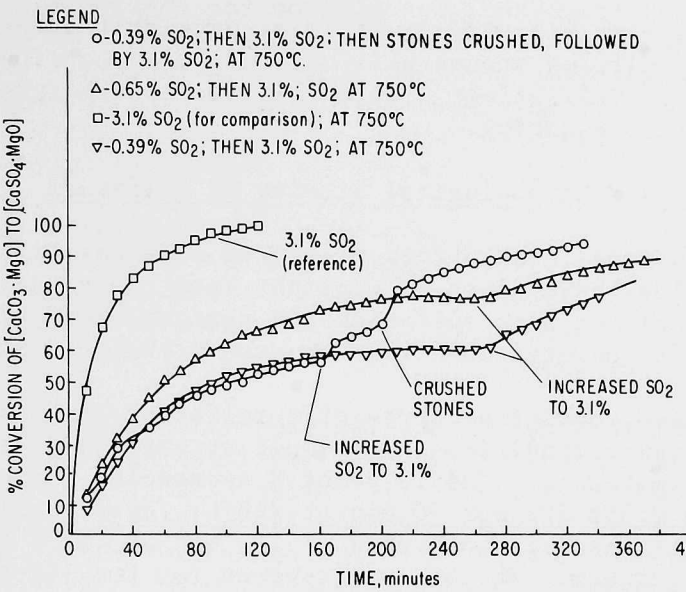

Fig. III-7. Plots of % Conversion vs Time for Sulfation Reaction of Half-Calcined 1337 Dolomite under the Reaction Conditions Described in the Legend.

From curves c and d in Fig. III-7, it is evident that, at the low SO_2 concentrations of 0.39% and 0.65%, the conversion of $CaCO_3$ in the dolomite stone to $CaSO_4$ stops after a finite reaction time and that conversion is less than complete. The data obtained in the earlier work, shown as curve a, indicate that with 3.1% SO_2 in the reacting-gas mixture, essentially complete conversion can be obtained. These preliminary results suggest that the extent of conversion of $CaCO_3$ to $CaSO_4$ might be a function of the SO_2 concentration in the reactant-gas mixture. It should be noted that, in the mathematical model described above, the assumption is made that complete conversion of $CaCO_3$ in the half-calcined dolomite stones is always attainable and not a function of SO_2 concentration.

The incomplete conversion of the $CaCO_3$ in the half-calcined dolomite stones at low SO_2 concentrations might involve a process whereby a structural change in the $CaSO_4$ product layer occurs that, in effect, blocks diffusion of SO_2 through the $CaSO_4$ product layer. This possible simple explanation led to the experiments (curves c and d) in which the SO_2 concentration was varied during the reaction. If by some process, SO_2 diffusion is indeed blocked, one would expect that once the reaction has stopped at some fractional conversion value, it would not proceed even if the SO_2 concentration should be increased. Figure III-7, curves c and d, shows that reaction does indeed start again when the SO_2 concentration is increased. However, the reaction rate after increasing

the SO_2 concentration to 3.1% was much lower than that observed when fresh half-calcined dolomite stones were sulfated with a 3.1% SO_2 gas mixture from the beginning to the end of the reaction (see curve a). The mathematical model in its present simple form is incapable of explaining these experimental results.

From curve b in Fig. III-7, it is evident that after the half-calcined, partially sulfated stones were crushed, the reaction rate was higher than before crushing. This effect is probably due to exposure of new $CaCO_3$ surfaces as a result of crushing.

3. Structural and Morphological Studies of Sulfation

Crystal-chemical considerations, based on x-ray diffraction and optical microscopy studies, have given new insight into the structural and morphological details associated with sulfation and regeneration. The following discussion pertains to observations made on stones that had undergone sulfation.

Figure III-8 shows the course of a sulfation reaction experiment with time under the following conditions: A sample at point A is the half-calcined (at 800°C) starting material. Sample point B represents the sample condition after reaction with 0.39% SO_2 for 70 min at 750°C. Sample point C represents the state of the material after a period of 168 min at 750°C but with no SO_2 in the reactive-gas stream. The SO_2 was removed for the 168-min interval in order to note any structural or morphological changes (changes in composition or crystallite size) which might arise as a result of sintering for this

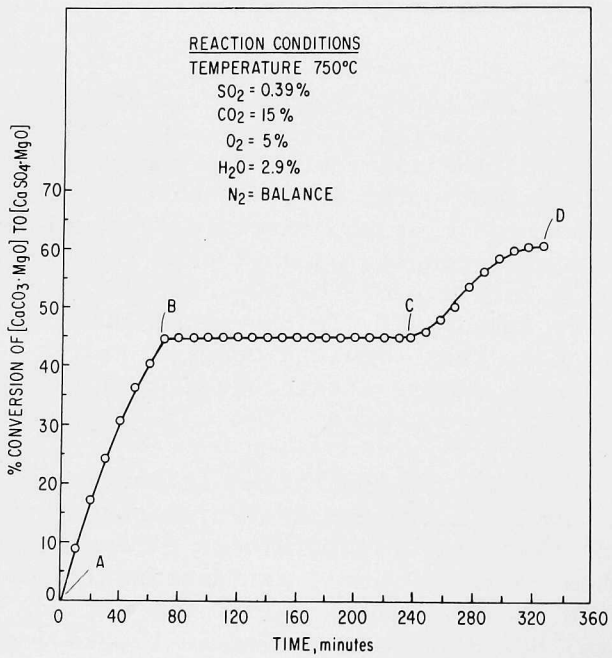

Fig. III-8.

Plot of % Converstion vs Time, Employing Kinetic Data for a Sulfation Reaction Experiment to Initiate Structural and Morphological Investigations.

interval. At sample point D, the SO_2 concentration of 0.39% had been restored and maintained for an additional 90 minutes. Aliquots of stones were removed at points A, B, C, and D for x-ray, microscopic, and electron microprobe studies.

a. X-ray Diffraction Studies. The diffraction pattern of the initial 1337 dolomite shows it to be very crystalline, with a small amount of fine material (the crystals are readily observed under low magnification with an optical microscope). The stones are fairly soft, but nevertheless the dolomite crystals within the stone are fused together in a random (crystallographic) orientation to produce adherence.

All x-ray diffraction observations have been made at room temperature. The removal of a TGA sample produces a rapid quench, and it is assumed that the quenched sample represents the condition of the material at elevated temperatures. X-ray measurements at elevated temperatures are planned in order to check the validity of the assumption.

The x-ray diffraction pattern of sample A (Fig. III-8) shows MgO and $CaCO_3$, both exhibiting very small crystallites, but with the $CaCO_3$ probably disordered. The MgO crystallites have a size of the order of 1000Å or less. The lack of resolution of the CuKα doublet for $CaCO_3$ indicates crystallite sizes of 300-1000Å, but the rapid drop-off in intensity with angle strongly suggests some disorder or thermal effect. There is also a tendency for ordering on the 104 planes (natural cleavage faces) of $CaCO_3$. The ordering is so pronounced that clusters of large pseudo-crystals are produced. Under some half-calcining conditions, the $CaCO_3$ crystals may show more or less tendency for preferred orientation, as indicated below in the section on half-calcination. Nevertheless, the characteristics described above may be quite general, for they agree fairly well with studies made by Wilsdorf and Haul[32,33] on transparent single crystals of dolomite.

In sample B, MgO is present, with $CaSO_4$ appearing with the $CaCO_3$.

MgO is present in sample C, but the volume of CaSO has decreased substantially in comparison to the amount observed in sample B. This may be caused by the nonuniform behavior of individual stones.

In sample D, the results are essentially unchanged from those of sample C.

The $CaSO_4$ seems to be in the same condition (small crystallite size or disorder, or both) as the $CaCO_3$ from which it was derived. In addition, the preferred orientation (and the sizes of the associated pseudo-crystals) of the $CaCO_3$ decrease as sulfation progresses. After sulfation, the stones become harder and under low-power magnification seem to exhibit the same characteristic coarse pore structure that is observed in the dolomite stage.

b. Microscopy and SEM Studies. Optical examination of untreated dolomite shows a crystal size range between 30 and 300 micrometers. Upon half-calcining, it is found that the single crystals of dolomite are replaced by grains--that is, a crystal seems to convert to a grain of about the same shape, with the grains still held together to produce a coarse pore structure similar to that found in the original dolomite.

MgO cannot be detected with certainty. It would be expected, on the basis of the x-ray results, that aggregates of MgO could be seen but that single crystals of MgO would be below the limit of visibility. Calcite crystals are observed, however, with a size range of 1-15 micrometers and with an average size of about 3 micrometers (30,000Å). Extinction in polarized light of the calcite crystals is always undulatory, indicating strain or disorder. In view of the small size of these crystals, it is questionable whether stresses would be present. It is quite possible that the origin of these crystals lies in the tendency of small crystallites to align in preferred orientation to simulate a larger pseudo-crystal, as indicated by the x-ray diffraction patterns. The undulatory nature of the extinction would then arise from incomplete and inexact alignment along crystallographic directions.

Oil-immersed calcite grains viewed in transmitted light show narrow rivulets or stringers about 1 micrometer wide, which exhibit high relief when the calcite grain is in a position of zero relief. It is suspected that these stringers are MgO, but their small size precludes a refractive index determination. Additional studies should lead to an understanding of the nature of the MgO distribution, but for the time being the stringers distributed in the calcite crystals are considered to be the MgO phase.

After sulfation, microscopic examination shows that these calcite crystals become reduced in size, in accordance with the x-ray observations. However, a most interesting morphological change is found optically: the calcite crystals do not sulfate uniformly. Figure III-9a depicts an irregularly-shaped calcite crystal that exhibits nonuniform extinction. Upon sulfation, a crystal is found to exhibit both $CaSO_4$ and $CaCO_3$ crystallites adhering together as shown in Fig. III-9b. This condition is found even on the periphery of stone that is about 50-60% sulfated.

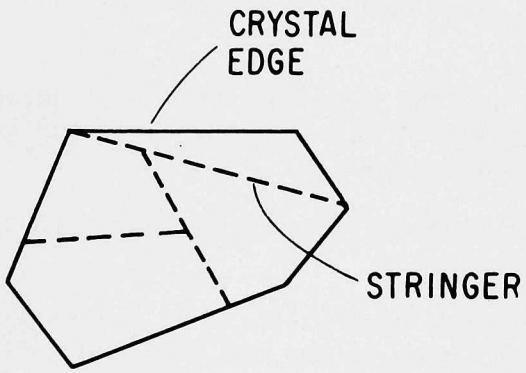

Fig. III-9a.

Appearance of Stringers in a Calcite Crystal Exhibiting Non-Uniform Extinction.

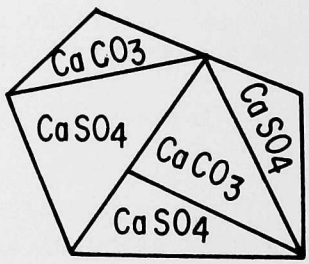

Fig. III-9b.

Distribution of Aggregated $CaCO_3$ and $CaSO_4$ Crystals After Partial Sulfation.

Figure III-10 shows a 75X magnification of the edge of a stone removed from point D (Fig. III-8). The individual grains are apparent. The band along the periphery in which the grains are pronounced constitutes the region of primary sulfation. SEM studies confirm the observation that the periphery of a stone is being sulfated first. Figures III-11 and III-12 show typical SEM results. These were obtained on a stone taken at point C (Fig. III-8), corresponding to about 45% sulfation. Figure III-11a shows a calcium scan across the entire stone; Fig. III-11b, a sulfur scan across the entire stone; and Fig. III-11c outlines five areas on the stone that were analyzed in detail for calcium, magnesium, and sulfur. Figure III-12 shows the results of the analyses of these five areas. It is apparent that even though calcium and magnesium are uniformly distributed across the stone, sulfur for the most part is distributed only in its periphery. With this information, a tentative structural model for the sulfation process can be developed.

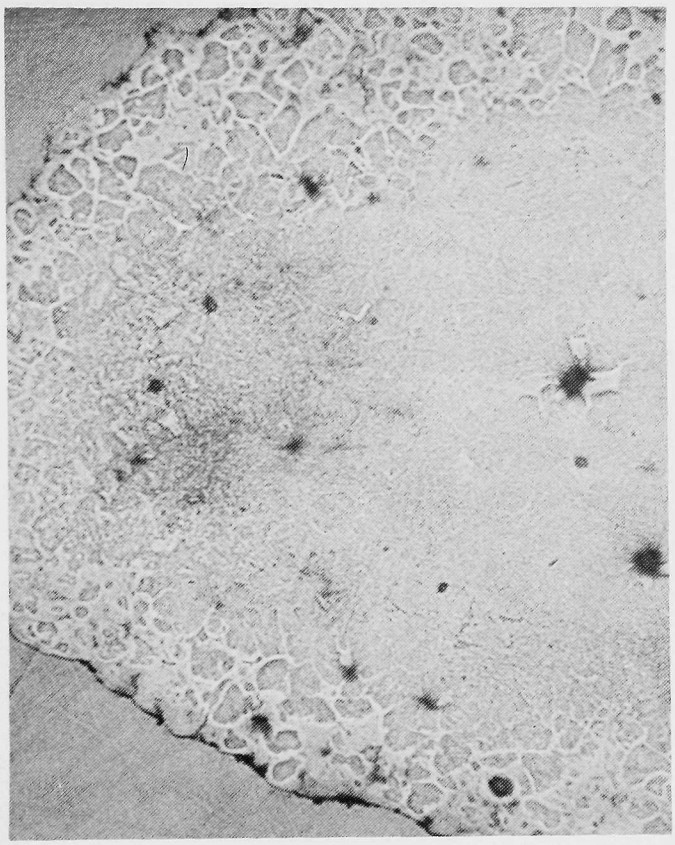

Fig. III-10.

Stone Removed at Point D, Fig. III-8.
Individual grains of stone apparent.
The band, along the periphery of stone,
where grains are most pronounced, is
the region of primary sulfation.

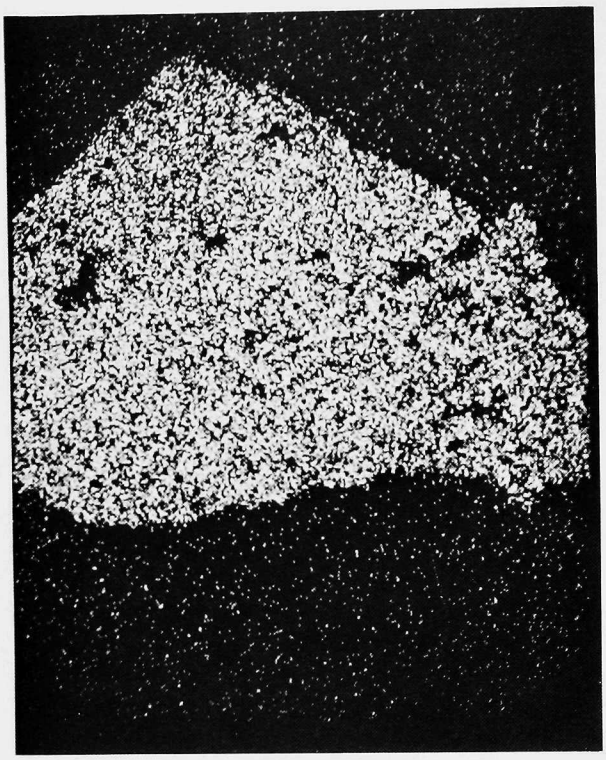

(a)

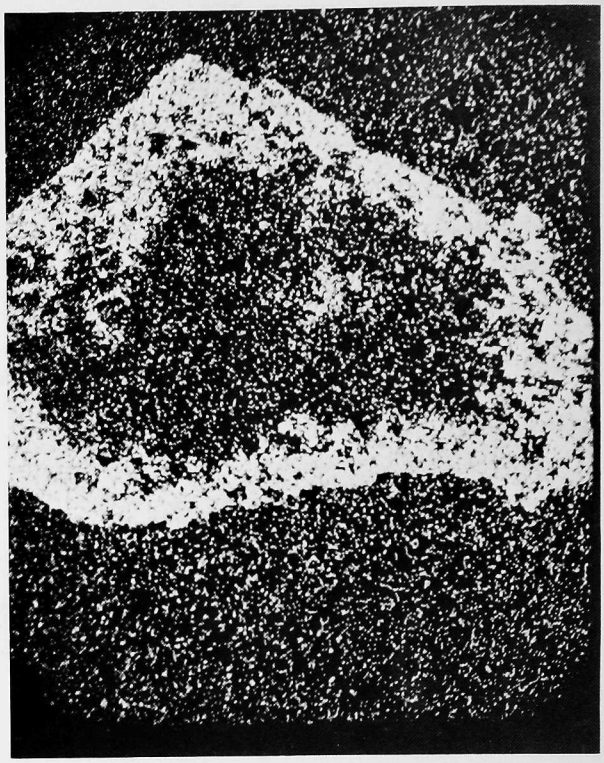

(b)

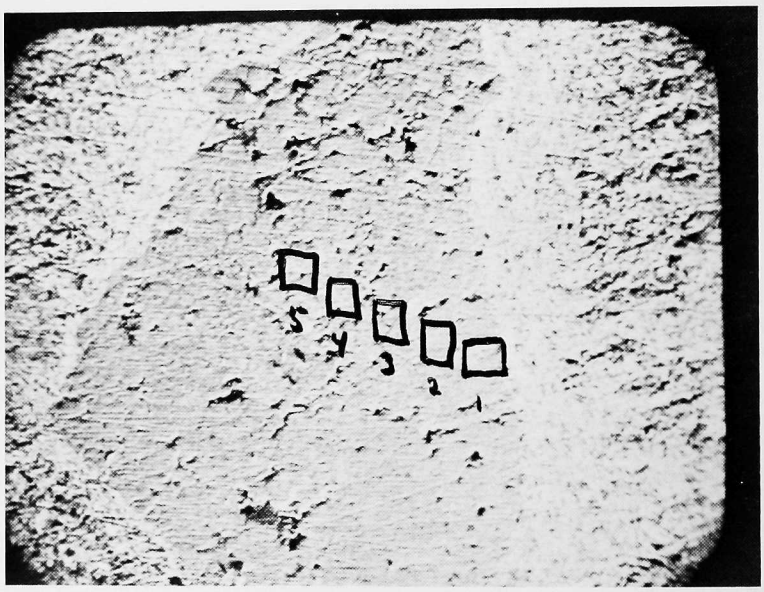

(c)

Fig. III-11.

SEM Results on a Stone Taken from Point C in Fig. III-8. Fig. 11a shows a Ca X-ray scan across the entire stone, Fig. III-11b a S X-ray scan across the entire stone, and Fig. III-11c outlines five areas on the stone analyzed in detail for the presence of Ca, Mg, and S (see Fig. III-12).

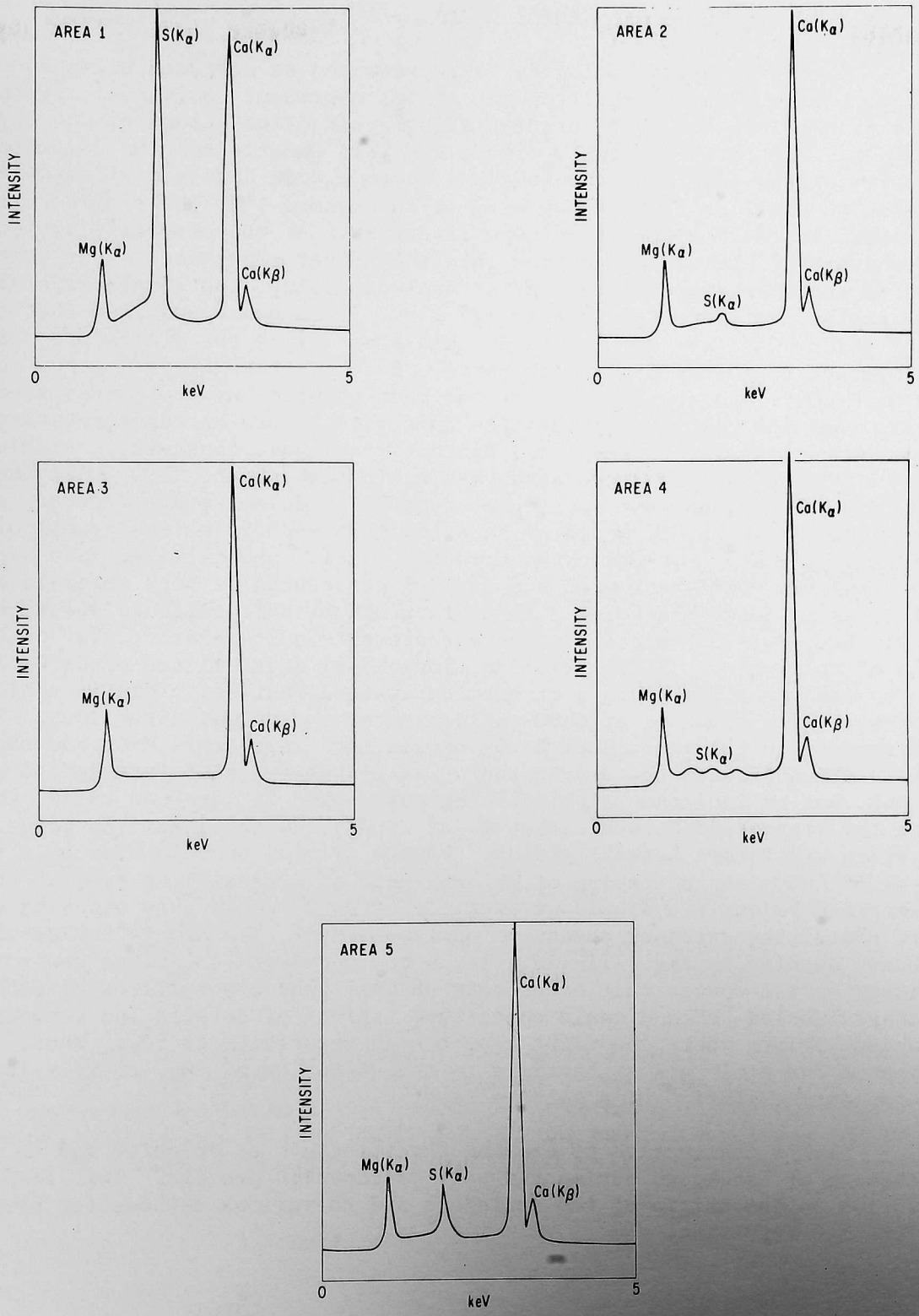

Fig. III-12.

SEM Results of Analysis for Presence of Ca, Mg, and S in the Five Areas of the Stone Described in Fig. III-11c.

4. Development of Structural Model

In Fig. III-13a, dolomite is represented as composed of macroscopic crystals of $CaMg(CO_3)_2$. The irregular shapes represent individual crystals, and the arrows indicate that the crystallographic orientations of the crystals are random. The total aggregate of the crystals constitutes the dolomite stone. Voids between the crystals, labeled "a", contain some finely divided dolomite crystals, so small as to be a powder. It is assumed that the single crystals of dolomite are held together by some intergrowth of the crystals, or perhaps by a tendency of the powder to grow into the larger crystals. Alternatively, a hydrate could be responsible. After half-calcining, the single crystals become grains, as indicated in Fig. III-13b. It is quite possible that the initial voids, "a", are maintained at this stage since the grains are still held together to maintain good adherence. Each of these grains is now composed of $CaCO_3$ + MgO aggregates. It has been pointed out that x-ray studies indicate that the calcite crystallites aggregate by preferred orientation into large pseudo-crystals. As Haul and Wilsdorf[32,33] have observed, a single crystal of dolomite will serve as a base against which the $CaCO_3$ will develop and orient. Hence, as long as single crystals of dolomite are present as shown in Fig. III-13a, it would be expected that each dolomite crystal will serve as a base for developing the oriented calcite crystallites into aggregates. This is consistent with the crystal structures of both dolomite and calcite, as is described below. A single grain of half-calcined dolomite is shown in Fig. III-13c, and this figure represents a speculative view of the makeup of the grain. In Fig. III-13c, individual crystallites of $CaCO_3$ are shown to tend to align along a crystallographic direction. This is a simplistic view for the symmetry of $CaCO_3$ allows three equivalent directions. The black shading in the individual $CaCO_3$ crystallite represents MgO, and the black shadings between the aggregated crystallites are also intended to represent MgO, but as isolated material. Regions marked "b" are new voids, now within the grain (and between crystals of $CaCO_3$), as distinct from voids, "a", which are formed between grains. Figure III-13d shows a view of a pseudo-crystal of $CaCO_3$ as consisting of an aggregate of crystallites tending to order. As described below, the single crystallite of $CaCO_3$ could show stacking disorder, containing extended sheets of entrapped MgO. The MgO is indicated by the heavy shading in Fig. III-13d. It is now necessary to define new voids, by virtue of the spaces that occur between unaligned crystallites of $CaCO_3$. These are labeled "c" and could constitute regions of defects and various vacancies--points where one might expect high reactivity to SO_2. Thus, the aggregated MgO could act as barriers to the diffusion of SO_2, thereby leading to nonuniform sulfation of a calcite crystal.

It is instructive to examine the structure of dolomite and to consider a mechanism of breakdown during the half-calcination process. This leads to a suggestion on the origin of the stringers and to various methods for breaking down the MgO formation.

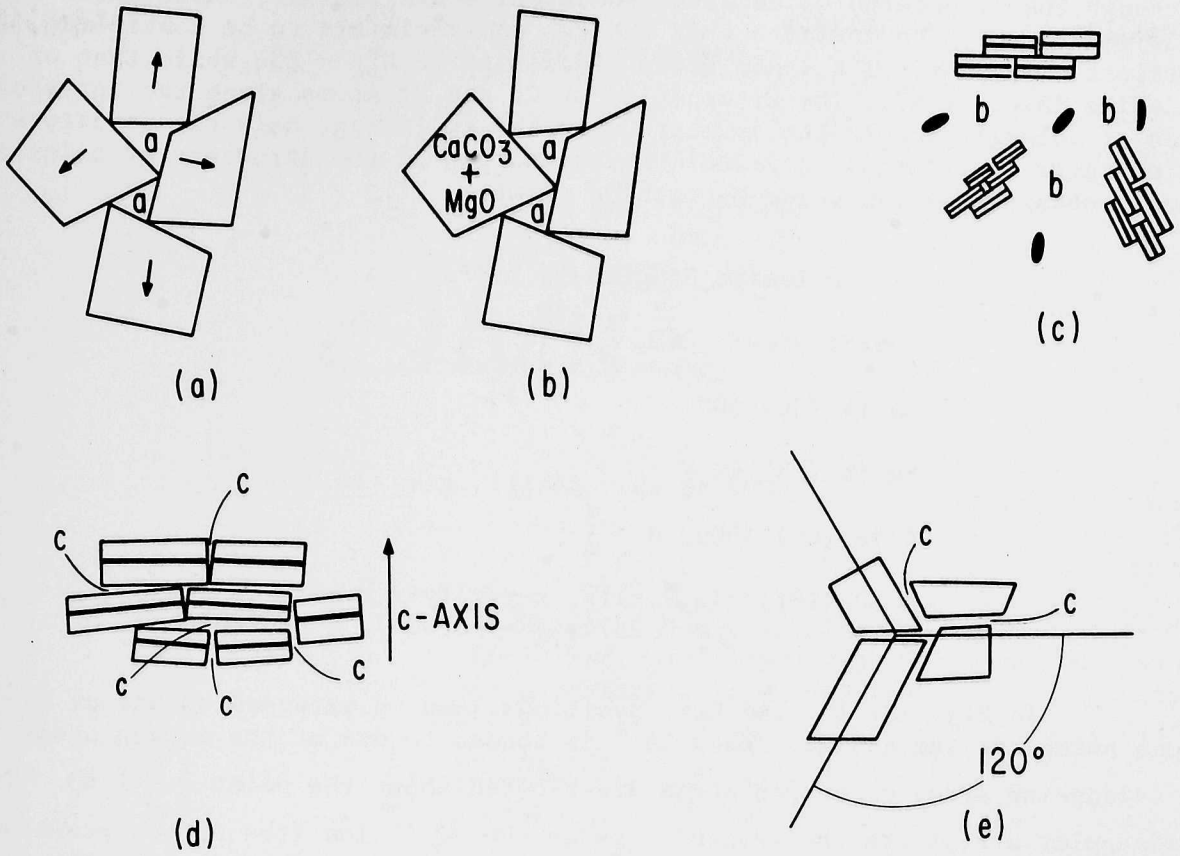

Fig. III-13.

Dolomite Stone.

a, b. dolomite stone before and after half-calcination.
c. aggregation characteristics.
d. nonuniform orientation of crystallites normal to c-axis.
e. nonuniform orientation in a-a plane of hexagonal axis.

Calcite, $CaCO_3$, possesses rhombohedral symmetry. The rhombohedral angle is 46°6', as distinct from the cleavage rhomb angle of 101°55'. However, it is convenient to describe the structure in terms of hexagonal symmetry. Dolomite, $CaMg(CO_3)_2$, is also rhombohedral, but can, in a similar manner, be referred to hexagonal symmetry. The hexagonal cell dimensions are (including $MgCO_3$):

	a(Å)	c(Å)
$CaCO_3$	4.99	17.06
$CaMg(CO_3)_2$	4.80	16.00
$MgCO_3$	4.62	14.99

Although the structures of calcite and dolomite are similar, basic differences in symmetry serve to indicate that the two materials are to be considered distinct compounds. The space group of calcite is D_{3d}^6 - $R\bar{3}c$ while that of dolomite is C_{3i}^2 - $R\bar{3}$. The alternation of Ca and Mg atoms along the threefold axes of dolomite lowers the symmetry. In the following, only the structure of dolomite is considered. A visual representation of the structure of calcite can be obtained by replacing Mg with Ca atoms.

Dolomite $CaMg(CO_3)_2$ Z = 3

Coordinates: $000, \frac{1}{3}\frac{2}{3}\frac{2}{3}, \frac{2}{3}\frac{1}{3}\frac{1}{3}$ +

Ca in (3a) 000

Mg in (3b) $00\frac{1}{2}$

C in (6c) $\pm 00u$, $u \sim \frac{1}{4}$

O in (18f) $\pm(x,y,z)(\bar{y}, x-y, z)(y-x, \bar{x}, z)$ with
$x = 0.2374$, $y = -0.0347$, $z = 0.2440$

In Fig. III-14, the Ca^{2+} positions lead to extended sheets of Ca^{2+} ions normal to the c-axis. Each Ca^{2+} is bonded to one of the oxygen atoms of a triangular array of oxygen atoms distributed about the point $\frac{2}{3}\frac{1}{3}$ 1.43. These triangular arrays are the oxygen atoms of the CO_3^{2-} ion (the carbon positions are omitted for clarity). Another oxygen array is distributed about the point $\frac{1}{3}\frac{2}{3}\overline{1.43}$. All arrays at z = ±1.43Å are extended sheets of oxygen atoms normal to the c-axis. Each Ca^{2+} ion is, therefore, bonded to six oxygen atoms. As shown in Fig. III-15, Mg^{2+} ions appear at positions $\frac{1}{3}\frac{2}{3}$ 2.67. Clearly, each Mg^{2+} ion is bonded also to oxygen atoms at a height z = 1.43Å. However, more CO_3^{2-} groups arise at a height of 3.91Å and are distributed about the points 0, 0, 3.91. Consequently, each Mg^{2+} ion is also bonded to six oxygens. As before, the oxygens at z = 3.91Å form extended sheets normal to the c-axis. This buildup of sheets of atoms, with Mg^{2+} and Ca^{2+} ions sharing the same neighboring oxygen atoms, continues the entire length of the c-axis (c = 16.00Å) within the unit cell. A view normal to the c-axis is shown in Fig. III-16. The shorter distance between Mg^{2+} - CO_3^{2-} planes arises from the smaller radius of the magnesium ion. The above layering, of course, extends throughout the entire (macroscopic) crystal of dolomite.

Since each Ca^{2+} ion shares a common oxygen atom with a Mg^{2+} ion, in half-calcining, each CO_3^{2-} ion must break down to form O^{2-} ions. An alternative way to view this is to remember that the oxygen atoms are symmetrically equivalent; that is, they are derived from an 18-fold set. Figure III-17 shows a view of a possible mechanism for half-calcination based upon the above structure.

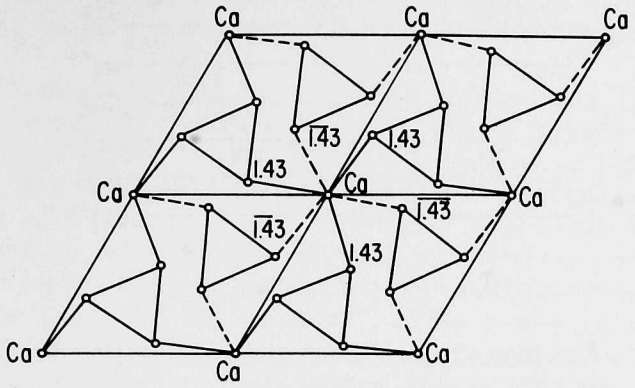

Fig. III-14. Ca at 000.

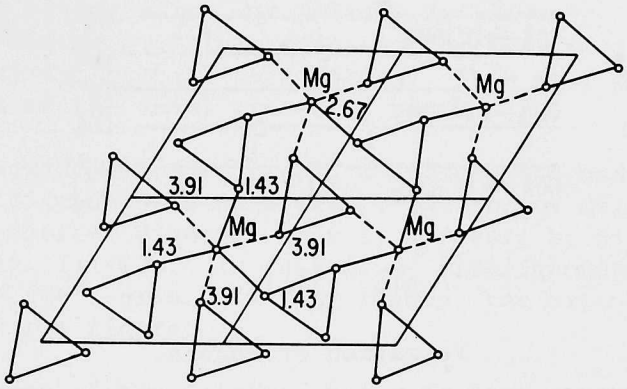

Fig. III-15. Mg at $\frac{1}{3}$ $\frac{2}{3}$ 2.67.

In Fig. III-17, each CO_3^{2-} ion is depicted as breaking down to form O^{2-} ions. A Mg^{2+} ion combines with O^{2-} to form MgO, and since Mg^{2+} ions are near each other (corresponding to reasonable metal-metal distances) MgO nuclei can form readily. On the other hand, the $CaCO_3$ should also form easily since it is stable under the half-calcining conditions and the Ca^{2+} positions are close to those in the related dolomite configuration. Diffusion of Mg^{2+} ions or MgO from neighboring sheets can occur, but in this case, the formation of calcite sheets can act as barriers to the diffusion. Hence, there may be a limited buildup of MgO crystallites along the c-axis, but extended sheets or bands could occur in two dimensions normal to the c-axis. An idealized situation is shown in Fig. III-18.

However, in addition to the above picture, dolomite is expected to exhibit a mosaic structure, a feature it has in common with many crystals. This consists of faults, manifest as defects and dislocations, which will be a factor in hindering the alignment of the half-calcined crystallites. These regions can become pathways for diffusion of MgO to build up to macroscopic thickness, leading to stringers or, simply, aggregates of MgO. It remains to

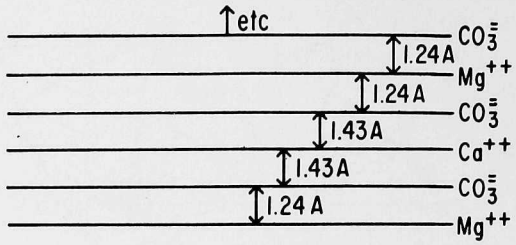

Fig. III-16.

Distribution of Ions Normal to c-axis Hexagonal.

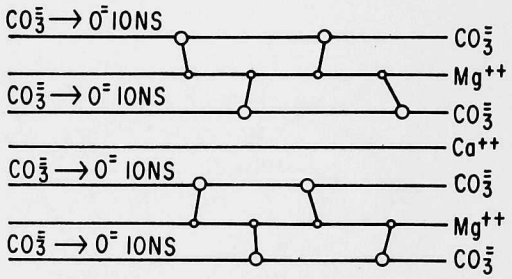

Fig. III-17.

Formation of Phases.

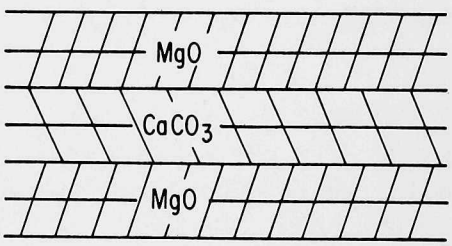

Fig. III-18.

Layering of Phases Showing Alternation of MgO and $CaCO_3$ Bands After Half-Calcination.

be determined if the stringers are indeed composed of MgO or have their origin in another process, as for example, cracks within a crystallite.

Nevertheless, the limits of growth imposed by the alternation of MgO and $CaCO_3$ within a crystallite to produce bands or sheets as depicted in Fig. III-18 would account for the small crystallite sizes observed for these phases. There is, however, a difference in the subsequent steps associated with half-calcining. MgO is cubic with a structure not compatible with that of either the dolomite or calcite structures, whereas calcite not only is compatible, but exhibits three equivalent directions. As indicated above, the 104 reflection of calcite was found to be "spotty." This plane corresponds to the three natural cleavage faces of $CaCO_3$, and the spottiness arises from the tendency of the crystallites to align normal to the 104 direction. If it is considered that the dolomite crystals have some mosaic character, and if, in addition, new defects are introduced during calcination, it might be expected that the reformed crystals of $CaCO_3$ will show configurations as indicated in Fig. III-13d, in which sections of crystals are displaced along the c-axis. In addition to the various defects, dolomite may contain impurity ions that can replace Ca and Mg atoms at the cation structure sites. At elevated temperatures, the thermal motion may become so anisotropic that certain metal-oxygen bonds may break preferentially during half-calcination. This will not change substantially the features of the model presented here.

Thus, stacking disorder within a crystallite and stacking disorder between the crystallites can be considered, the latter arising from their attempt to align. Another disorder arises, however, by virtue of the symmetry. This is shown in Fig. III-13e. In this case, misalignment can arise in a direction normal to the c-axis. In this figure, the extended sheets of MgO are in the plane of the figure.

The tendency of the calcite sheets to form oriented crystals, but leading to misalignment, could account for the undulatory nature of the extinction under polarized light. The model, in addition, suggests a variety of pores that could exist. Of particular interest is the pore configuration shown in Figs. III-13d and III-13e. The regions "c" have been defined as pores. Strictly speaking, these are regions of incomplete bonding--unsatisfied bonding--because of structure discontinuity across a boundary and may be the origin of van der Waals or other bonding to cause orientation along specified crystallographic directions. The pores "c" could well be regions of high reactivity to SO_2.

The model developed above has been established on the basis of limited x-ray diffraction and microscopic studies and, consequently, has many limitations. The pore blockage and barrier diffusion schemes are over-simplified. Changes in molecular volumes produce dynamic changes in channeling and pore makeup. The formation of $CaSO_4$ apparently does not occur by a simple process. Results of infrared studies of sulfation[34] show that complex sulfates build up on the surfaces of CaO. These sulfate layers could well be responsible for some limitation of continued sulfation. The nature of processes responsible for stone hardness and adherence must also be considered. Possibly, the formation of stable intermediate compounds, developed by an epitaxial mechanism, may lead to adherence, and the epitaxial layers could also participate as diffusion barriers. Finally, as will be shown, the degree of preferred orientation of the calcite varies with calcining conditions. Thus,

Figs. III-13c, III-13d, and III-13e may not be representative of the grain makeup. The model should, therefore, be looked upon as a guide, subject to modification as more information is obtained.

D. Half-Calcination Reaction (B. R. Hubble and S. Siegel)

In experiments carried out to help establish a structural model, it was noted that the $CaSO_4$ seemed to exhibit the small crystallite size or disorder present in the $CaCO_3$--certainly the small crystallite size-- and that the stone hardens substantially during sulfation with little change in shape. It was suspected, therefore, that some of the larger pore configurations are maintained during sulfation. However, other pore or channel arrangements change continuously, since the molecular volumes of CaO, $CaCO_3$, and $CaSO_4$ differ, leading to different space-filling requirements as reactions proceed. It seems evident, therefore, that when the stone is cycled through a series of sulfation and regeneration reactions and returned to a starting material, the regenerated material could exhibit an extensively modified micropore configuration compared with that in the original half-calcined stone. A question then arises as to whether a starting material with good sulfation characteristics can be regenerated to a starting material having the same characteristics--that is, can a good morphology be retained?

Preliminary results on the carbonation reaction presented below suggest that the regeneration process does not go to completion. This raises the question whether the morphology of half-calcined dolomite can have an effect on the extent of regeneration reactions. To resolve some of these problems, several experiments have been performed to study the modification of starting dolomite in order to obtain morphological information on half-calcined 1337 dolomite that can be correlated later with rates of the chemical reactions of interest. The experimental variables for the half-calcination reaction, Eq. (6), are temperature and CO_2 partial pressure.

In this systematic study of the calcination reaction and the morphology of the resulting half-calcined material, the following series of experiments was performed. 1337 dolomite was half-calcined at one-atmosphere pressure in an environment of 100% CO_2 at 640°C, 660°C, 680°C, 700°C, 720°C, and 740°C. Calcination of 1337 dolomite was also performed in an environment of 40% CO_2 at 640°C. The kinetic results obtained are shown in Fig. III-19 and III-20, where percent conversion is plotted against time. Some error may exist in these plots because of the manner in which percent conversion was calculated. Since many of the experiments did not go to completion, it was not possible to determine what weight loss corresponded to exactly 100% conversion. A common value was chosen for these calculations, corresponding to the average value obtained in many previous half-calcination experiments. Figure III-19 summarizes the results for an environment of 100% CO_2. Figure III-20 summarizes the results at 640°C for environments of 40% and 100% CO_2.

The half-calcination technique employed in this program has been to heat the dolomite in an environment of 40% CO_2 to 800°C at a rate of about 25°C/min. Under these experimental conditions, the half-calcination reaction has been completed in 20 to 25 min. From Fig. III-19, it can be seen that in the environment of 100% CO_2, the reaction rate is much lower, even at the highest temperature, 740°C. It is also apparent that in 100% CO_2 the reaction rate increases rapidly with temperature, particularly at temperatures above 660°C.

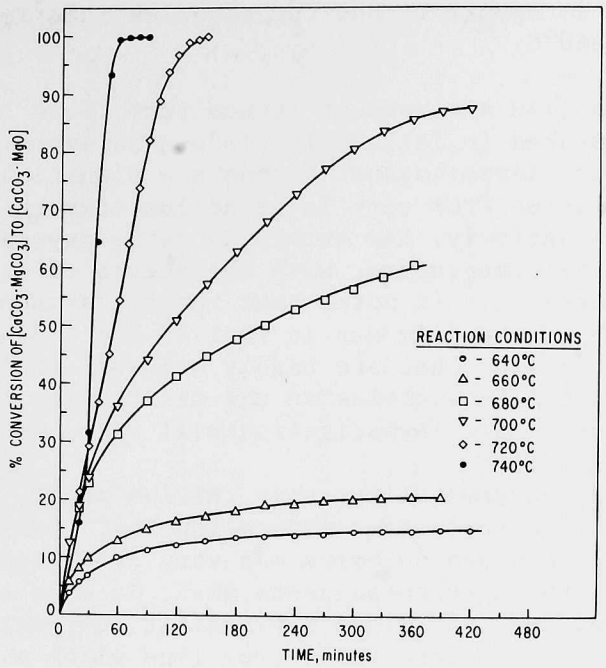

Fig. III-19.

Plots of % Conversion vs Time for Half-Calcination of 1337 Dolomite Under 100% CO_2 Environment as a Function of Temperature.

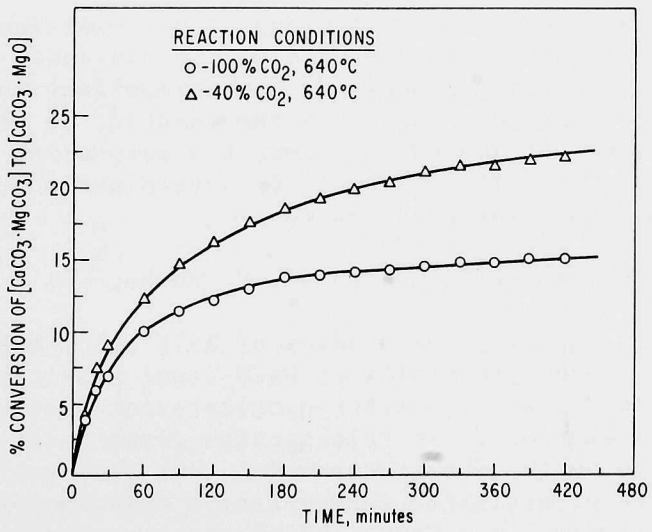

Fig. III-20.

Plots of % Conversion vs Time for Half-Calcination of 1337 Dolomite at 640°C as a Function % CO_2 Environment.

From Fig. III-20, it is apparent that the reaction rate increases with CO_2 partial pressure at 640°C.

The x-ray diffraction analyses of stones from these half-calcination experiments are summarized in Table III-3. For the experiments carried out in 100% CO_2, the following morphological trends are significant: The $CaCO_3$ pseudo-crystal size varies from very large at low temperature to small at high temperatures, or alternatively, the extent of $CaCO_3$ crystallite preferred orientation varies with temperature, with the degree of orientation decreasing as temperature increases. It is noted that the appearance of fairly large pseudo-crystals in the x-ray film may in fact be due to very small crystallites, perhaps 1000Å or so in size, that are highly oriented to form these crystals. The rapid drop-off in the intensities of the diffraction lines observed indicates some disorder. A microscopic investigation will yield more information on this.

In 100% CO_2, the MgO crystallite size remains small, regardless of the temperature. However, there is some indication that the intensities of the MgO lines in the half-calcined dolomite may vary from experiment to experiment. Visual examination of the pattern suggests that, in some cases, particularly at large scattering angles, the lines may exhibit sharpening. If this sharpening is real, and this can be determined from line width measurements, it may be a consequence of crystal growth.

A comparison of the extremes (*i.e.*, calcination at 100% CO_2 and 640°C and calcination at 40% CO_2 and 800°C) indicates a large difference in morphology. The observations when calcination took place at 100% CO_2 and 640°C reveal the largest pseudo-crystals (highly oriented) of $CaCO_3$, whereas calcination at 40% CO_2 and 800°C results in small pseudo-crystals of $CaCO_3$ (slight preferred orientation). The effect of CO_2 partial pressure at 640°C is much less drastic, in that the 40% CO_2 half-calcination leads to only smaller pseudo-crystals of $CaCO_3$--although still relatively well oriented.

These results show that the morphology of half-calcined dolomite can be controlled to some extent by choosing the conditions under which the reaction is carried out. By comparing kinetic data and resultant morphology of half-calcined stones, it is obvious that when the reaction is performed under conditions for which the reaction rate is low, the morphology indicates larger pseudo-crystals of $CaCO_3$. It remains to be determined whether the MgO structure is affected in a similar fashion.

E. Sulfation During Half-Calcination (L. H. Fuchs,* B. R. Hubble, S. Siegel)

In the previous section, the studies of half-calcination described were intended to isolate those properties of $CaCO_3$ (and possibly MgO) related to crystallite size and degree of preferred orientation that might have a bearing on the kinetics of reactions. In this section, experiments are discussed which were suggested by the structural model that proposes that MgO bands and stringers in calcite crystallites formed from a dolomite crystal can act as barriers to SO_2 diffusion into $CaCO_3$. Such an occurrence could explain the

---

*Chemistry Division, ANL.

Table III-3. Summary of X-ray Diffraction Analyses of 1337 Dolomite Stones from Half-Calcination Reaction Experiments.

Sample History	$CaMg(CO_3)_2$		MgO		$CaCO_3$		Quartz
	Crystallite Size[a]	Quantity	Crystallite Size	Quantity	Crystallite Size[b]	Quantity	Quartz
100% CO_2 at 640°C for approx. 7 hr	large	major	small	very minor	larger, very oriented	minor	
100% CO_2 at 660°C for approx. 7 hr	large		small	minor +	large, oriented	minor +	very minor
100% CO_2 at 680°C for approx. 6 hr	large	decrease	small	medium	large, less oriented	medium	medium
100% CO_2 at 700°C for approx. 2 1/4 hr	large		small	medium	medium, slight orientation	medium	
100% CO_2 at 700°C for approx. 7 hr	large	minor	small	major	small, slight orientation	major	very minor
100% CO_2 at 720°C for 2 1/3 hr	---	none	small	major	small, slight orientation	major	
100% CO_2 at 740°C for 1/2 hr	---	none	small	major	small, slight orientation	major	
40% CO_2 at 800°C for approx. 25 min	---	none	~1000Å	major	small, slight orientation	major	trace
40% CO_2 at 640°C for approx. 7 hr	large	major	small	minor	large, oriented	minor	

[a] It should be noted that the origin of the apparently larger dolomite crystals may be the result of initial decomposition of the finely divided material leaving the larger crystals to stand out in the diffraction pattern.

[b] Lack of resolution of the α, α_2 doublet serves to indicate that the crystallite size is the order of 1000Å in all experiments. However, they undergo preferred orientation so as to simulate single crystals. At the beginning of this series, the orientation is pronounced enough to produce fairly well-defined pseudo-crystals. However, as the temperature increases, the pseudo-crystals become smaller, with the orientation becoming more random.

nonuniform sulfation of $CaCO_3$ crystallites. The purpose of these experiments was to determine if free ions or MgO molecules not yet fully aggregated into the characteristic three-dimensional structure would react with SO_2 and O_2 during the reaction time of the half-calcination process.

The experiments were performed as follows: The flow of the sulfation reaction gas mixture over the 1337 dolomite stones was started at a temperature below that at which the half-calcination reaction would normally begin; then the temperature was raised to that at which half-calcination under 40% CO_2 partial pressure would proceed. In this experiment, therefore, sulfation and half-calcination reactions proceeded simultaneously (thus closely simulating conditions in a fluidized-bed combustion process).

X-ray diffraction analysis of the resulting reaction product showed the presence of a new phase not previously reported in the sulfation of sorbent additives--$Mg_3Ca(SO_4)_4$.* This compound was first reported by J. J. Rowe *et al.*[35] Following the x-ray identification of this new phase formed in the sulfation-half-calcination experiment, the compound was also confirmed by optical microscopic study of the reacted stone. Its distribution in the stone was established, and microscopic amounts were removed for additional x-ray investigation, leading to verification of the identity of the phase. The amount of compound formed varied from experiment to experiment, but in at least one case a substantial amount was formed. Also, in a recent experiment in which a synthetic dolomite of composition $CaCO_3/MgCO_3>1$ was half-calcined and then sulfated, examination showed a major amount of $Mg_3Ca(SO_4)_4$.

The experiment using a particular synthetic dolomite suggests that the binary compound can be formed under various reaction conditions. Therefore, it is concluded that the chemistry associated with the formation of this compound may be a new and significant variable in the cyclic use of dolomite in sulfur emission control chemistry. The formation of $Mg_3Ca(SO_4)_4$ could indicate a breakdown of the MgO sheets. This merits further study, but for the present, difficulty is encountered in making a quantitative estimate of the amount of this compound present. However, information from optical microscopy is available on its location within the 1337 dolomite particles. Figures III-21 and III-22 show representative photomicrographs of particles containing the compound. The occurrence of the binary sulfate, $Mg_3Ca(SO_4)_4$, is found to be confined to those surfaces within the particles that are exposed to the gas during the reaction (darkened areas); it occurs as thin rims on the peripheries and on the walls of interior cavities. In addition, $CaSO_4$ and MgO have always been present as associated phases on x-ray samples taken from these rims. The occurrence of this phase is of interest for two reasons: (a) sulfation during calcination is the more realistic situation for the reaction of dolomite in a fluidized bed, and (b) the mineral huntite, $Mg_3Ca(CO_3)_4$, occurs in nature. One might speculate that huntite may be formed as a transient species and that this is the phase that in fact reacts with SO_2.

---

*The identification of $Mg_3Ca(SO_4)_4$ was made by B. Tani, Analytical Chemistry Laboratory, CEN.

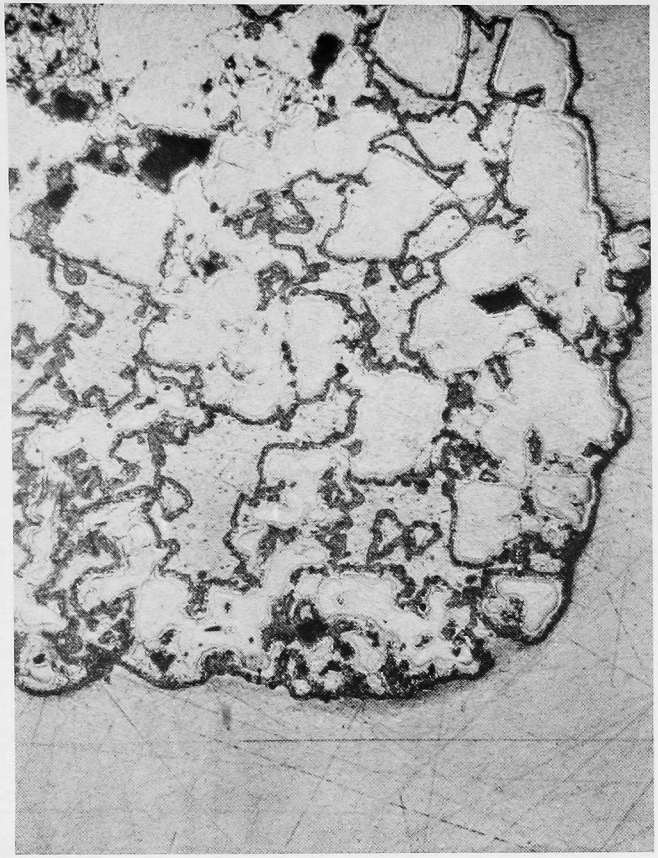

Fig. III-21.

1337 Dolomite Particle Showing Location of [$CaSO_4 \cdot 3MgSO_4$] within the Particle. Dark ribbons are [$CaSO_4 \cdot 3MgSO_4$] and have been discolored by exposing sample to air.

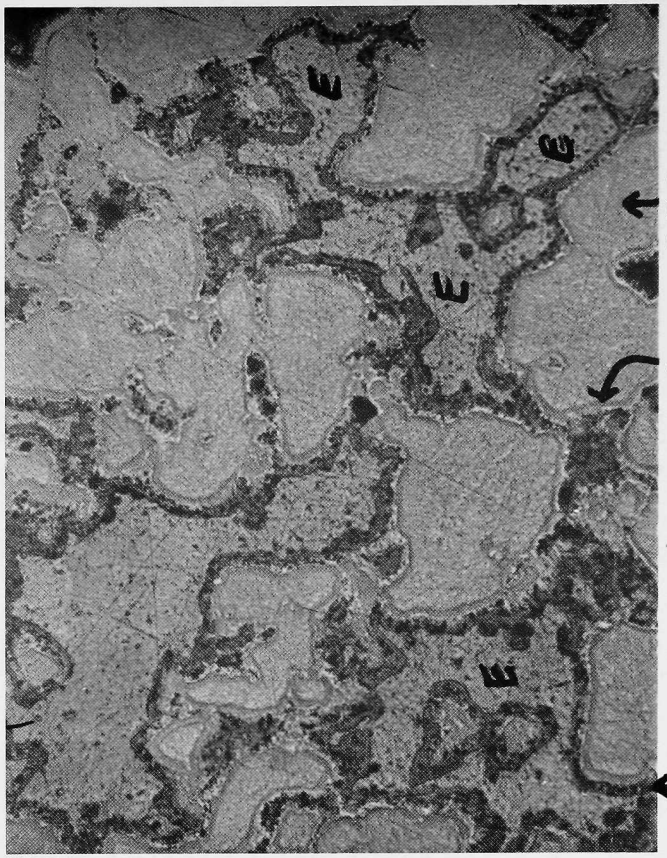

Fig. III-22.

Another 1337 Dolomite Particle Showing Location of [$CaSO_4 \cdot 3MgSO_4$] Within the Particle.

It is hoped that $Mg_3Ca(SO_4)_4$ and $Mg_3Ca(CO_3)_4$ can be prepared in sufficient quantity in order to study their properties, particularly to note if the carbonate reacts with SO_2 directly to form the sulfate double salt. If this occurs, a pretreatment of the dolomite that would lead to the production of substantial amounts of $Mg_3Ca(CO_3)_4$ might be considered.

F. Sulfation of Synthetic Dolomite (L. H. Fuchs,* H. R. Hoekstra,* B. R. Hubble, S. Siegel)

1. Modification of the Structure of Dolomite

In the above discussions, the possible role of MgO acting as a barrier to diffusion of SO_2 in the un-reacted half-calcined dolomite has received primary consideration, but the role of the various pores must also be examined. In Fig. III-13 voids are depicted between the various $CaCO_3$ and MgO aggregates. On sulfation, these voids can be reduced in size because of the larger molecular volume of $CaSO_4$. This model is useful in explaining the variation in the yield of $CaSO_4$ for various concentrations of SO_2 in the gas stream. Thus, $CaSO_4$ will form within $CaCO_3$ crystals (as demonstrated by the microscopy studies, Fig. III-9b). The $CaSO_4$, along with the MgO, could then become the barriers to diffusion. If the SO_2 concentration is low, heat developed during the reaction can be dissipated to the $CaCO_3$-$CaSO_4$-MgO aggregate. Under these conditions, the voids are reduced in size as $CaSO_4$ builds up. However, if the SO_2 concentration is high, the heat of reaction is not dissipated rapidly enough; as a result, stresses continuously rupture the $CaCO_3$-$CaSO_4$-MgO aggregate to expose fresh $CaCO_3$, thereby increasing the yield of $CaSO_4$. Under this condition, new voids would be created within the $CaCO_3$-$CaSO_4$-MgO complex.

If pore size within the half-calcined dolomite and the morphology of the $CaCO_3$ crystals, as well as the nature of the MgO matrix, are important in establishing the nature of the sulfation curve, it is possible to achieve a high degree of variability for these quantities by the use of synthetic dolomites.

Goldsmith and his co-workers (University of Chicago) have published extensively on the $CaCO_3$-$MgCO_3$ phase diagram and on the production of dolomites. In particular, Graf and Goldsmith[36] have described the production of synthetic dolomites, including a series of compounds called protodolomites. Their work is not reviewed here in detail, but one example is given below.

With certain starting materials, treated in the presence of H_2O and CO_2 at temperatures from 25°C to 450°C, a variety of dolomites can be produced. At elevated temperatures, dolomite is formed in which Ca^{2+} and Mg^{2+} are ordered in the structures. At lower temperatures, a dolomite-like material, protodolomite, is formed. X-ray studies by Graf and Goldsmith on these protodolomites reveal the absence of superstructure lines characteristic of dolomite, variable displacement in the 006 reflection over narrow compositional changes, and general diffuseness in the x-ray reflections. They interpret the results as indicating that the ordering of the calcium and magnesium atoms is not

---

*Chemistry Division, ANL.

consistently maintained and suggest that the ions may segregate into calcium-rich or magnesium-rich planes that do not occur in simple succession. They also consider the possible existence of small domains that approach ideal dolomite in composition and ordering but with the composition of a given cation plane changing from domain to domain.

The variability in the position of the 006 line relative to other diffraction lines for slight variations in the Ca/Mg ratios indicates that distances between planes normal to the c-axis vary. In pure dolomite, the Ca-6(0) distances are 2.40Å, whereas for Mg-6(0) they are 2.11Å. These are values to be expected on the basis of ionic radii sums and therefore indicate no unusual bonding variation. The variability of the 006 reflection thus suggests instability or strain in the structure. Hence, such a structure can lead to a starting material with considerable randomness in the Ca^{2+} and Mg^{2+} positions, small crystallite size, and strain. One might speculate that half-calcination of this protodolomite would lead to pore configurations and aggregation characteristics of the $MgO-CaCO_3$ mixture that differ from those reported for the presently used dolomite. In addition, the activity of $CaCO_3$ may be substantially altered.

Accordingly, a number of synthetic dolomites have been produced. Only one has been used in systematic TGA experiments, and the results are encouraging. Sulfation curves and two regeneration cycles are reported in this section. The starting material was compressed into a pellet and fractured into numerous pieces. At the start of sulfation, the fragments were quite soft, comparable in texture with natural dolomite. However, after the third sulfation cycles, the fragments were found to be very hard, and microscopic examination revealed a very fine grain size with a small degree of porosity existing within the grains. In this case, diffusion may be by way of grain boundaries.

2. Chemistry of Synthetic Dolomites

A number of protodolomite syntheses have been carried out by mixing 1M solutions of $MgCl_2$ and $CaCl_2$, then adding a 10% excess of K_2CO_3 to precipitate the alkaline earth ions. After the precipitates were allowed to stand for 6 to 96 hr, at either 25°C or 60°C, they were centrifuged and washed repeatedly with water until the rinse water gave a negative Cl^- test. The precipitates were then dried at 100°C and finally at 200°C to constant weight.

The products were investigated by x-ray diffraction and by infrared and thermal (DTA-TGA) analysis. The results tend to confirm the work of Berner,[37] which indicates that the presence of Mg^{2+} ions slows the crystal growth of calcite (dolomite) but does not affect aragonite crystallization. In addition, magnesium does not enter the aragonite structure as it does with calcite to form dolomite. As a result, most syntheses resulted in a mixture comprising aragonite and basic magnesium carbonate as the principal products, with minor amounts of protodolomite. Results were not always reproducible; one preparation contained a major amount of dolomite.

Attempts to increase the dolomite concentration by adding K_2CO_3 to the $CaCl_2$ solution before $MgCl_2$ was added were not successful. Apparently, the initial gel-like precipitate formed at 25°C subsequently recrystallizes to aragonite and/or dolomite. Further work is required to determine conditions under which protodolomite synthesis is maximized.

The dolomite-aragonite ratios can be determined by x-ray diffraction analysis and can be approximated quickly from the infrared spectrum. One of the carbonate bending modes in aragonite appears at ~850 cm^{-1}, while the corresponding dolomite absorption occurs at 870 cm^{-1}.

Thermal analysis of the products indicates that decomposition occurs at the following temperatures when samples are heated in air:

$$Mg(OH)_2 \cdot MgCO_3 \xrightarrow{200^\circ} MgO + MgCO_3 \xrightarrow{300^\circ} MgO \quad (25)$$

$$CaCO_3 \xrightarrow{600^\circ} CaO \quad (26)$$

$$MgCa(CO_3)_2 \xrightarrow{525^\circ} MgO + CaCO_3 \xrightarrow{600^\circ} MgO + CaO \quad (27)$$

3. TGA Sulfation and Regeneration Experiments

A few experiments of a survey nature have been performed to obtain information on the reactive properties of the synthetic dolomites. The particular synthetic dolomite used was prepared with a composition of $CaCO_3/MgCO_3>1$. The purposes of the experiments were (a) to establish whether the synthetic dolomite would react with SO_2, (b) to determine if the sulfated form could be reduced and carbonated, and (c) to gain information on the integrity of the synthetic upon being carried through a number of these reactions.

Since the synthetic was in powder form, it was formed into thin pellets using a press and 17,000 lb/in.^{2} pressure. These pellets were then broken into small chips not more than a few millimeters in size. Microscopic observations revealed a soft texture similar to that of natural dolomite. The small chips were used in the following TGA studies.

In the first sulfation experiment, the synthetic dolomite was half-calcined and reacted with 0.39% SO_2, 5% O_2, 15% CO_2, and 2.9% H_2O. A 77% conversion to the sulfate in a reaction time of 150 min suggests that its reactivity is at least as high as that of 1337 dolomite. The TGA results were confirmed by x-ray diffraction analysis. Microscopic examination showed that the sulfated form of the synthetic had little pore structure, in contrast to the large pore structure system of 1337 dolomite. However, other sulfated synthetic dolomites have been found to exhibit porosity.

This initial sulfation experiment was followed by a series of reactions based on the two-step regeneration method, Eqs. (8) and (9), using the same synthetic starting material. In this study, the synthetic dolomite chips were sequentially fully calcined, sulfated, reduced, carbonated (cycle 1); fully calcined, sulfated, reduced, carbonated (cycle 2); and fully calcined, sulfated (cycle 3). Figures III-23, III-24, and III-25 summarize the TGA results. Figure III-23 presents plots of weight gain vs. time for the three sulfation reactions, Fig. III-24 presents plots of weight loss vs. time for the two reduction reactions, and Fig. III-25 presents plots of weight gain vs. time for the two carbonation reactions. X-ray analysis of materials obtained at the end of this series of reactions showed $CaSO_4$ and MgO to be the major phases present.

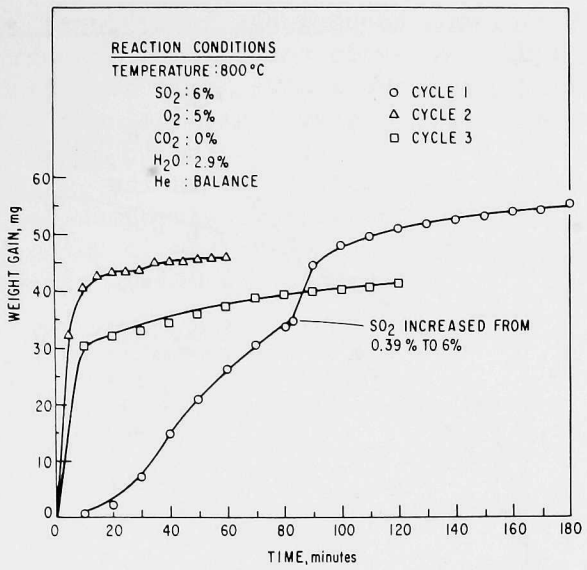

Fig. III-23.

Plots of Weight Gain vs Time for Sulfation Reaction of Fully-Calcined Synthetic Dolomite.

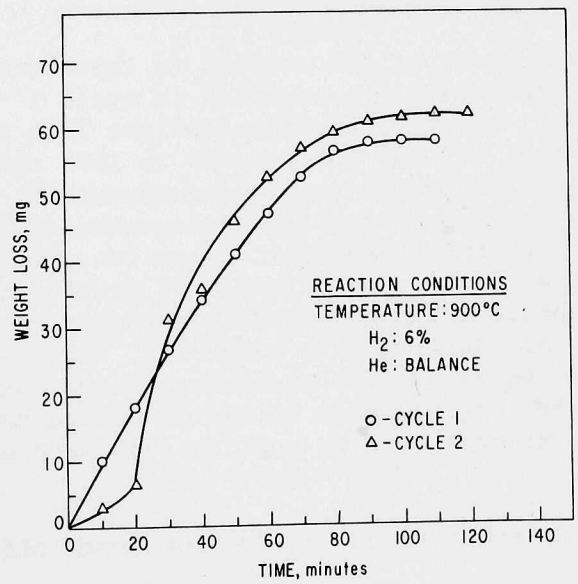

Fig. III-24.

Plots of Weight Loss vs Time for Reduction Reaction of Synthetic Dolomite.

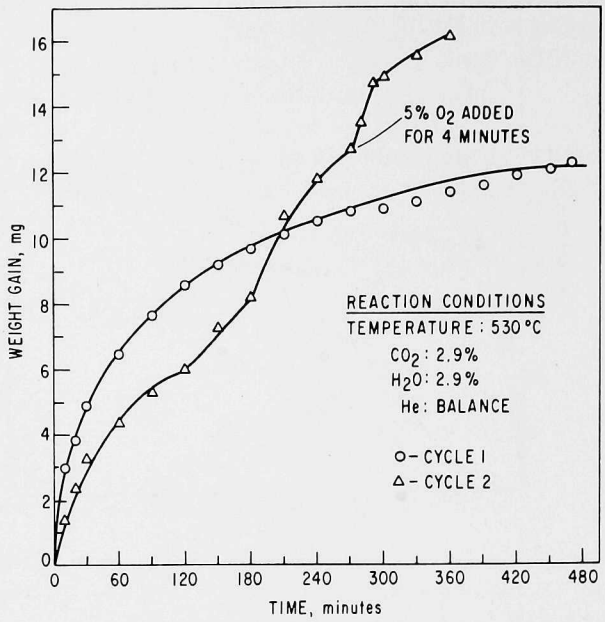

Fig. III-25.

Plots of Weight Gain vs Time for Carbonation Reaction of Synthetic Dolomite.

The following observations related to these results are noted. The total weight gain for the sulfation reaction in cycle 1 (Fig. III-23) corresponds to 95% conversion; however, the total weight loss for the reduction reaction in cycle 1 (Fig. III-24) corresponds to 160% conversion. This result is difficult to explain and is not presently understood. Although these TGA curves are not as smooth as curves obtained for studies involving 1337 dolomite, they serve to indicate that the synthetic dolomites undergo the reactions related to cyclic use as sorbent materials. Of particular interest is the observation that synthetic chips appeared to harden, even at the end of one sulfation reaction. Yet, despite this hardening, they retained their good reaction properties in terms of final weight gains or losses in subsequent reactions. This result suggests that integrity of synthetic dolomites may not be the limitation one might expect in applications such as fluidized-bed combustion processes.

Continued TGA and chemical studies of synthetic dolomites are planned.

The increased rate of weight gain observed in the carbonation reaction of cycle 2 when O_2 was added to the reactive-gas stream for a short time suggested a source of error that might exist in performing such cyclic experiments. Observed weight gains for the sulfation reaction may in part be due to the oxidation of the sulfide form of the sorbent, which still exists when 100% conversion has not been achieved in the carbonation reaction. An experiment confirming this possibility was performed with 1337 dolomite that had been

half-calcined, sulfated completely, and reduced completely. The results of the experiment on the reduced form of the stone are shown in Fig. III-26 where weight gain is plotted against time. The stones were first reacted with 5% O_2 at 800°C for one minute, resulting in a weight gain; then the stones were cooled to 750°C before again being reacted with 5% O_2 for an additional 25 minutes; and finally 3% SO_2 was added to the 5% O_2 for an additional 100 minutes and an additional weight gain occurred. X-ray diffraction analysis of stones from the end point of the experiment indicated that the major phase present was $CaSO_4$; very little CaS was observed.

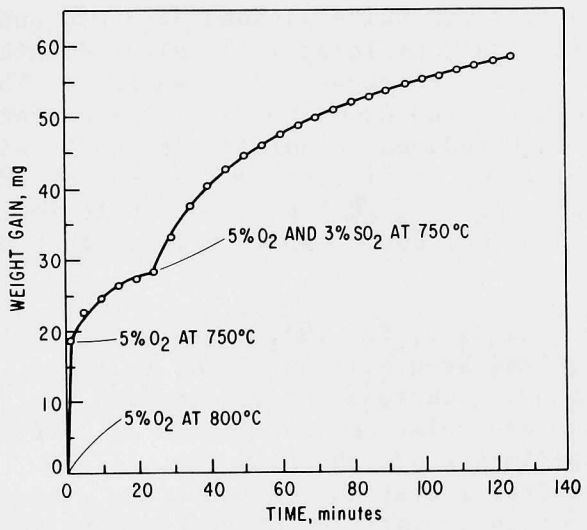

Fig. III-26.

Weight Gain vs Time for CaS·MgO Reacting with O_2, and O_2 and SO_2.

G. Two-Step Regeneration Process (W. I. Wilson)

The two-step process to regenerate a reactive additive from the sulfated form of the sorbent reagent material is indicated by Eqs. (8) and (9)

$$[CaSO_4 \cdot MgO] + 4H_2 \rightarrow [CaS \cdot MgO] + 4H_2O \quad (8a)$$

$$[CaSO_4 \cdot MgO] + 4CO \rightarrow [CaS \cdot MgO] + 4CO_2 \quad (8b)$$

$$[CaS \cdot MgO] + H_2O + CO_2 \rightarrow [CaCO_3 \cdot MgO] + H_2S \quad (9)$$

Equation (8) represents the reduction reaction and Eq. (9) the carbonation reaction. Preliminary TGA kinetic experiments on these two reactions and the results obtained are reported here.

In the TGA experiments on the reduction reaction, the reactive gas mixtures were blended from pure helium and a 6% H_2 in He mixture, using rotameters in the manner previously described in detail for the sulfation reaction mixtures.[31]

Initial attempts to reduce sulfated 1337 dolomite to the sulfide at 800°C were not successful. Experiments performed using analytical-grade $CaSO_4$ in place of the sulfated 1337 stone indicated that temperatures near 900°C were required to reduce the sulfate to sulfide at a pressure of one atmosphere, when dilute hydrogen in helium was used as the reducing gas.

A series of experiments was then performed by the following procedure: A sample of dolomite 1337 was half-calcined at 850°C and sulfated at 800°C, using a simulated flue gas containing 1.1% sulfur dioxide, until 65 to 75% of the available calcium had been converted to sulfate. The stone was then calcined to convert the unreacted $CaCO_3$ to CaO. The sulfate in the partially converted stone was then reduced to sulfide at 900°C using various hydrogen concentrations and humidity conditions. The results, shown in Fig. III-27, indicated that the reaction (Eq. 8a) goes to completion. Data obtained with H_2O present are not plotted, but clearly indicate that H_2O does not affect the reaction rate.

The carbonation reaction, Eq. (9), has also been studied, using 1337 dolomite samples that had been half-calcined, sulfated, and reduced by the procedure outlined above. Carbonation was carried out at 530°C, using mixtures of helium and various equimolar concentrations of carbon dioxide and water. Results of these experiments are shown in Fig. III-28. The data are more scattered than those from sulfation and reduction experiments. This result might be expected because preparation of the sulfide involves a number of steps and it is unlikely that uniform starting materials for the recarbonation

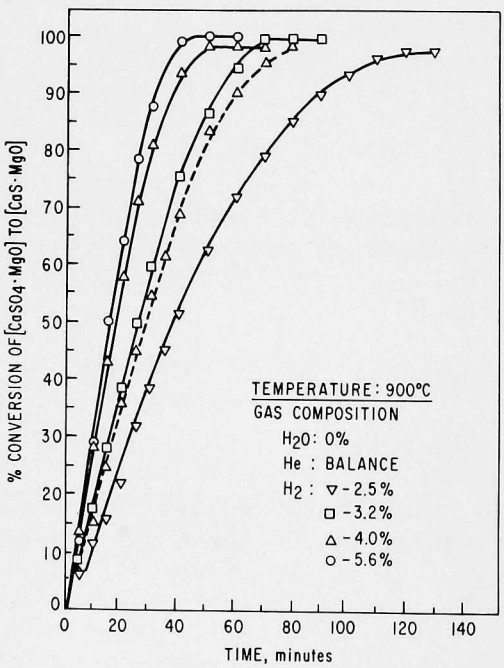

Fig. III-27.

Plots of % Conversion vs Time for Kinetic Data for the Reduction of Sulfated Dolomite and Reagent Grade Calcium Sulfate by Hydrogen (Solid lines represent various H_2 concentrations used with dolomite; broken line represents 4.0% H_2 with analytical reagent-grade $CaSO_4$ pellet).

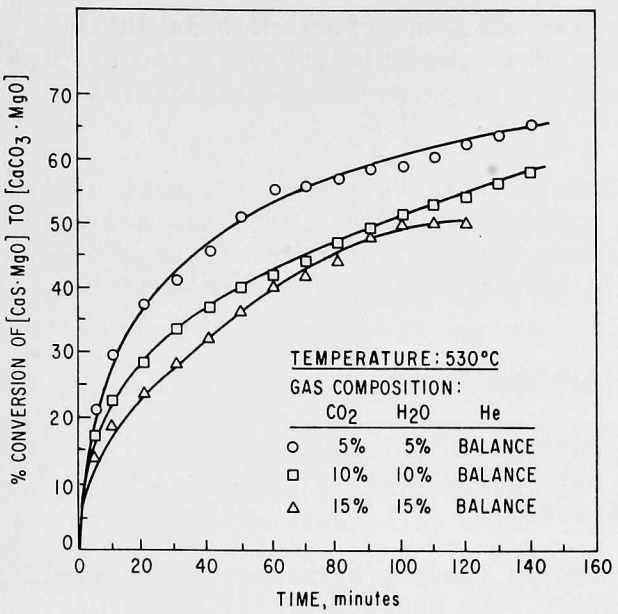

Fig. III-28.

Percent Conversion vs Time for Various Equimolar CO_2:H_2O Concentrations at 530°C Employing Kinetic Data for the Carbonation Reaction.

step were obtained. Also, problems associated with H_2O vapor concentrations, obtained by the thermostated humidifier technique referred to earlier, make these results open to some doubt. This reaction will be investigated thoroughly with the experimental apparatus modified to replace the thermostated humidifier technique.

H. Sulfate-Sulfide Regeneration Method (L. H. Fuchs,* H. R. Hoekstra,* B. R. Hubble, S. Siegel)

The feasibility of the solid-solid reaction

$$3CaSO_4 + CaS \rightarrow 4CaO + 4SO_2 \qquad (28)$$

is documented;[38,39,40] in fact, the reaction has been used as a method of producing SO_2. In addition, this reaction has been the subject of study from time to time as a possible scheme for regenerating dolomite or limestone.[39,40] However, there is in the literature no detailed examination of the process--perhaps because it could entail a solid-solid reaction mechanism which depends on pore size and the associated separation of the reacting phases.

The initial interest in this reaction was based on the observation that a sulfated synthetic dolomite showed no visible pore structure within the sulfate crystals, suggesting that the reacting solid species would be in intimate contact. In addition, microscopic observations indicated that the sulfation reaction in 1337 dolomite occurs in small grains, separated by the larger pores. Based on this information, it was speculated that the large

---

*Chemistry Division, ANL.

pores found in dolomite may not necessarily play an important role in the various diffusion processes. To consider this possibility, a series of preliminary TGA/x-ray diffraction experiments were performed employing 1337 dolomite.

The procedure used in these experiments is as follows: A sample of 1337 dolomite was sulfated completely after half-calcination. This was followed by the reduction with H_2 at 900°C to reduce the sulfate form of the stones to the sulfide, to obtain a 3:1 molar ratio as required by the chemical reaction given by Eq. (11)

$$3[CaSO_4 \cdot MgO] + [CaS \cdot MgO] \rightarrow 4[CaO \cdot MgO] + 4SO_2 \qquad (11)$$

This step was followed by heating the stones to about 950°C under a flow of one atmosphere of pure helium. Stones were removed at various stages of reaction (Eq. 11) for x-ray diffraction analysis.

A number of problems were encountered in these preliminary experiments. In initial attempts, the dolomite particles were not completely sulfated because of instrumental difficulties. This resulted in a substantial amount of residual CaO in the stones before the solid-solid reaction could take place. In addition, in the regeneration reaction, any or all of the phases (MgO, CaO, $CaCO_3$, $CaSO_4$, CaS, etc.) can be present in the x-ray diffraction patterns of the samples, leading to difficulty in interpretation of the data. In the past, visual examination of the x-ray diffraction patterns has permitted semi-quantitative estimates of growth or decrease of chemical species during a reaction. However, for this regeneration reaction, it became necessary to develop a method for quantitative measurements of various phases present in the diffraction patterns. A description of the x-ray technique developed for this purpose is described below. Use of the method on stones from a TGA run is then described.

The use of standards does not seem feasible at present, since standards cannot reproduce the line widths, disorder, or impurities present in a sample. Therefore, line intensities derived from the diffraction pattern of the particular sample under study must be used for quantitative measurements. This approach also has the advantage of eliminating the necessity of preparing large numbers of standards with various concentrations of the different phases.

The intensity expression for a powder diffraction line recorded by the Debye-Scherrer method is

$$I_{hkl} = K\, N^2\, p\, F^2_{hkl} \left(\frac{1 + \cos^2 2\theta}{\sin^2\theta \cos\theta}\right) V \qquad (29)$$

The constant, K, includes the wavelength and various fundamental constants. The remainder of the expression contains the crystallographic quantities. N is the number of unit cells per unit volume, p is the multiplicity of the reflection, the function within the parenthesis is the combined Lorentz-polarization factor, F_{hkl} is the crystal structure factor, and V is the volume

of material in the beam. The structure of the phase must be known in order to obtain F_{hkl}, which is derived from

$$F_{hkl} = \sum_n f_n e^{2\pi i(hx_n + ky_n + lz_n)} \tag{28}$$

where f_n is the atomic scattering factor for atom n; x_n, y_n, and z_n are the coordinates of the n^{th} atom; and hkl are the Miller indices. The structures of all the pertinent phases are known, and the F-values can accordingly be calculated readily from the structures.

Presently, the intensities of the lines produced in the powder diffraction pattern are deduced from densitometer tracings. The inherent errors of this method are approximately ±5-8%. A substantial error arises because of the nonlinear density characteristics of very weak or very intense lines, but this error can be reduced by selection of appropriate diffraction lines. Unfortunately, the overlap of lines is so severe that the analysis must be based on a limited number of specific reflections. In addition, resolution is lost because of the finite width of the densitometer beam, scattering by film grain, and other factors. Many of the errors will be eliminated when diffractometer techniques are developed.

If only two phases are present in the sample, the individual volumes can be determined easily. By choosing appropriate diffraction lines for the two samples of volumes, V_1 and V_2, one can write

$$I_1 = K_1V_1 \text{ and } I_2 = K_2V_2, \tag{31}$$

from which it follows that

$$\frac{I_1}{I_2} = K' \frac{V_1}{V_2} \tag{32}$$

Since $V_1 + V_2 = 100\%$, the individual volumes can be deduced readily. If three phases are present and the volume of one is invariant, the volume of the other two may likewise be determined.

Error estimates have been obtained by measurement of a pattern of a fully calcined dolomite. In this sample, only MgO and CaO need to be considered. The small amount of α-SiO_2 that is generally present in 1337 dolomite samples is insignificant. The following intensity ratios are observed and can be compared to calculated intensity ratios.

Line Pair	Ratio Calculated	Ratio Observed
CaO_{111}/MgO_{220}	1.67	2.05
CaO_{111}/MgO_{200}	0.894	0.916
CaO_{220}/MgO_{200}	1.50	1.25
CaO_{220}/MgO_{220}	2.90	2.80

The calculated intensity ratios are based on the composition of 1337 dolomite, *i.e.*, $Ca_{1.14}Mg_{0.86}(CO_3)_2$. In order to assess errors, the molecular weights of CaO and MgO have been computed from observed intensity ratios, using the above intensity expressions. These are shown in Table III-4, where the relative volumes have been obtained from the intensity ratios. The corresponding molecular weights have been normalized relative to the known molecular weights of CaO and MgO.

Table III-4. Summary of Molecular Weights Computed from Observed Intensity Ratios of Fully-Calcined 1337 Dolomite.

Line Pair	Relative Volume, CaO	Molecular Weight, CaO	Relative Volume, MgO	Molecular Weight, MgO
CaO_{111}/MgO_{220}	0.709	61.64	0.291	35.63
CaO_{111}/MgO_{200}	0.730	63.46	0.270	33.06
CaO_{220}/MgO_{200}	0.621	53.99	0.379	46.40
CaO_{220}/MgO_{220}	0.664	57.73	0.336	41.14
	Calculated Ave.	59.21	Calculated Ave.	39.06
	Actual	56.08	Actual	40.31
	Error	5.6%	Error	3.1%

Clearly, if several or more diffraction lines could be used in deriving volumes, the average weights determined from these lines would approach the actual weights more closely. However, in practice, it is necessary to consider the maximum error arising from one line pair. Thus, in the above table, the maximum error in determining the weight of CaO was 13%, whereas that for MgO was 18%. Errors ranging up to 20% or so must therefore be expected.

For half-calcined dolomite using only one reflection pair, the observed intensity ratio $ICaCO_{3_{113}}/IMgO_{220} = 1.14$, whereas the calculated value is 1.34. The observed ratio leads to molecular weights listed in Table III-5. In this case, the calculated molecular weights differ from actual values by about 9%, based upon one observation. Additional line pairs could not be used.

The above intensity expressions, utilizing the observed intensity ratios, were used to establish errors of the method, following the procedure outlined. In practice, these equations cannot be used conveniently, for at least three variable phases are present; CaO, $CaSO_4$, and CaS. Instead, working curves are employed, based on the fact that when only CaO and MgO, $CaCO_3$ and MgO, or $CaSO_4$ and MgO are present in the sample (corresponding to completely calcined, half calcined, or completely sulfated dolomites, respectively), the ratios of

Table III-5. Molecular Weights of $CaCO_3$ and MgO Obtained from Observed Intensity Ratios of Half-Calcined 1337 Dolomite.

Line Pair	Relative Volume, $CaCO_3$	Molecular Weight, $CaCO_3$	Relative Volume, MgO	Molecular Weight, MgO
$CaCO_{3_{113}}/MgO_{220}$	0.787	92.57	0.213	43.81
	Actual	100.09	Actual	40.31
	Error	7.5%	Error	8.7%

the calcium salt to the MgO line intensities represent maximum volumes of the particular calcium salt, if it is assumed that the volume of MgO is constant. For example, in a half-calcined dolomite, the various $ICaCO_3/IMgO$ ratios correspond to the maximum amount of $CaCO_3$ that can be found in the material. This maximum volume can be normalized to correspond to the volume of 1.14 moles of $CaCO_3$ or to the molecular weight itself. This determines the 100% point on the working curve. The other point, 0% $CaCO_3$, would then correspond to $ICaCO_3/IMgO = 0$, and a straight line establishes the working curve. Use of a straight line introduces an error in the low-$CaCO_3$ concentration range because of the nonlinear density characteristics of weak lines recorded photographically. A correction can be applied, but in view of the other errors, it is not considered here.

In Fig. III-29, working curves are shown that can be used for deriving CaO, $CaCO_3$, and $CaSO_4$ concentrations. Insofar as possible, experimental line ratios have been used. Theoretical values would not include the effects of absorption, thermal motion, and disorder; hence, the observed values are probably more realistic. In the case of $CaSO_4$, no pattern for fully sulfated material was available and theoretical line ratios had to be used.

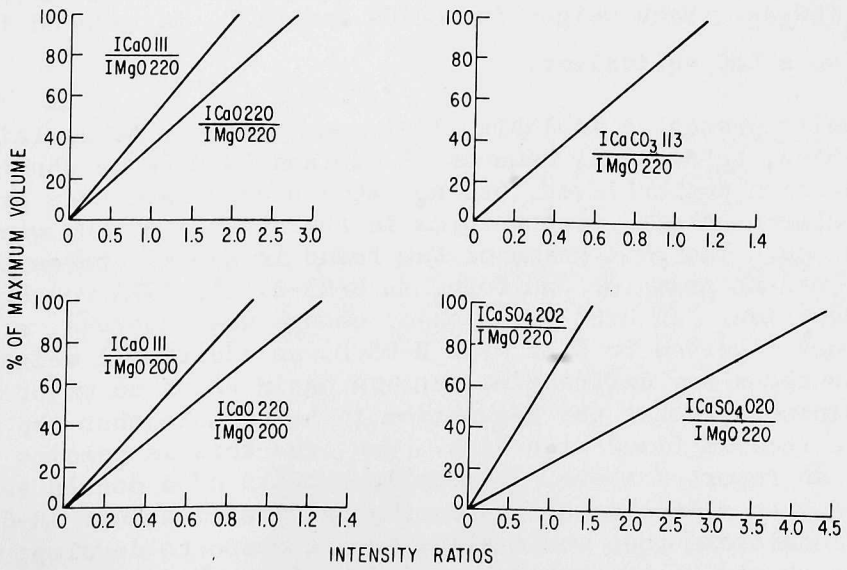

Fig. III-29. Working Curves for Quantitative Determination of CaO, $CaSO_4$ and $CaCO_3$.

Generally, it is found that only the 220 reflection of MgO can be used as a reference line, since other MgO reflections suffer too much interference. Even for the 220 line of MgO, the 214 line of $CaSO_4$ and the 215 line of $CaCO_3$ always interfere. The data in Table III-6 show the degree of interference. All lines superimpose fairly closely so that peak heights of the interferences can be subtracted. Strictly speaking, the intensity distribution over an angular range should be subtracted, but this cannot be done conveniently from a densitometer tracing.

Table III-6. Extent of Interference in X-ray Patterns.

Phase	hkl	sin θ
$CaSO_4$	214	0.5168
MgO	220	0.5171
$CaCO_3$	215	0.5228

With a suitable analytical method available, it was possible to study the following regeneration process in more detail:

$$3[CaSO_4 \cdot MgO] + [CaS \cdot MgO] \rightarrow 4[CaO \cdot MgO] + 4SO_2 \qquad (11)$$

Preliminary studies have indicated that CaO can be produced by this reaction. As an example of the results, one experiment is described below in some detail. In this experiment (identified as H-65), a half-calcined and sulfated dolomite sample was partially reduced to produce CaS. The stones were then heated under helium at 945°C for various times, and aliquots were isolated for the x-ray study. In Table III-7, percentage volumes of the chemical species, calculated from observed intensity ratios, are shown in the fourth column. These values are reduced to give molecular weights based on the formula, $Ca_{1.14}Mg_{0.86}(CO_3)_2$. Each weight for $CaCO_3$ and $CaSO_4$ is reduced in the sixth column to give a CaO equivalent.

The results presented in Table III-7 cannot as yet be explained in detail. Thus, for H-65-A, substantial amounts of CaO and $CaCO_3$ were observed--not only was 100% sulfation not achieved, but no $CaCO_3$ should have been present. In H-65-B, the effect of high temperatures in the absence of CO_2 was to convert the $CaCO_3$ to CaO. The 29.1 grams of CaO found in H-65-B corresponds well with the 28.8 equivalent grams of CaO found in H-65-A. The TGA weight loss arises from CaS production. In H-65-C, no major change was observed, although a weight loss was observed in TGA. For H-65-D, an additional weight loss was observed, but the x-ray diffraction pattern again shows no major change. It should be pointed out that the assumption is being made that the amount of MgO in the sample remains fixed with time. How true this is remains to be determined since, as reported above, detectable amounts of a double salt $Mg_3Ca(SO_4)_4$ may be formed when sulfation occurs during half-calcination. H-65-B was prepared under conditions that would allow such a phase to develop; hence, consideration should be given to the buildup of the CaO. In run H-65-E,

Table III-7. Summary of Results of Application of X-ray Technique to H-65 Experimental Series.

Sample	Sample History	Chemical Species	Volume Percent	Molecular Weight, g	Molecular Weight in CaO Equivalents	Comments
H-65-A	Half-Calcined, sulfated to constant weight, CO_2 removed to calcine remaining $CaCO_3$	CaO	14	8.95	8.95 } 28.77	
		$CaCO_3$	31	35.37	19.82 }	
		$CaSO_4$	69.5	107.7	44.39	
H-65-B	H-65-A partially reduced	CaO	45.5	29.1	29.1	
		$CaSO_4$	33	51.2	21.1	CaS observed
H-65-C	H-65-B heated under He for 15 min	CaO	48	30.69	30.69	
		$CaSO_4$	25.5	39.55	16.30	CaS observed
H-65-D	H-65-B heated under He for approx. 36 min	CaO	42	26.85	26.85	
		$CaSO_4$	31	48.08	19.82	CaS observed
H-65-E	H-65-B heated under He for approx. 61 min	CaO	74	47.31	47.31	
		$CaSO_4$	21	32.57	13.43	CaS observed
H-65-F	H-65-B heated under He for approx. 89 min	CaO	64.5	41.2	41.2	
		$CaSO_4$	24.5	38.0	15.7	little CaS present

a very substantial increase in the CaO content was observed, even though CaS was still detected. An anomaly arises in H-65-F, for although the CaO content remained essentially the same as in H-65-E, very little CaS was detected. It is believed that much of the irregular behavior stems from the nonuniform response of individual stones to the sulfation and regeneration steps. This difficulty can be overcome by the use of larger samples to ensure more representative analytical results.

In Fig. III-30, the percentage of the maximum attainable CaO content (Table III-7)(based on a CaO max of 63.93 g) is shown as a function of time. In spite of the anomalies, there is no doubt that the amount of CaO now present was about 70% of maximum. Unfortunately, the content of CaO in the starting material was 42%. The extent to which CaO can be formed when the initial CaO content is zero (*i.e.*, after 100% sulfation) remains to be determined. However, the results of other experiments to date have also been encouraging in indicating that the solid-solid regeneration reaction does indeed proceed.

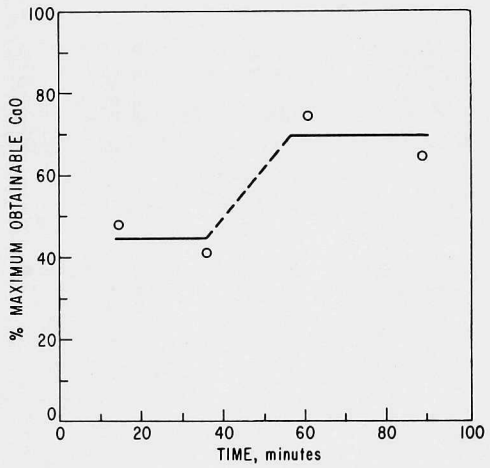

Fig. III-30.

Percent Yield of CaO vs Reaction Time for the Sulfate-Sulfide Reaction.

I. Stone Adherence (L. H. Fuchs*, B. R. Hubble, S. Siegel)

Prior to any chemical reactions, the 1337 dolomite stones are soft and easily fragmented. They are composed of aggregates of small crystals ranging in size from 30 to 300 micrometers. The x-ray diffraction patterns indicate, however, that finely divided dolomite is also present. The adherence of the stone may be attributed to an intergrowth of the crystals or perhaps some bonding involving a hydrate.

As reported above in the section on the sulfation reaction, the half-calcined stones develop grains of about the same size as the crystals from which they were derived, but the stones still show adherence. Two sources of bonding may be considered.

---

*Chemistry Division, ANL.

First, the calcite crystallites maintain a preferred orientation relative to the original dolomite crystal[31,32] so that the general shape of the original crystal persists. Observations regarding the persistence of grain size are based on a microscopic study of a limited number of stones. It is established, however, that the crystallites can be substantially randomized by proper choice of the calcining conditions. Nevertheless, some preferred orientation is always observed. Hence, if this persistence in orientation is assumed, it can be surmised that individual clusters (grains) adhere to other grains by way of van der Waals or other forces.

Second, the presence of α-quartz may permit the formation of stable silicates that could act as a cement. There is some merit in this consideration, since in dolomite stones with high α-quartz content, the silica can disappear at high temperatures to form a calcium magnesium silicate. This has been observed in x-ray studies.

Following sulfation, or even on regeneration and sulfation, adherence is maintained, with a noticeable hardening of the stones. The hardening is very pronounced in one of the synthetic dolomites. The integrity of the stones is maintained in spite of the very large molecular volume changes taking place during the various reactions. Bonding may arise from the following causes: (1) A $CaSO_4$-CaS eutectic may form. This has been suggested in the literature.[41] (2) A stable $CaSO_4$ hydrate may form and persist between the grains. (3) A Mg-Ca complex may develop at the interfaces of the grains. (4) An expitaxial bond may form. Law *et al.*[34] have carried out an infrared study of the sorption of SO_2 on CaO. This work has led to the identification of $(S_xO_y)^{-m}$ species resulting from polymerization. Although their temperature conditions do not correspond to present higher temperature requirements, the study does suggest that an expitaxial relationship may exist, leading to bonding.

In a number of cases, as in Fig. III-31, the microscopic studies have revealed the presence of narrow bands around the grains containing the reactants. The bands generally are only a few micrometers in width and do not lend themselves to easy study, but may be characterized if detailed analysis of these bands can be accomplished.

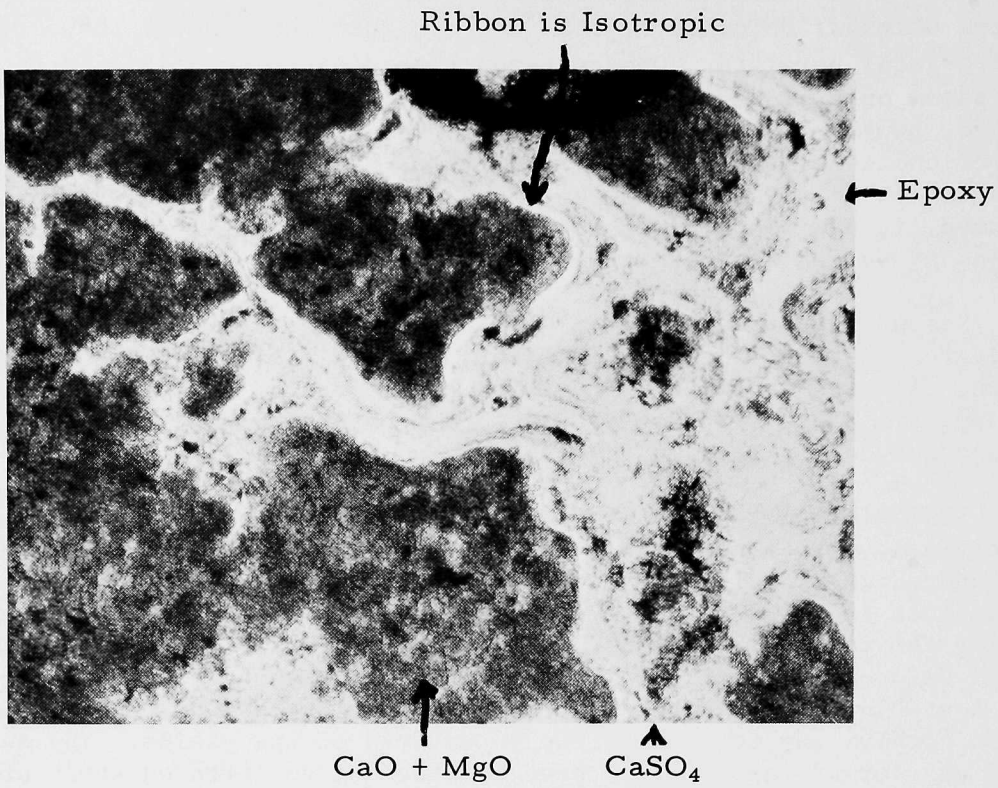

Fig. III-31.

Thin Section Enlargement (305x) of 1337 Stone in Reduced State Exhibiting Unidentified Isotropic Bands Surrounding Grains.

REFERENCES

1. C. M. Shy and J. F. Finklea, Environ. Sci. Technol. *7*, 204 (1973).

2. M. O. Amdur and M. Corn, Amer. Ind. Hyg. Assoc. J. *24*, 326 (1963).

3. *Chemical Engineering Division Physical Inorganic Chemistry Annual Report, July 1973 - June 1974*, USAEC Report ANL-8123, p. 43 (1974).

4. P. T. Cunningham, S. A. Johnson, and R. T. Yang, Environ. Sci. Technol. *8*, 131 (1974).

5. N. J. Harrick, *Internal Reflection Spectroscopy* (Interscience Publishers, New York, 1967).

6. D. Leaky, R. Siegel, P. Klotz, and L. Newman, Atmos. Environ. *9*, 319 (1975).

7. G. Herzberg, *Molecular Spectra and Molecular Structure II. Infrared and Raman Spectra of Polyatomic Molecules* (Van Nostrand Reinhold Co., New York, 1945).

8. F. A. Miller, C. H. Wilkins, Anal. Chem. *24*, 1253 (1952); F. A. Miller, A. L. Carlson, F. F. Bentley, and W. H. Jones, Spectrochim. Acta *16*, 135 (1960); R. J. Gillespie and E. A. Robinson, Can. J. Chem. *40*, 644 (1962); P. Dhamelincourt, G. Palavit, and S. Noël, Bull. Soc. Chim., France (1971) 2849.

9. Y. Mizutani and T. A. Rafter, "Isotopic Composition of Sulfate in Rain Water, Gracefield, New Zealand," New Zealand J. Sci. *12*, 69 (1969).

10. E. Meszaros, "Evidence of the Role of Indirect Photochemical Processes in the Formation of Atmospheric Sulfate Particulate," Aerosol Sci. *4*, 429 (1973).

11. R. A. Cox, "Some Experimental Observations of Aerosol Formation in the Photo-oxidation of Sulfur Dioxide," Aerosol Sci. *4*, 473 (1973).

12. P. Urone and W. H. Schroeder, "SO_2 in the Atmosphere: A Wealth of Monitoring Data, but Few Reaction Rate Studies," Environ. Sci. Tech. *3*, 436 (1969).

13. R. M. Lloyd, "Oxygen Isotope Behavior in the Sulfate-Water System," J. Geophys. Res. *73*, 6099 (1968).

14. W. A. Pryor and U. Tonellato, "The Exchange of ^{18}O between Sodium Thiosulfate-^{18}O and Water," J. Amer. Chem. Soc. *89*, 3379 (1967).

15. P. W. Schenk and R. Stendel, "Oxides of Sulfur," Chap. 11, in *Inorganic Sulfur Chemistry*, G. Nickless, ed., pp. 367-418, Elsevier, New York, N.Y. (1968).

16. ASTM Designation D516-68, "Standard Methods of Test for Sulfate Ion in Water and Waste Water," 1973 Annual Book of ASTM Standards, Part 23, pp. 425-426.

17. R. N. Clayton and S. Epstein, "The Relationship between $^{18}O/^{16}O$ Ratios in Coexisting Quartz, Carbonate, and Iron Oxides from Various Geological Deposits," Geology *66*, 352-371 (1958).

18. A. Longinelli and H. Craig, "Oxygen-18 Variations in Sulfate Ions in Sea Water and Saline Lakes," Science *156*, 56-59 (1967).

19. T. A. Rafter, "Oxygen Isotopic Composition of Sulfates. Part 1, A Method for the Extraction of Oxygen and its Quantitative Conversion to Carbon Dioxide for Isotope Ratio Measurements," New Zealand J. Sci. *10*, 493-510 (1967).

20. Y. Mizutani, "An Improvement in the Carbon-Reduction Method for the Oxygen Isotopic Analysis of Sulfates," Geochem. J. *5*, 69-77 (1971).

21. Y. Horibe, K. Shigehara, and Y. Takakuwa, "Isotope Separation Factor in Carbon Dioxide-Water System and Isotopic Composition of Atmospheric Oxygen," J. Geophys. Res. *78*, 2625-2629 (1973).

22. S. Epstein and T. Mayeda, "Variation of ^{18}O Content of Waters from Natural Sources," Geochim. and Cosmochim. Acta *4*, 223-224 (1953).

23. M. Majzoub, "Une Méthode d'Analyse Isotopique de l'Oxygéne sur des Microquantites d'Eau Determination des Coefficients de Partage a l'Equilibre de l'Oxygéne 18 entre H_2O et CO_2; D_2O et CO_2," J. Chem. Phys. *63*, 563-568 (1966).

24. C. Huygen, "The Sampling of Sulfur Dioxide in Air with Impregnated Filter Paper," Anal. Chim. Acta *28*, 349-360 (1963).

25. ASTM Designation D1339-72, "Standard Methods of Test for Sulfite Ion in Water," 1973 Annual Book of ASTM Standards, Part 23, p. 436.

26. G. Cortecci and A. Longinelli, "Isotopic Composition of Sulfate in Rain Water, Pisa, Italy," Earth Planet. Sci. Lett. *8*, 36-40 (1970).

27. ASTM Designation D1739-70, "Standard Method for Collection and Analysis of Dustfall (Settleable Particulates)," 1973 Annual Book of ASTM Standards, Part 23, pp. 893-894.

28. C. M. Stevens and L. Krout, "Method for the Determination of the Concentration and the Carbon and Oxygen Isotopic Composition of Atmospheric Carbon Monoxide," Inst. J. Mass Spect. Ion Phys. *8*, 251 (1972).

29. S. G. Chang and T. Novakov, "Formation of Pollution Particulate Nitrogen Compounds by NO-Soot and NH_3-Soot Gas-Particle Surface Reactions," Atmos. Environ. *9*, 1-10 (1975).

30. T. Novakov, S. G. Chang, and A. B. Harker, "Sulfates as Pollution Particulates: Catalytic Formation on Carbon (Soot) Particles," Science *186*, 259-261 (1974).

31. *Chemical Engineering Division Physical Inorganic Chemistry Annual Report, July 1973 - June 1974*, USAEC Report ANL-8123, pp. 47-52 (1974); R. T. Yang, P. T. Cunningham, W. I. Wilson, and S. A. Johnson, Advan. Chem. Series *39*, 149 (1975).

32. H. Wilsdorf and R. Haul, Nature *167*, 945 (1951).

33. R. Haul and W. Wilsdorf, Acta Cryst. *5*, 250 (1952).

34. M. J. Law *et al.* Environ. Sci. Technol. *5*, 1191 (1971).

35. J. J. Rowe, G. W. Morey, and C. C. Silber, J. Nucl. Chem. *29*, 925 (1967).

36. D. Graf and J. Goldsmith, Geology *64*, 173 (1956).

37. R. A. Berner, Geochim. Cosmochim. Acta *39*, 489 (1975).

38. B. Newmann, Z. Angew. Chem. *39*, 1537 (1926).

39. Vogel *et al.*, ANL/ES-CEN-1005.

40. R. C. Hoke *et al.* Combustion, 6-12, (Jan. 1975).

41. D. L. Keairns *et al.*, Westinghouse Research Laboratories, EPA Contract No. 63-02-0217 (Dec. 1973).